THEORETICAL STUDIES OF UNCONVENTIONAL SUPERCONDUCTIVITY IN Sr_2RuO_4

THEORETICAL STUDIES OF UNCONVENTIONAL SUPERCONDUCTIVITY IN SR_2RUO_4

By

WEN HUANG, M.SC.

A Thesis

Submitted to the School of Graduate Studies

in Partial Fulfilment of the Requirements

for the Degree

Doctor of Philosophy

McMaster University

Abstract

In this thesis we study the edge currents and the multi-band superconductivity in the unconventional superconductor Sr_2RuO_4.

Numerous measurements have given strong support for a topologically non-trivial time-reversal symmetry breaking chiral p-wave state in this material. However, the spontaneous edge current expected for this order has eluded experimental detection. In this thesis, we present a general theoretical description of the edge currents in chiral superconductors. Our results elucidate the connection between the edge currents and the topological property of the chiral pairing. On this basis, we argue that superconducting gap anisotropy, combined with surface disorder, may provide an explanation for the absence of observable edge currents in Sr_2RuO_4. In addition, contrary to intuitive expectations, the integrated edge current is found to identically vanish for any non-p-wave chiral superconductor in the continuum limit– a result which may be connected with the orbital angular momentum problem in chiral superfluids, such as the A phase of ^{3}He. In lattice models, the integrated edge current may not vanish in non-p-wave superconductors but, in general, is substantially smaller compared to that of a simple chiral p-wave.

In a separate study, we investigate the multi-band nature of the superconductivity in Sr_2RuO_4, via explicit microscopic calculations of the multi-band interactions. Our results indicate comparable pairing correlations on all of the bands and the existence of soft collective phase fluctuations–a Leggett mode. We also examine the possibility of alternative time-reversal symmetry breaking multi-band superconductivity which does not necessarily require chiral p-wave pairing.

Acknowledgements

Five years have passed since I began my PhD at McMaster. Except for an unpleasant gain of age, I have every reason to believe that this has been a rewarding journey. Along the way I have had a terrific fortune of being alongside a group of exceptional individuals. They helped me grow over the years and shaped me into my present being. It is to them I owe my sincerest gratitude.

Without a doubt, my advisor Prof. Catherine Kallin comes on top of the list. I consider it a privilege to be Catherine's student. She introduced me to the field of Sr_2RuO_4 and has been extremely patient in providing critical guidance throughout the years. She is always willing to discuss physics with me, never hesitates to challenge me with questions which often strike at the heart of the problems we are attacking. This thesis, more precisely my PhD, would never have become possible without her constant support and encouragement. Far beyond this, Catherine taught me how to conduct a quality research. I am fortunate to have witnessed her deep physical insight, as well as her meticulous and unrelenting pursuit of precision and fundamental interpretations of complex physics. Her uncompromising style of research will have a long-lasting impact on my career. During the course of my PhD, I was also extremely fortunate to be given many great opportunities outside of McMaster and an invaluable freedom to pursue various directions. For all of these, I will remain eternally grateful to Catherine.

I am also indebted to other members of my supervisory committee, Prof. John Berlinsky and Prof. Sung-Sik Lee. John has always been kind to offer valuable career advices. I must thank him for his great help during my search for a postdoctoral position. And, throughout my PhD, my research benefited tremendously from the discussions with him. I hope that there will be opportunities to work more closely with him. Sung-Sik's influence on me reaches beyond my thesis research. Through his courses and many other occasions, I have always been immensely impressed by his remarkable proficiency in untangling profound subjects and presenting them with the utmost clarity. He is an inspirational physicist to look up to.

vi

Preface

This is a sandwich thesis based on four publications, which appear in the following order:

- Chapter 3   W. Huang, E. Taylor, C. Kallin, *Vanishing edge currents in non-p-wave topological chiral superconductors*, Phys. Rev. B **90**, 224519 (2014).
  WH performed numerical calculations; WH and ET conducted theoretical analyses; CK supervised the project. All authors discussed and wrote the draft.

- Chapter 4   W. Huang, S. Lederer, E. Taylor, C. Kallin, *Nontopological nature of the edge current in a chiral p-wave superconductor*, Phys. Rev. B **91**, 094507 (2015).
  WH performed numerical calculations; WH, SL and ET conducted theoretical analyses; CK and ET supervised the project. All authors discussed and wrote the draft.

- Chapter 5   S. Lederer, W. Huang, E. Taylor, S. Raghu, C. Kallin, *Suppression of spontaneous currents in Sr_2RuO_4 by surface disorder*, Phys. Rev. B **90**, 134521 (2014).
  SL and WH performed numerical calculations; SL, WH and ET conducted theoretical analyses; CK and SR supervised the project. All authors discussed and wrote the draft.

- Chapter 6   W. Huang, T. Scaffidi, M. Sigrist, C. Kallin, *Leggett modes and multi-band superconductivity in Sr_2RuO_4*, arXiv:1605.03800 (accepted to Phys. Rev. B).
  WH performed theoretical analyses, TS carried out numerical calculations; CK and MS supervised the project. All authors discussed and wrote the draft.

All of the published papers appear with the permission of the American Physical Society.

To my beloved mother, Xiao-Rong Liu

Table of Contents

List of Figures

Chapter 1

Introduction

One hundred years after its discovery,[1] superconductivity remains one of the most extensively studied quantum mechanical phenomena in condensed matter physics. The advent of the celebrated Bardeen-Schrieffer-Cooper (BCS) theory[2] more than five decades ago laid the foundation of a microscopic understanding of this novel quantum state. Many more superconductors have since been discovered, some with unconventional properties beyond the original BCS description. Among them, strontium ruthenate (Sr_2RuO_4)[3] stands out, thanks to its unusual superconducting order[4].

Sr_2RuO_4 is a perovskite oxide iso-structural to to one of the parent compounds of the well known cuprate superconductors,[5] La_2CuO_4 (Fig. 1.1). However, unlike the latter which is a anti-ferromagnetic Mott insulator[6] in the absence of chemical doping, normal state Sr_2RuO_4 is a non-magnetic metal with three bands crossing the Fermi level (Fig. 1.1)[7, 8]. Above the superconducting transition and below about $30K$, the compound behaves like a Fermi liquid but with considerable mass enhancement indicative of strong electron correlations[4]. The three bands consist primarily of the Ru t_{2g} d-orbitals $- d_{xz}$ (xz), d_{yz} (yz) and d_{xy} (xy)[9, 10]. Due to the layered structure of the crystal, the bands exhibit minuscule interlayer hopping along the crystalline c-axis (z-direction). As a consequence, the bands cross the Fermi level forming cylindrical-shaped Fermi surface sheets around the k_z-axis in the Brillouin zone[7,
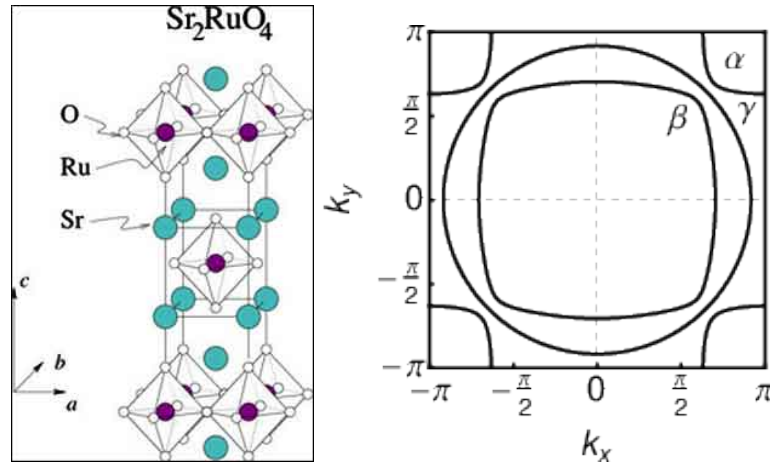
Figure 1.1: Schematics of a) the crystal structure of Sr_2RuO_4, and b) its three Fermi surfaces in a two-dimensional Brillouin zone.

8]. Among them, two quasi-one-dimensional (1D) bands, dubbed α- and β-bands, originate mainly from the hybridized xz and yz-orbitals which hop dominantly along the respective x- and y-directions; while the quasi-2D γ-band arises primarily from the xy-orbital. The three d-orbitals are further hybridized by a significant atomic spin-orbit coupling[10, 11, 12].

Below we summarize the main features of the unconventional superconductivity in Sr_2RuO_4. For more exhaustive discussions the readers are referred to existing reviews, Refs [4, 13, 14, 15, 16, 17].

1.1 Spin-triplet odd-parity pairing in Sr_2RuO_4

The superconductivity in Sr_2RuO_4 was first discovered by Maeno in 1994 [3], with a rather low transition temperature $T_c \sim 0.93K$. The T_c was subsequently improved to $1.5K$ for higher quality samples [4, 16].

One of the first indications of the unconventional nature of the superconductivity of Sr_2RuO_4 was the strong suppression of T_c due to impurity doping[18]. This is not expected in conventional

s-wave superconductors, and is most commonly attributed to the unconventional nature of the Cooper pairing where the superconducting gap averages to zero around the Fermi surface.

Early evidence for spin-triplet pairing stemmed from both NMR Knight shift [19] and Neutron scattering [20] measurements, both of which saw constant spin susceptibility across the superconducting transition down to the lowest accessible temperatures. In the absence of spin-orbit coupling, constant spin susceptibility below T_c is peculiar to superconductors with triplet pairing for a magnetic field perpendicular to the direction of zero-spin projection of the triplet Cooper pairs (see below). Specific to a spin quantization axis parallel to the magnetic field, the Cooper pairs are formed with electrons carrying the same spin. Thus the development of superconductivity does not hinder spin polarization. In contrast, spin polarization is suppressed in a spin-singlet superconductor as it requires breaking the Cooper pairs.

The Pauli exclusion principle necessarily implies odd parity for the spatial wave function of a triplet Cooper pair, namely, the wave function must change sign upon an exchange of the coordinates of the two electrons constituting the Cooper pair. More formally, $\Delta_k = -\Delta_{-k}$. This is supported by phase-sensitive measurements on superconducting quantum interference devices (SQUID) by Nelson *et al* [21]. In these experiments, as is expected for a single-domain odd parity order parameter, when the magnetic flux threading the junctions is zero, the critical current reaches a minimum (maximum) for devices with junctions on the opposite (same) sides of the crystal.

By convention, a generic triplet pairing gap may be written as,

$$\Delta_{\sigma\sigma'}(k) = i[(d(k)\cdot\sigma)\sigma_y]_{\sigma\sigma'} = \begin{pmatrix} -d_1(k) + id_2(k) & d_3(k) \\ d_3(k) & d_1(k) + id_2(k) \end{pmatrix} \tag{1.1}$$

where the so-called $\hat{d}$-vector $d(k) = (d_1, d_2, d_3)$ denotes the spin configuration of the pairing and the k-dependence characterizes the structure of the superconducting gap. Physically, for the triplet states considered here, the $\hat{d}$-vector denotes the direction along which the spin of the Cooper pair has zero projection. For example, taking the spin quantization axis to be along the c-axis orthogonal to the 2D plane, for an out-of-plane $\hat{d}$ state, one arrives at $\Delta_{\uparrow\uparrow} = \Delta_{\downarrow\downarrow} = 0$ and $\Delta_{\uparrow\downarrow} = \Delta_{\downarrow\uparrow} = d_3(k)$. Other $\hat{d}$-vector states may be similarly obtained.

There is a further recent verification of the odd parity triplet pairing: the observation of half-quantum-vortex (HQV) in the cantilever magnetometry measurements by Jang *et al* [22] on mesoscopic ring-shaped samples. A HQV is formed when the $\hat{d}$-vector rotates by $180°$ as the phase of orbital part of the Cooper pair wave function winds by π around the vortex core. It may also be viewed, when taking the spin quantization axis to be orthogonal to the $\hat{d}$-vector, as a topological excitation where the order parameter of only one of the two spin species winds by a phase of 2π. However, the existence of these excitations has not yet been confirmed in more recent transport studies [23, 24], and questions remain regarding the stability of HQV under various experimental conditions [25, 26, 27, 28].

1.2 Time reversal symmetry breaking pairing

Another novel property of Sr_2RuO_4 is the possibility of time-reversal symmetry breaking (TRSB) superconductivity. Evidence of TRSB came first in μSR [29] where weak internal magnetic fields were observed below T_c. Later Kerr effect measurements [30] observed a rotation of the polarization angle of the reflected linearly polarized light normally incident to the sample below T_c. A further indirect verification is a Josephson interferometry measurement[31] and a point contact spectroscopy[32], which indicate the existence of domains of time-reversed superconducting order parameters.

This peculiar property, combined with the triplet and odd-parity nature of the pairing, makes chiral $p_x + ip_y$ order the most probable candidate ground state for Sr_2RuO_4. Such a novel state breaks time-reversal symmetry in the sense that Cooper pairs carry non-vanishing and quantized orbital angular momentum $L_z = \pm \hbar$, similar to the so-called A-phase of ^{3}He[33]

In conjunction with the tetragonal crystal lattice structure and the finite spin-orbit coupling on the Ru orbitals, a chiral p-wave state should exhibit an out-of-plane $\hat{d}$-vector and the order parameter belongs to the two-dimensional E_u representation of the underlying D_{4h} point group.[34] More explicitly,

$$\Delta_{\sigma\sigma'}^{\text{chiral}}(k) = \begin{pmatrix} 0 & \Delta_0(k_x \pm ik_y) \\ \Delta_0(k_x \pm ik_y) & 0 \end{pmatrix}. \tag{1.2}$$

In the absence of spin-orbit coupling which breaks spin rotation invariance, the chiral state is degenerate with the so-called helical state analogous to ^{3}He B-phase[33],

$$\Delta_{\sigma\sigma'}^{\text{helical}}(k) = \begin{pmatrix} \Delta_0(-k_x \pm ik_y) & 0 \\ 0 & \Delta_0(k_x \pm ik_y) \end{pmatrix}, \tag{1.3}$$

which has an in-plane $\hat{d}$-vector orientation and preserves time reversal invariance by virtue of the opposite chiral pairing associated with the two spin species. It is widely believed that spin-orbit coupling in Sr_2RuO_4 pins the $\hat{d}$-vector to the $\hat{c}$-axis, thereby favoring the chiral pairing[35].

1.2.1 Topological chiral superconductivity The quantized angular momentum carried by the Cooper pairs leads to a non-trivial topological property for the ground state. This may be

illustrated using the example of continuum systems, where the gap function of a generic chiral pairing reads,

$$\Delta_k = \Delta_0 \left(\frac{k_x + ik_y}{k_F} \right)^m \equiv \Delta_0 (k/k_F)^m e^{im\theta_k} \ , \ m = 1, 2, ... \tag{1.4}$$

where m denotes the orbital angular momentum of the associated Cooper pairs, e.g. $m = 1$, 2 and 3 for chiral p-,d-, and f-waves, respectively; and θ_k is the angle of wavevector k with respect to the x-axis. Remarkably, the quantized orbital angular momentum coincides with an integer topological invariant that defines the topology of the ground state: the Chern number [38, 39],

$$C \equiv \frac{1}{4\pi} \int d^2k \, \hat{h} \cdot \left(\partial_{k_x} \hat{h} \times \partial_{k_y} \hat{h} \right) = m, \tag{1.5}$$

Here the $\hat{h}$ denotes a pseudospin given by $\{\text{Re}[\Delta_k], -\text{Im}[\Delta_k], \xi_k\}$ and $\hat{h} = \vec{h}/|\vec{h}|$, with $\xi_k \equiv \varepsilon(k) - \mu$ giving the normal state single-particle dispersion. Physically, the Chern number counts the Berry phase acquired by the pseudospin as it winds adiabatically on the torus of the 2D Brillouin zone[40, 41].

The attribution of non-trivial topology, i.e. the non-vanishing Chern number, is not limited to continuum models, but also extends to generic lattice systems, as long as the state remains fully gapped. More generically, a chiral pairing may be expressed as,

$$\Delta_k = \Delta_1 f_1(k) + i\Delta_2 f_2(k). \tag{1.6}$$

Here both of the two components of the order parameter, Δ_1 and Δ_2, are real, and the form factors $f_1(k)$ and $f_2(k)$ are any lattice harmonics that transform the same way as the appropriate basis functions do under the lattice point group symmetry operations.[42] For example, in a square lattice, the simplest chiral p-wave reads $\Delta_k \sim \sin k_x + i \sin k_y$. Usually, form factors

pertaining to higher harmonics signify substantial gap anisotropy, as can be seen by taking
$|\Delta_k| = \sqrt{|\Delta_1 f_1(k)|^2 + |\Delta_2 f_2(k)|^2}$.

Finally, the core of a HQV in a chiral p-wave superconductor supports a zero-energy Majorana mode [43, 39, 44]. These exotic particles are their own anti-particles [45]. Their existence are robust against local perturbations and relies purely on a topological property embedded in a HQV [44]. Multiple Majorana modes in the same system introduce ground state degeneracy and result in non-Abelian braiding statistics when the HQV's move around each other [46], a remarkable property which may be utilized for quantum computing [47]. This constitutes an important motivation for investigating the unconventional superconductivity in Sr_2RuO_4.

1.2.2 Edge current and orbital angular momentum paradox   Similar to quantum Hall insulators or Chern insulators, a chiral superconductor supports chiral edge modes. These modes have Majorana character [48], and their existence is a manifestation of the non-trivial topology of the bulk state[49]. The number of the chiral edge branches equals the Chern number, while their chirality is protected by the topology of the chiral ground state and is hence robust against local perturbations.

The existence of chiral edge modes leads naturally to the expectation of spontaneous currents at the edge of the system. A related problem has been studied for decades in relation to the intrinsic orbital angular momentum in thin films of ^{3}He A-phase (see e.g. [33, 36, 37]). In analogy to the Bose-Einstein condensate (BEC) limit with tightly-bound molecules, since each Cooper pair carries a quantized orbital angular momentum $\langle L_z \rangle = \hbar/2$, a system of N particles is intuitively expected to acquire a total orbital angular momentum $\langle L_z^{\text{tot}} \rangle = N\hbar/2$. Note that for a $U(1)$-breaking state, particle number is not conserved, and these expectations

are only accurate up to a factor of $1 - (\Delta/E_F)^2$. Generalizing to higher angular momentum Cooper pairing, $\langle L_z^{\text{tot}} \rangle = mN\hbar/2$, where $m = C$ is the Chern number. An alternative argument would suggest that, in the BCS limit only particles within a thin shell of the Fermi level are paired, resulting in an extra factor of Δ/E_F for the expected value of the angular momentum, i.e. $\langle L_z^{\text{tot}} \rangle = \frac{\Delta}{E_F} \frac{mN\hbar}{2}$. A third argument would suggest that, since the average size of the Cooper pairs, parameterized by the coherence length ξ, is much larger than the inter-particle spacing, k_F^{-1}, the Cooper pairs strongly overlap and cancel the orbital current generated by one another. This leads to a much stronger suppression of the orbital angular momentum $\langle L_z^{\text{tot}} \rangle = \left(\frac{\Delta}{E_F} \right)^2 \frac{mN\hbar}{2}$. The orders-of-magnitude difference in the various predictions constitutes the so-called angular momentum paradox. Many have contributed insights since the question was initially raised (see e.g. [50, 51, 52, 53, 54, 55, 56]). Recently, Stone and Roy[48] and Sauls[57], studying chiral p-wave superfluids, showed explicitly that the total angular momentum is indeed given by $N\hbar/2$. However, this is not a direct consequence of summing up contributions from the $N/2$ Cooper pairs as mentioned above. More importantly, as we shall see in this thesis, the conclusion is drastically different for chiral superfluids with $m > 1$.

A more practical problem, which motivated part of this thesis, arises in relation to Sr_2RuO_4. Like the spontaneous angular momentum, the spontaneous currents at the edges or domain walls are expected as a direct consequence of the chiral p-wave pairing in Sr_2RuO_4 [58, 59]. Here, a domain wall separates real space domains of Cooper pairing with positive and negative chiralities. Strikingly, efforts to detect the signature magnetic fields generated by these spontaneous surface currents have so far returned null results. These include scanning SQUID and scanning Hall probe microscopies [60, 61, 62], which consistently placed a strict upper bound for the spontaneous current approximately 10^{-3} times smaller than what was predicted for a simple one-band isotropic chiral p-wave model for Sr_2RuO_4 [58]. Such an apparent
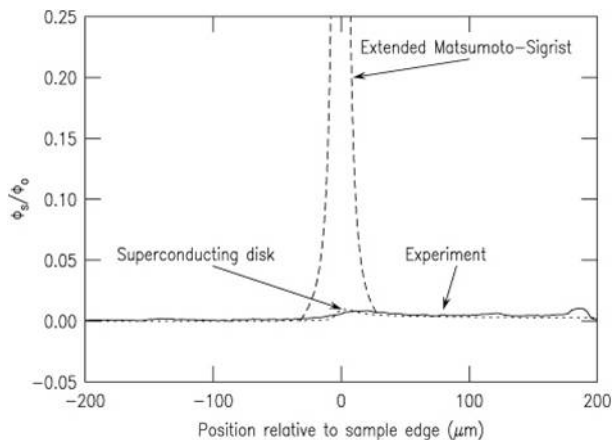
Figure 1.2: Scanning SQUID measurement by Kirtley et al. [60], showing significant discrepancy between the measured and theoretically predicted magnetic signals as the SQUID pick-up loop scans across a sample edge.

contradiction imposes stringent constraints on theories of unconventional superconductivity in Sr_2RuO_4.

Over the years, a fair amount of work has emerged, attempting to reconcile chiral p-wave order and the absence of edge currents in Sr_2RuO_4. Early on, Ashby and Kallin [63] explored the suppression of edge current due to surface disorder as recently indicated in, e.g. a junction tunneling measurement [64]. The surface suppression was later substantiated by numerical BdG calculations of more realistic anisotropic chiral p-wave models for this material [65, 66].

Meanwhile, Imai et al [67] showed that the spontaneous current at an ideal edge remains substantial in multi-band chiral p-wave models of Sr_2RuO_4 in which superconductivity resides dominantly on the quasi-1D bands. Interestingly, in the limit of weak inter-orbital mixing (due to both hybridization and spin-orbit coupling), the nearly flat edge dispersion associated with the quasi-1D orbitals promotes the formation of spin polarization at the boundary, which the authors argued would at least partially negate the magnetic field generated by the spontaneous

current. However, they also noted that the spin polarization is less pronounced in the presence of stronger inter-orbital mixing.

Alternative arguments for the absence of observable surface currents have been proposed, such as the formation of small domains [31, 61] which might cancel the expected signal in scanning probes. However, to obtain the required degree of cancellation, the domain size would have to be smaller than a micrometer [14, 15]. This is not compatible with the Josephson phase sensitive [21] and the Kerr effect [30] measurements, both of which indicate single domain sizes substantially larger than a few micrometers.

1.2.3 Plan of this thesis Part of the goal of this thesis is to develop a most generic description for the edge currents in chiral superconductors and superfluids. We will first formulate in Ch.2 general theories of the spontaneous current in superconductors with TRSB, using both phenomenological and semiclassical analyses. We then present in Ch.3 a rather surprising finding, that the integrated edge current vanishes identically for all non-p-wave chiral superconductors in the continuum limit. Extensions to generic lattice models are also discussed. Next in Ch.4, we explore the connection between the edge current and the intrinsic topology of the chiral ground state. Finally, in Ch.5 we present a self-consistent numerical Bogoliubov de-Gennes (BdG) calculation of the edge current in a multi-band model of Sr_2RuO_4, where the effect of strong surface disorder is systematically investigated.

1.3 Superconducting mechanism
Shortly after the discovery of superconductivity in Sr_2RuO_4, Rice and Sigrist [34], and independently Baskaran [68], proposed spin-triplet pairing, motivated by the strong Hund's coupling between the Ru d-orbitals which favors spin-triplet correlations. More studies [69, 35, 70, 71, 72, 73, 74, 75, 76, 77, 78] have

followed, based almost exclusively on unconventional mechanisms associated with Coulomb correlations and to some extent their associated bosonic charge and/or spin density wave fluctuations.

Among these studies, spin density-wave proposals include: 1) Ferromagnetic fluctuations on the γ-band due to a filling proximate to a van-Hove singularity, and 2) strong incommensurate spin-density-wave fluctuations arising from the quasi-nested $\alpha\&\beta$-bands. This leads to the expectation that superconductivity is primarily driven by one of the two subsets of bands – quasi-2D γ-band or quasi-1D $\alpha\&\beta$-bands, and that the passive band(s) exhibit much weaker Cooper pairing by proximity.

Nevertheless, throughout the years, a picture has emerged that superconductivity arises concurrently on all of the three bands in Sr_2RuO_4. Experimentally, this is evident in, e.g. the specific heat measurements, which below T_c do not show any anomaly indicative of the existence of a weaker superconducting gap on a subdominant band.[79, 80] Theoretically, a weak-coupling renormalization group analysis by Scaffidi *et al* [77] predicts comparable gap amplitudes on all of the bands in a range of band and interaction parameters believed to be appropriate to Sr_2RuO_4. However, this is still an unresolved issue, and both experimental[81] and theoretical[82, 72, 75, 76, 78] indications also exist in support of a state where one subset of the bands dominates superconductivity.

1.3.1 Plan of this thesis   In Ch.6, we ask the question of how the superconducting order parameters of the three-bands in Sr_2RuO_4 interact with each other, and explore possible novel physics resulting from the multi-band interactions. Based on microscopic weak coupling calculations, we explicitly evaluate the effective multi-band interactions in the leading superconducting channels for various regions of interaction parameter space. Our results in-

dicate comparable superconducting correlations on the two subsets of bands, which lead to comparable gaps on the bands. We also argue that the comparatively weaker interactions between the two subsets of bands in general result in a relatively soft collective phase mode, the Leggett mode. In addition, we also examine the possibility of exotic multi-band TRSB triplet superconductivity which does not necessarily involve chiral p-wave pairing.

Chapter 2

Edge currents in time-reversal symmetry breaking (TRSB) superconductors: General Theories

2.1 Introduction

This chapter will present general theories of edge currents in chiral superconductors. The discussions are not limited to chiral *p*-wave states, but include higher angular momentum Cooper pairing states, such as chiral *d*- and *f*-wave, etc, as well as other superconducting order parameters with TRSB. We provide both phenomenological and semiclassical analyses to elucidate the relation between the edge currents and the underlying superconducting order. In particular, it will become clear that the edge current depends rather sensitively on the structure of the gap functions of the two chiral components.

The phenomenological analysis, based on a Ginzburg-Landau effective theory, yields a powerful qualitative description of the edge current. On the other hand, the semiclassical argument provides an intuitive explanation to the comparatively smaller edge current in non-*p*-wave and anisotropic *p*-wave chiral superconductors.

This chapter will concentrate on scenarios with sharp confining edges, i.e. the carrier density drops to zero abruptly over the length scale of the order of k_F^{-1} which is much smaller

than the coherence length. This is most relevant to solid state superconductors where it is not feasible to engineer a spatial variation of the particle density while retaining superconductivity. The soft edge limit, where the density varies over a length scale larger than or at least comparable to the coherence length, will be discussed in the next chapter. Unless otherwise specified, we shall focus on single-band systems in this chapter.

2.2 Ginzburg-Landau effective theories

To understand the appearance of edge currents in a TRSB superconductor, one may start from an effective field theory that encapsulates the low energy electromagnetic responses of the system. Such an effective theory can be obtained from a gradient expansion of the action of a superconductor given by the following[83, 84],

$$S = \int d\tau d^d r \left(\frac{|\Delta|^2}{V} - \mathrm{Tr} \ln \hat{G}^{-1} \right), \tag{2.1}$$

where Δ is the superconducting order parameter, $-V$ is the effective interaction which mediates Cooper pairing, and the Gor'kov Greens function $\hat{G}$ is obtained via the following relation,

$$\hat{G}^{-1} = \begin{pmatrix} -\partial_\tau - \hat{H}_0 & \Delta \\ \Delta^* & -\partial_\tau + \hat{H}_0^* \end{pmatrix}, \tag{2.2}$$

where $\hat{H}_0$ is the single-particle normal state Hamiltonian. An appropriate perturbative expansion of (2.1) depends on the temperature regime under consideration. At $T \simeq T_c$, $\Delta(T)/T \ll 1$, hence an expansion with respect to Δ/T may be performed, resulting in an effective Ginzburg-Landau theory (see Appendix A for details). For a generic two-component superconducting state given by $\Delta_k = \Delta_1 f_1(k) + \Delta_2 f_2(k)$, the effective time-independent Ginzburg-Landau action reads [42],

$$S[\Delta^*, \Delta] = \int d\mathbf{r}\ [\frac{\alpha_1(T)}{2}|\Delta_1|^2 + \frac{\alpha_2(T)}{2}|\Delta_2|^2$$

$$+ \frac{\beta_1}{4}|\Delta_1|^4 + \frac{\beta_2}{4}|\Delta_2|^4 + \frac{\beta_{12}}{4}|\Delta_1|^2|\Delta_2|^2 + \frac{\beta'}{4}(\Delta_1^*\Delta_2 + \Delta_1\Delta_2^*)^2 + O(|\Delta|^4)$$

$$+ k_1|\mathcal{D}_x\Delta_1|^2 + k_1'|\mathcal{D}_y\Delta_1|^2 + k_2|\mathcal{D}_y\Delta_2|^2 + k_2'|\mathcal{D}_x\Delta_2|^2$$

$$+ k_3(\mathcal{D}_x^*\Delta_1^*\mathcal{D}_y\Delta_2 + c.c.) + k_4(\mathcal{D}_x^*\Delta_2^*\mathcal{D}_y\Delta_1 + c.c.) + ...],\qquad(2.3)$$

where "..." stands for higher order gradient contributions, $\mathcal{D}_i = \partial_i - ieA_i$ is a covariant derivative, $\alpha_j(T) \propto (T - T_{c,j})/T_{c,j}$ where $T_{c,j}$ is the transition temperature of the j-th component of the gap, and the β and k coefficients may be obtained in the expansion and are related to the structure (form factor) of the two superconducting gap components, $f_1(k)$ and $f_2(k)$, as well as the underlying band structure. In particular, it can be shown that all of the β-coefficients are positive, which immediately implies a ground state with (complex) TRSB order parameter, i.e. $\Delta_1^*\Delta_2 + \Delta_1\Delta_2^* = 0$. This is consistent with the maximal condensation energy gain when the two components form a complex superposition to reduce the number of nodes in the superconducting gap.

Furthermore, if the two components are degenerate [42], i.e. if they belong to an irreducible two-dimensional representation of the underlying lattice point group, $T_{c,1} = T_{c,2}$, $\beta_1 = \beta_2$, $k_1 = k_2$ and $k_1' = k_2'$. In general, the form of the action may be deduced on the basis of symmetry considerations. One can check that all of the terms in (2.3) preserve the required global $U(1)$ symmetry. And in the case of two degenerate components, such as for a chiral p-wave on a tetragonal lattice, the D_{4h} point group symmetries are manifest once we impose the relations mentioned above.
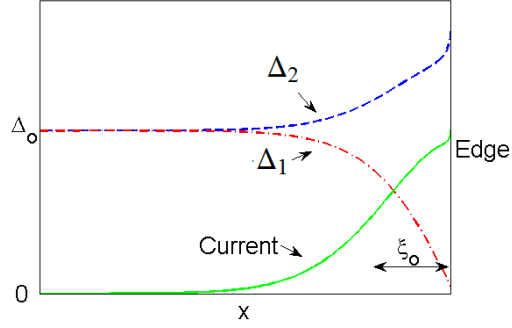
Figure 2.1: The emergence of edge current at a sharp edge. The distinct spatial variations of the two components of chiral order parameter at the edge give rise to a spontaneous current parallel to the edge. The order parameter components are obtained from self-consistent BdG calculations.

Consider an ideal, translation invariant sharp edge at $x = 0$ running along the y-axis. Thus edge current, if any, would flow parallel to y-axis. Since the edge acts as a translational-invariance breaking perturbation along the x-direction, it drives the two order parameter components Δ_1 and Δ_2 to deviate from their bulk values near the edge (Fig.2.1). This is the origin of edge currents in a TRSB superconductor. To see this more explicitly, note that

$$j_y = \frac{1}{e}\frac{\partial S}{\partial A_y} = 2e(k_1'|\Delta_1|^2 + k_2|\Delta_2|^2)A_y + e(k_3 + k_4)(\Delta_1^*\Delta_2 + \Delta_1\Delta_2^*)A_x$$
$$+ 2k_3\mathrm{Im}[(\partial_x\Delta_1^*)\Delta_2] - 2k_4\mathrm{Im}[\Delta_1^*(\partial_x\Delta_2)]. \tag{2.4}$$

The second term vanishes because $\Delta_1^*\Delta_2 + \Delta_1\Delta_2^* = 0$ in a TRSB state. If we ignore screening effects (i.e. dropping the terms proportional to the vector potential), (2.4) becomes,

$$j_y = 2k_3\mathrm{Im}[(\partial_x\Delta_1^*)\Delta_2] - 2k_4\mathrm{Im}[\Delta_1^*(\partial_x\Delta_2)]. \tag{2.5}$$

It now becomes apparent that current along y arises as a response to the order parameter gradients along x (Fig.2.1). In other words, the physics of this Hall-like current response stems from a current-order parameter gradient correlation. Moreover, one can show that the k_3 and k_4 coefficients that govern these correlations as in (2.3) are given by (Appendix A),

$$
\begin{aligned}
k_3 = k_4 &= \frac{\partial^2}{\partial_{q_x}\partial_{q_y}} T \sum_{iw,k} [-G_0(iw,k+q)G_0(-iw,-k)f_1(k)f_2(k)]\,|_{q=0} \\
&\propto \langle v_x(k)v_y(k)f_1(k)f_2(k)\rangle_{FS}
\end{aligned}
\tag{2.6}
$$

where $G_0(iw,k) = 1/(iw - \xi_k)$ is the usual normal state Greens function, w is the fermionic Matsubara frequency, and the bracket in the second line of (2.6) represents a line integral over the Fermi surface.

With $k_3 = k_4$, it is obvious that no current should emerge if the two order parameters exhibit the same spatial variation. Nevertheless, the distinct behaviour of Δ_1 and Δ_2 near an edge is in fact guaranteed by their symmetries. Take the simple chiral p-wave as an sample. Upon a reflection of the two components about the y-axis, Δ_1 (k_x) component changes sign, while Δ_2 (k_y) does not. Thus Δ_1 must fall to zero right at the edge, while Δ_2 may stay the same (in reality it varies due to quartic and higher order couplings with Δ_1 as in (2.3)), as can be seen in Fig.2.1. Since the order parameters vary over a length scale of the coherence length ξ from the edge, the current is also concentrated over the same length scale in the same regime.

In a charged superfluid, screening (Meissner effect) arising from the first term in (2.4) results in an opposite current distributed over a magnetic penetration depth of the surface,[42, 58, 63] leading to vanishing integrated current. The local current distribution is non-vanishing, but its maximum magnitude is reduced by screening.

Thus far, we have seen that edge currents may arise in the presence of spatially varying order parameter components in a TRSB superconductor, and the current thus-generated is dictated by an overall coefficient k_3. This is a very powerful phenomenological criterion. As a simple test, one may examine the edge current at the (10) surface of simple $d_{xy} + is$ and $d_{x^2-y^2} + is$ superconductors on a square lattice, for which we obtain, respectively,

$$k_3 \propto \langle v_x(k)v_y(k) \sin k_x \sin k_y (\cos k_x + \cos k_y) \rangle_{FS} \neq 0, \text{ and}$$

$$k_3 \propto \langle v_x(k)v_y(k)(\cos k_x - \cos k_y)(\cos k_x + \cos k_y) \rangle_{FS} = 0 \qquad (2.7)$$

where we have assumed simple harmonics for the gap structure of the respective components. The vanishing k_3 in the second line can be inferred from symmetry and is independent of the band and gap structures. This immediately suggests vanishing edge current (at this lowest order, see below) for $d_{x^2-y^2} + is$ and finite edge current for $d_{xy} + is$ at a (10) surface, as has been discussed in an earlier study.[59]

To further corroborate the GL theory, we compare in Fig.2.2 the predictions based on the value of k_3 and the numerical BdG calculations of the integrated edge current at a sharp edge of a chiral p-wave model on a square lattice (see the publication in Chapter 5 for an introduction to the self-consistent numerical BdG calculations). It is not difficult to see the qualitative agreement between the two throughout the entire range of chemical potentials relevant to the tight binding band structures considered.

It is also easy to see from (2.6) that k_3 may be generically smaller for TRSB superconductors whose gap components change sign more frequently across the Fermi surface. This suggests a mechanism for reducing the edge current in realistic models of a chiral p-wave superconductor, as will be elaborated in our publications to be presented in Ch.4.
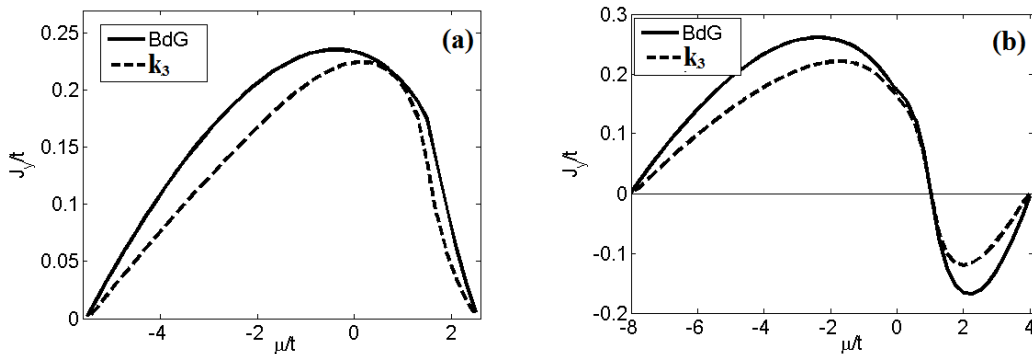
Figure 2.2: Comparison between the total edge current obtained from GL theory and numerical self-consistent BdG calculations on a square lattice chiral p-wave model with $\Delta_k = \Delta_0(\sin k_x + i \sin k_y)$. The tight-binding single particle spectrum is given by $\xi_k = -2t(\cos k_x + \cos k_y) - 4t' \cos k_x \cos k_y - \mu$, with $t'/t = 0.3$ in (a) and $t'/t = 1$ in (b).

Finally, it should be stressed that (2.4) and (2.5) only constitute the lowest order contribution to the current, which vanishes when k_3 is zero. However, higher order gradient terms in the effective action (2.3), such as $(\mathcal{D}_x^3 \Delta_1)^* \mathcal{D}_y \Delta_2$, may not vanish. These additional contributions can generate small yet non-vanishing local current distribution, as has been found in a recent study of edge currents in non-p-wave chiral superfluids[85]. Furthermore, due to the reduced lattice symmetry, subdominant superconducting components may be induced at the boundary, which might also lead to finite local current.

2.3 Semiclassical theories

Here we turn to a semiclassical perspective which provides a more intuitive picture of the edge current in a TRSB superconductor.

By analytically solving the BdG equation in the presence of an ideal sharp edge, the energy dispersion and wavefunctions of the quasi-particle states, including those of the edge modes if present, may be obtained. These analyses are most easily done assuming constant amplitude of the order parameter components at the boundary. Note this is not in contradiction with
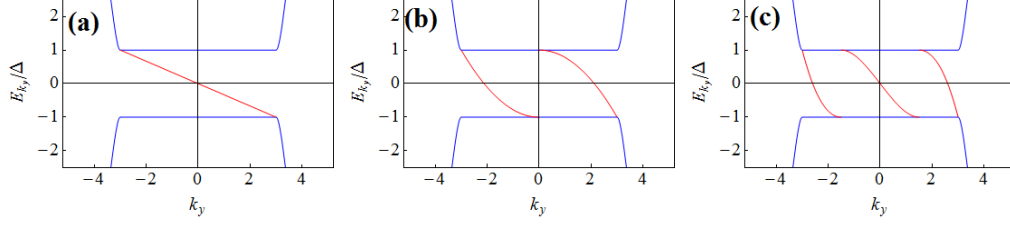
Figure 2.3: Edge dispersion of chiral p-, d- and f-wave superconductors, or Chern insulators with Chern number $C = 1, 2, 3$.

the Ginzburg-Landau argument in the previous section, as the energy spectrum thus obtained corresponds exactly to that in the presence of realistic order parameter profiles at the edge, due to the absence of spectral flow (see Chapter 4). The edge current can be subsequently evaluated. For illustrative purpose, we focus below on the topologically non-trivial chiral superconductors and investigate the contribution from their edge states alone. Earlier studies specific to chiral p-wave can be found in Refs [59, 48, 57]. For more details of our analyses, see Appendix B. The BdG Hamiltonian for a chiral superfluid is given by,

$$\hat{H}_k = \psi_k^\dagger \begin{pmatrix} \xi_k & \Delta(\frac{k_x+ik_y}{k_F})^m \\ \Delta^*(\frac{k_x-ik_y}{k_F})^m & -\xi_{-k} \end{pmatrix} \psi_k \tag{2.8}$$

where the Nambu spinor $\psi_k = (c_{k,\sigma}^\dagger, c_{-k,\sigma'})^T$, and m gives the angular momentum of the Cooper pairs. In inversion symmetric case, $\xi_k = \xi_{-k}$, the same form of Hamiltonian matrix also describes a Chern insulator[86] with the same Chern number m, but with a different spinor in particle-particle basis, $\psi_k = (c_{a,k}, c_{b,k})^T$. For convenience, we focus here on the continuum limit where $\xi_k \sim k^2$.

Despite the topological equivalence and the same edge state dispersion at an open boundary (Fig.2.3), there exists a crucial distinction between a chiral superconductor and a Chern insulator resultant from the $U(1)$ symmetry breaking of a chiral superfluid. More concretely,

the current operator is $j_k = \partial_k \hat{H}_k$ for a Chern insulator, while $j_k = \partial_k \xi_k \sigma_0$ for a chiral super-conductor (σ_0 is a 2×2 identity matrix). This has important consequences the current carried by the individual quasi-particle states.

In a Chern insulator, the current carried by a state is given by its group velocity $\partial_k E_k$. This implies the topological protection of the edge current, as the total current would then be entirely determined by the number and chirality of the edge dispersion and is independent of the details of the edge spectrum. More concretely, $J_{\text{tot}} \propto C\Delta_0/2$ where Δ_0 is the size of the gap. However, an edge state in a chiral superfluid carries a current that is given by $\sim \partial_k \xi_k = k/m^*$, where m^* is the effective mass. A semiclassical understanding of this is the following. The edge mode of a chiral superconductor is an equal-amplitude linear superposition of particle and hole components, i.e. $\gamma_k = \frac{1}{\sqrt{2}}(c_{k,\sigma}^\dagger + i c_{-k,\sigma'})$. Thus charge current is oblivious to the group velocity of this charge-neutral mode. Meanwhile, the opposite motion of the constituting electron and hole components, one with momentum k and the other $-k$, provides a net flow of charge current. Combined with the energy and momentum distributions of the edge modes as in Fig 2.3, a striking difference between p-wave and non-p-wave chiral superconducting ground states immediately becomes obvious: in the former, all of the individual occupied chiral modes carry current that flows in the same direction, while in the latter, the contributions from multiple branches of occupied states can cancel each other. Thus the edge state contribution is significantly smaller for non-p-wave chiral superconductors–a somewhat counterintuitive conclusion which otherwise follows naturally from our semiclassical reasoning.

One can further show that, due to the symmetry properties peculiar to the continuum limiting cases, the integrated edge state contribution vanishes exactly for non-p-wave pairings. The total bulk state contribution can also be analytically evaluated and shown to be identically
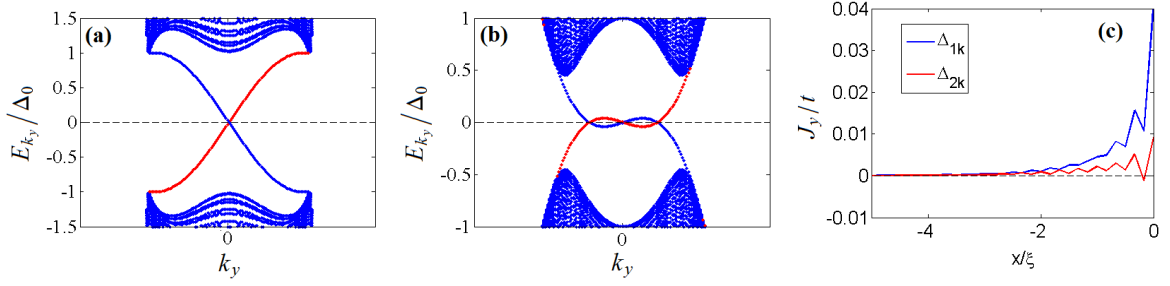
Figure 2.4: Low energy dispersion (a,b) and numerical BdG edge current distribution (c) for two chiral p-wave models on a square lattice, with periodic boundary along y and open boundaries in x-direction. The modes plotted in red are the edge states belonging to one of the edges. The single-particle tight-binding dispersion reads $\xi_k = -2t(\cos k_x + \cos k_y) - 4t' \cos k_x \cos k_y - \mu$, with $\mu = -1.5t$ in both (a) and (b). The superconducting gap function is $\Delta_{1k} = \Delta_0(\sin k_x + i \sin k_y)$ in (a) and $\Delta_{2k} = \Delta_0(\sin k_x \cos k_y + i \cos k_x \sin k_y)$ in (b). In (c), the x-coordinate is measured with respect to a length scale defined by $\xi = v_F/\Delta_0$ with $v_F \simeq 1$ and $\Delta_0 = 0.2t$.

vanishing (see Appendix B). Thus the total integrated current also vanishes [87]. These results will be elaborated in Ch.3.

Away from the continuum limit in lattice models, the current can be non-zero for non-p-wave chiral pairing, but would still be smaller than for a simple chiral p-wave. That the integrated current need not vanish may be understood by the fact that the locations of the zero-crossings of the chiral edge dispersion in lattice models are constrained by lattice symmetries, thus the currents carried by the multiple chiral edge branches may not exactly cancel as they did in the continuum limit. In addition, for anisotropic chiral p-wave models, additional zero-energy-crossings of the edge dispersion may also occur, introducing cancellations between the occupied edge states carrying opposite momenta, thus reducing the overall spontaneous current (see Fig.2.4) [88, 89], consistent with the discussions in the previous section.

Chapter 3

Vanishing edge currents in non-p-wave topological chiral superconductors

3.1 Preface   The edge current and orbital angular momentum of chiral p-wave superfluids have been studied extensively, largely due to the experimental realization of chiral p-wave superfluidity in ^{3}He[33, 36, 37] and potential relevance to Sr_2RuO_4. Here, we take one small step further by studying the edge current and orbital angular momentum in chiral superconductors with higher angular momentum Cooper pairing. A intuitive and obvious expectation is that, the total edge current of a chiral d-wave superconductor is twice as large as that of a chiral p-wave since the angular momentum per Cooper pair is twice as large. However, this turns out to be incorrect.

Our conclusion is threefold: 1) while the integrated edge current is non-zero for chiral p-wave, it vanishes for all non-p-wave chiral superconductors in the continuum limit; This also implies vanishing total orbital angular momentum when the latter is confined to a finite-size disk; 2) the integrated edge current, and hence orbital angular momentum, may be recovered for non-p-wave chiral superconductors in the presence of a soft edge where the Cooper pair

density varies slowly; 3) for a non-p-wave chiral superconductor on a lattice, the edge current can be nonzero but is generically smaller compared to that of a chiral p-wave.

These results are verified with numerical BdG calculations and are in agreement with the phenomenological and semiclassical theories presented in the previous chapter, as well as a concurrent study using a different analysis[90]. A few subsequent works have also substantiated and elaborated on this study[66, 85, 91, 92]. Our conclusions hold meaningful implications for the orbital angular momentum problem in ^{3}He-A[33, 37, 36] and the edge current problem in putative or proposed chiral superconductors such as Sr_2RuO_4, UPt_3[93], $SrPtAs$[94], $Na_xCoO4 \cdot yH_2O$[95], dopped graphene[96], etc.

3.2 Publication

Vanishing edge currents in non-p-wave topological chiral superconductors

Wen Huang,[1] Edward Taylor,[1] and Catherine Kallin[1,2]

[1]*Department of Physics and Astronomy, McMaster University, Hamilton, Ontario, Canada L8S 4M1*

[2]*Canadian Institute for Advanced Research, Toronto, Ontario, Canada M5G 1Z8*

The edge currents of two-dimensional topological chiral superconductors with nonzero Cooper pair angular momentum—e.g., chiral p-, d-, and f-wave superconductivity—are studied. Bogoliubov–de Gennes and Ginzburg-Landau calculations are used to show that in the continuum limit, *only* chiral p-wave states have a nonzero edge current. Outside this limit, when lattice effects become important, edge currents in non-p-wave superconductors are comparatively smaller, but can be nonzero. Using Ginzburg-Landau theory, a simple criterion is derived for when edge currents vanish for non-p-wave chiral superconductivity on a lattice. The implications of our results for putative chiral superconductors such as Sr_2RuO_4 and UPt_3 are discussed.

I. INTRODUCTION

Two-dimensional topological chiral superconductors break time-reversal symmetry by virtue of the fact that the Cooper pairs have nonzero orbital angular momentum. For simple orbital eigenstates of the (z component of the three-dimensional) angular momentum operator such as p-, d-, and f-wave states, the Cooper pairs each carry $m\hbar$ of angular momentum, with nonzero integer magnetic quantum numbers m. In a finite sample of such a superconductor (for convenience, in this paper we will not distinguish between chiral superconductors and neutral chiral superfluids such as ^{3}He, using "superconductor" to describe both), this Cooper pair orbital angular momentum is expected to give rise to a spontaneous edge current and related to this, a nonzero *total* angular momentum.

For p-wave superconductors, both the edge current and total angular momentum have been studied extensively (see, e.g., Refs. [1–5]), largely due to the fact the chiral p-wave A phase of ^{3}He is the only system which is known to be definitely chiral. At the same time, the perovskite superconductor Sr_2RuO_4 is widely believed to be chiral p wave [6–8], although magnetic fields consistent with the expected edge current have yet to be detected [9–11]. This last fact in particular has generated considerable interest in the question of what exactly is the relationship between topological chiral superconductivity and edge currents. Although it can be strongly suppressed by disorder [5,12] as well as gap anisotropy and band effects [13], the edge current and total angular momentum of a chiral p-wave superconductor are generically *large*, the latter for instance being $L_z = N\hbar/2$ [4,14] in the continuum limit for an ideal surface at $T = 0$, where N is the total number of fermions.

In this paper, we generalize previous studies of the edge current in chiral p- and d-wave superconductors [15–18]. In addition to being a problem of intrinsic theoretical interest, giving greater insight into the nature of the edge current in chiral p-wave superconductors for instance, this work will be relevant in the quest to find non-p-wave chiral superconductors such as the possibly chiral f-wave superconductor UPt_3 [19,20]. In contrast to the generically large edge current in chiral p-wave superconductivity, we find that the edge current in states with higher orbital Cooper pair angular momentum

can vanish, depending on details of the lattice. All our results are for unscreened currents.

Drawing on analytic semiclassical Bogoliubov–de Gennes (BdG) and Ginzburg-Landau (GL) calculations for continuum systems, we show that, amongst chiral pairing states that are eigenstates of the angular momentum operator, only chiral-p superconductors have a nonzero edge current. Our results extend to three-dimensional (3D) superconductors by considering eigenstates of the z-component $\hat{L}_z$ of the orbital angular momentum operator: only states with magnetic quantum number $m = 1$ give rise to a nonzero edge current. This means, e.g., that the 3D f-wave state $k_z^2(k_x + ik_y)$ with $m = 1$ has an edge current, but the $m = 2$ state $k_z[(k_x^2 - k_y^2) \pm 2ik_xk_y]$ does not. The latter is the continuum analog of a possible order parameter for UPt_3.

Turning to lattice models, numerical BdG and GL calculations are used to understand how these results carry over from the continuum. Away from the continuum limit, the edge current along axes of high symmetry can be nonzero even for non-p-wave chiral states, although for all cases studied, it is reduced as compared to that for chiral p wave on a square lattice. In some cases, such as chiral f wave on a triangular lattice, we find that the integrated current is extremely small. In all cases where we find such a small integrated current, the local current oscillates over a small length scale comparable to the lattice spacing with an amplitude that decreases linearly with Δ_0/E_F [18] and hence, vanishes in the weak-coupling limit. A general condition for which the edge current vanishes consistent with our BdG results is derived within GL theory.

We start in Sec. II by presenting our semiclassical analysis for systems in the continuum limit. The implications of our results for the problem of the total angular momentum are discussed in Sec. III. There, a Chern-Simons-like [4,13,21,22] expression for the current is also discussed in connection with the possibility of a "soft" edge, where the density vanishes slowly as compared to the coherence length. Apart from this section, and also a brief discussion given in Sec. V, we leave implicit that all our results are for a sharp edge, where the density vanishes over a distance on the order of the mean interparticle spacing k_F^{-1}.

Turning our focus to lattice models, in Sec. IV, results are given for numerical BdG calculations of the edge current for

WEN HUANG, EDWARD TAYLOR, AND CATHERINE KALLIN

chiral p-, d-, and f-wave order parameters in some representative lattice systems: $p_x + ip_y$ on a square lattice, $d_{x^2-y^2} + id_{xy}$ on square and triangular lattices, and $f_{x(x^2-3y^2)} + if_{y(3x^2-y^2)}$ on a triangular lattice. In Sec. V, we reproduce our continuum as well as numerical lattice BdG results using GL theory. A summary of our results is given in Sec. VI along with a discussion of their relevance for systems such as Sr$_2$RuO$_4$ and UPt$_3$, which have been proposed as candidate chiral superconductors.

II. EDGE CURRENT IN THE CONTINUUM LIMIT OF CHIRAL SUPERCONDUCTORS

We begin by using semiclassical Bogoliubov–de Gennes calculations to understand properties of the edge current for an edge in two-dimensional continuum chiral superconductors. For continuum systems, the Cooper pair eigenstates

$$\Delta_{\mathbf{k}} = \Delta_0 \left(\frac{k_x + ik_y}{k_F}\right)^m \equiv \Delta_0 (k/k_F)^m e^{im\theta}, \quad m = 1,2,\dots \tag{1}$$

of the 2D angular momentum operator are characterized by the magnetic quantum number m. θ is defined such that $\mathbf{k} = k[\cos\theta, \sin\theta]$. Not only does the magnetic quantum number give the angular momentum $m\hbar$ per Cooper pair, it also is equal to the Chern number (or skyrmion number of the BdG Hamiltonian) [23],

$$m = C \equiv \frac{1}{4\pi} \int d^2 k \, \hat{h} \cdot \left(\partial_{k_x}\hat{h} \times \partial_{k_y}\hat{h}\right), \tag{2}$$

which counts the number of zero-energy edge modes. Here $\vec{h} = \{\text{Re}[\Delta_{\mathbf{k}}], -\text{Im}[\Delta_{\mathbf{k}}], \xi_{\mathbf{k}}\}$ and $\hat{h} = \vec{h}/|\vec{h}|$, with $\xi_{\mathbf{k}} \equiv \epsilon(\mathbf{k}) - \mu$ the single-particle dispersion.

The Bogoliubov–de Gennes (BdG) equation for the order parameter (1) is

$$\begin{bmatrix} h_0 & \Delta_0\left(\frac{k}{k_F}\right)^m e^{im\theta} \\ \Delta_0\left(\frac{k}{k_F}\right)^m e^{-im\theta} & -h_0^* \end{bmatrix} \begin{bmatrix} u \\ v \end{bmatrix} = E \begin{bmatrix} u \\ v \end{bmatrix}, \tag{3}$$

where $h_0 \equiv -\frac{\hbar^2}{2m^*}\nabla^2 - \mu$ and we have used m^* to denote the fermion mass to avoid confusion with the magnetic quantum number. We seek solutions of (3) for the situation where there is an edge parallel to the x axis, at $y = 0$. This edge is implemented using the boundary condition $u(y=0) = v(y=0) = 0$.

A spontaneous current arises at an edge due to both current-carrying Andreev-scattered edge states as well as the reflection of continuum states [4]. The corresponding solutions

$$\hat{\Psi} = \sum_{\sigma=\pm} \sigma \begin{bmatrix} a_\sigma(y) \\ b_\sigma(y) \end{bmatrix} e^{ik_F x \cos\theta + i\sigma k_F y \sin\theta} \tag{4}$$

of the BdG equations are thus completely parametrized by the incident angle θ; see Fig. 1. In (4), the $\sigma = \pm$ components of the solution represent the transmitted (specular reflection) and reflected (Andreev reflection) solutions, respectively. Note that for our chosen geometry, this angle is the same as the one that enters the order parameter (1). The minus sign ($\sigma = -1$) attached to the reflected solution means that the vanishing of the wave function at the edge becomes $\hat{\Psi}_-(0) = \hat{\Psi}_+(0)$, where $\hat{\Psi}_\sigma^\dagger \equiv [a_\sigma, b_\sigma]$. The current density *per spin component*
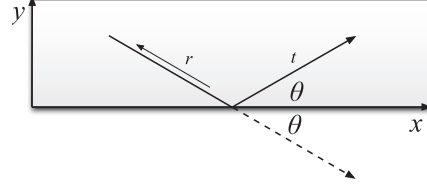
FIG. 1. Specular (t) and Andreev (r) reflection of a quasiparticle off an ideal edge at $y = 0$. Adapted from Ref. [4].

corresponding to this solution is thus

$$j_x(y > 0) = \frac{\hbar}{4m^* i}[\hat{\Psi}^\dagger \partial_x \hat{\Psi} - (\partial_x \hat{\Psi}^\dagger)\hat{\Psi}]$$
$$= \frac{\hbar k_F \cos\theta}{2m^*} \sum_{\sigma=\pm} \hat{\Psi}_\sigma^\dagger \hat{\Psi}_\sigma. \tag{5}$$

As noted in Ref. [4], the seemingly extra factor of $1/2$ in this expression is needed to compensate the double counting in the particle-hole basis spanned by $\hat{\Psi}$.

To solve the BdG equations, (3) and (4), we adopt the elegant approach used by Stone and Roy [4] to solve the $m = 1$ problem and map these equations onto the one-dimensional "twisted mass" Dirac problem. The density $\sum_\sigma \hat{\Psi}_\sigma^\dagger \hat{\Psi}_\sigma$ of quasiparticle states receives contributions from the bound edge state as well as the "charge" $Q_m(\theta)$ arising from the phase-shifted bulk continuum states that accumulates at the edge. Each bound state has unit normalization and thus its contribution to the integrated current is obtained by integrating (5) over the values of θ for which the edge mode spectrum is negative (i.e., occupied):

$$J_{\text{edge}} = \int_{\text{occupied}} \frac{k_F \sin\theta d\theta}{2\pi} \left(\frac{\hbar k_F \cos\theta}{2m^*}\right). \tag{6}$$

The contribution to the current from bulk continuum states is similarly

$$J_{\text{bulk}} = \int_0^\pi \frac{k_F \sin\theta d\theta}{2\pi} Q_m(\theta) \left(\frac{\hbar k_F \cos\theta}{2m^*}\right). \tag{7}$$

In Appendix A we use the solutions of the twisted-mass Dirac problem to show that the edge mode spectrum and accumulated charge are given by piecewise functions

$$E^{(0)} = (-1)^j \Delta_0 \cos(m\theta) \text{ for } \frac{(j-1)\pi}{m} \leqslant \theta < \frac{j\pi}{m} \tag{8}$$

and

$$Q_m(\theta) = \frac{m\theta}{\pi} - j \text{ for } \frac{(j-1)\pi}{m} \leqslant \theta < \frac{j\pi}{m}, \tag{9}$$

with $j = 1 \dots m$. The edge mode dispersion means that the occupied edge states correspond to incident angles $\theta \in [0, \pi/2m], [\pi/m, 3\pi/2m], \dots, [(m-1)\pi/m, (m-1/2)\pi/m]$, and (6) becomes

$$J_{\text{edge}} = \frac{\hbar k_F^2}{16\pi m^*} \sum_{j=1}^m \left[\cos\frac{(2j-2)\pi}{m} - \cos\frac{(2j-1)\pi}{m}\right]. \tag{10}$$

Using (9) in (7), the bulk state contribution to the current is

$$J_{\text{bulk}} = -\frac{\hbar k_F^2}{4\pi m^*} \sum_{j=1}^{m} \left[\frac{m}{8\pi} \left(\sin \frac{(2j-2)\pi}{m} - \sin \frac{2j\pi}{m} \right) \right.$$
$$\left. + \frac{1}{4} \cos \frac{(2j-2)\pi}{m} \right]. \quad (11)$$

For chiral p wave ($m = 1$), the bulk contribution is half in magnitude as the current carried by the chiral edge states, and flows in the opposite direction: $J_{\text{edge}} = \hbar k_F^2/(8\pi m^*)$ and $J_{\text{bulk}} = -\hbar k_F^2/(16\pi m^*)$ [4]. The total edge current per spin component can thus be written as $J = n\hbar/4m^*$, where $n = k_F^2/4\pi$ is the number density per spin component. This value is consistent with numerical BdG calculations in the continuum limit of lattice models [13] (for simple lattice models at least, iterating BdG to full self-consistency has negligible impact on our results). It is also the edge current needed to produce a macroscopic angular momentum $N\hbar/2$ for N fermions in a disk [4] (see below).

On the other hand, the edge state and continuum state contributions (10) and (11) vanish independently *for all* $m > 1$, a fact that can be proved by induction. Thus the total edge current is identically zero for any chiral superconductor with Cooper pair angular momentum $>\hbar$. Note that although multiple chiral edge branches with the same chirality exist for $m > 1$, the contributions to the current exactly cancel among those chiral branches. In the continuum at least, p wave is special [13]! As noted in the Introduction, this result extends to 3D superconductors by considering eigenstates of the z component $\hat{L}_z$ of the orbital angular momentum operator: only states with magnetic quantum number $m = 1$ give rise to a nonzero edge current.

III. TOTAL ANGULAR MOMENTUM

Before discussing how the continuum limit results carry over to lattice models of chiral superconductivity, we briefly touch on a problem of some historic interest, namely the angular momentum carried by a disk of a neutral chiral superfluid [24]. The fact that the edge current vanishes for $m > 1$ Cooper pair states means that a superfluid of N fermions arising from these states will not have a macroscopic total angular momentum

$$L_z = \frac{N\hbar m}{2}. \quad (12)$$

Such a macroscopic angular momentum would arise if there is a local current density [4,5] $j(x) \sim Nmv_F\Delta_0 \exp(-x/\xi_0)$ confined within a coherence length of the edge at weak coupling. It is moreover the expected result in the strong-coupling "BEC limit" [2,25], where the number of Cooper pairs (i.e., the condensate occupation) asymptotes to $N/2$. For p-wave pairing, the edge current indeed gives rise to a total angular momentum given by (12) for both an ideal sharp edge [4,5] as well as a soft one [14]. For higher-angular momentum pairing, however, our BdG results suggest that (12) is not true in general.

We define the total angular momentum of a disk of radius R as

$$L_z = \int_{r \leqslant R} d\mathbf{r} m^* (\mathbf{r} \times \mathbf{j})_z. \quad (13)$$

Recall that m^* is the fermion mass. A nonzero local current $\mathbf{j}(\mathbf{r})$ only arises if the density or order parameters components vary in space. Thus, for a disk having a sharp edge, wherein the density vanishes over an atomic scale at the edge, the only current is the edge current we have discussed in previous sections. For higher-angular momentum Cooper pair states with $m > 1$, the total angular momentum is zero.

At the same time, if the edge is softened, such that the density vanishes over a length scale much longer than the BCS coherence length, the local edge current per spin component is given by [4,13,21,22]

$$\mathbf{j}(\mathbf{r}) = -\frac{\hbar C}{8\pi} (\hat{z} \times \nabla) A_0(\mathbf{r}). \quad (14)$$

Here $A_0(\mathbf{r})$ is an external potential that gives rise to the slow density variation and C is the Chern number (2) which, as noted earlier, is equal to the magnetic quantum number m in continuum systems for Cooper pair states that are eigenstates of the angular momentum. We have confirmed using numerical BdG (not shown) that the current is restored as the edge is softened, in agreement with the lattice discretized form of (14), with $\partial_x A_0(x) \to A_0(x_{i+1}) - A_0(x_i)$. Some discussion of the origin of this "Chern-Simons-like" contribution is given in Sec. V.

Using (14) in (13), for a rotationally invariant potential $A_0(\mathbf{r}) = A_0(r)$, and using the equilibrium condition $\partial_r A_0(r) = (\partial \mu/\partial n)\partial_r n(r)$ with $\mu = 2\pi n/m^*$, the total angular momentum is

$$L_z = -\frac{\hbar C m^*}{4} \int_0^R dr r^2 (\partial \mu/\partial n) \partial_r n(r) = \frac{N\hbar C}{2}, \quad (15)$$

where $N = 2\pi \int_0^R dr r n(r)$. Thus, equating the Chern number with the magnetic quantum number m, when the density varies slowly, one recovers (12) for *all* cases with nonzero Cooper pair angular momentum. It is only when the density varies sharply that the total angular momentum vanishes for all states except p wave.

We note in passing that (14) is equivalent to the "intrinsic pair angular momentum" identified by Mermin and Muzikar, arising from the orbital angular momentum of the Cooper pairs. It indeed conspires to produce the expected macroscopic angular momentum (12) but only in general when the density varies slowly as compared to the BCS coherence length ξ_0. Such a situation can arise, for instance, in an ultracold atomic gas chiral superfluid confined in harmonic traps [14].

IV. EDGE CURRENT FOR LATTICE MODELS

We now turn to the question of whether our central continuum-limit result—the vanishing of the edge current in non-p-wave chiral superconductors—survives outside of this limit. Some indication of the answer can be found in the literature, which has largely focused on the possibility of chiral d-wave superconductivity in the cuprates [15–17] but also, more recently, chiral d-wave order in graphene [26–28]

and other materials [18,29,30]. A small (but nonzero) edge current along the [11] surface was reported in Ref. [16] for chiral $d_{x^2-y^2} + id_{xy}$ superconductivity on a square lattice. It is unclear, however, whether the calculation reported there allowed for the possibility that $d + is$ order (expected to produce a nonzero edge current [16,17]) develops near the surface. In lattices with hexagonal symmetry, away from the continuum limit, Ref. [18] finds a finite but small local current. Nonzero edge currents are also found for chiral d-wave superconductivity on a honeycomb lattice [28].

Here we expand on these results, presenting numerical BdG calculations of the unscreened edge current in a few representative one-band models: chiral p and d wave on a square lattice, as well as chiral f and d wave on a triangular lattice. The last has been proposed as a possible superconducting state in $Na_xCoO_2 \cdot yH_2O$ [29] and SrPtAs [30]. In contrast to p-wave pairing which has a large edge current along the axes of a square lattice, we find that the integrated edge current along the same axes is very small for $d_{x^2-y^2} + id_{xy}$ order, consistent with previous work [17]. The edge current is substantial for this state when placed on a triangular lattice, however. Considering chiral f-wave pairing on a triangular lattice, we find a very small integrated current. In all cases where we find such a small integrated current, the local current varies rapidly over a scale $\sim k_F^{-1}$ with amplitude decaying linearly with Δ_0/E_F, similar to that in Ref. [18]. We thus take our results to be indicative of a vanishing edge current in the weak-coupling limit of these cases.

Our BdG calculations are carried out in the standard way (see, e.g., Ref. [31] for details) using a strip geometry, with edges at $y = 0$ and $y = 300$ (in units where the lattice spacing is 1), and periodic boundary conditions imposed along x. Iterations are carried out to self-consistency. Although subdominant orders can often be induced at the surface, we ignore these for simplicity. For chiral $p_x + ip_y$ and $d_{x^2-y^2} + id_{xy}$ pairing on a square lattice, we use $\Delta_{\mathbf{k}} = \Delta_0(\sin k_x + i \sin k_y)$ and $\Delta_{\mathbf{k}} = \Delta_{01}(\cos k_x - \cos k_y) + i \Delta_{02} \sin k_x \sin k_y$, respectively. These are allowed by the underlying tetragonal point group (D_{4h}) symmetry of the lattice; they reduce to $(k_x + ik_y)/k_F$ and $(k_x + ik_y)^2/k_F^2$ in the continuum limit. Note the two d-wave components are in general nondegenerate on a square lattice and $\Delta_{01} \neq \Delta_{02}$. Using the same interaction strength for both channels, however, we find the d_{xy} component to be too small to reliably carry out calculations. To avoid this difficulty, we tune the interactions to give $\Delta_{01} \simeq \Delta_{02}$. Changing these values does not affect our conclusion in cases where the edge current vanishes, however. In addition, the numerical calculations we present are for systems with one electronlike Fermi surface around the Γ point. However, we have also done calculations for other scenarios and the discussion and conclusions which follow apply equally well to all cases.

The local currents near the edge at $y = 0$ for these two models are shown in Fig. 2. The local current for chiral d wave oscillates with an amplitude that decays linearly with Δ_0 [18]. In units of the lattice hopping t, the integrated current shown in Fig. 2 is $J \simeq 0.006t$, as compared to $J \simeq 0.12t$ for p wave, and we expect that in the $\Delta_0 \ll t$ limit, the integrated current vanishes for chiral d wave on a square lattice. This is true despite the fact that there are two chiral

FIG. 2. Spatial dependence of the local edge current $j_x(y)$ for chiral p- and d-wave order parameters on a square lattice with hopping t. The edge is at $y = 0$ and the local currents extend over several coherence lengths $\xi_0 \equiv t/\Delta_0 \sim 5$ (in units of the lattice spacing). Calculations are done using $\mu = -t$ in conjunction with the order parameters described in the text for a strip of width 300 lattice sites along y and with periodic boundary conditions along x.

zero-energy (Majorana) bound-state modes present on each edge; see Fig. 3. In fact, for the contribution to the edge current from the chiral edge modes, it is precisely because there is more than one edge state that the contribution vanishes as a result of canceling contributions. As much is evident from the continuum-limiting expressions (8) and (10) (we note that the former well describes the in-gap dispersion shown in Fig. 3 and also the spectra shown in Fig. 4 for d- and f-wave pairing on a triangular lattice).

For the triangular lattice, the chiral d-wave order takes the form of $\Delta_{\mathbf{k}} = \Delta_0[\cos k_x - \cos(\sqrt{3}k_y/2)\cos(k_x/2)] + i\Delta_0\sqrt{3}\sin(\sqrt{3}k_y/2)\sin(k_x/2)$, which also reduces to $(k_x + ik_y)^2$ in the continuum limit. A chiral f-wave state of the form $\Delta_{\mathbf{k}} = \Delta_{01}[\sin(2k_x) - 2\cos(\sqrt{3}k_y)\sin k_x] + i\Delta_{02}[2\sin(\frac{\sqrt{3}}{2}k_y)\cos(\frac{3}{2}k_x) - \sin(\sqrt{3}k_y)]$ can be realized on a triangular lattice with second and third neighbor odd-parity pairing. This gap function reduces to $(k_x + ik_y)^3$ in the
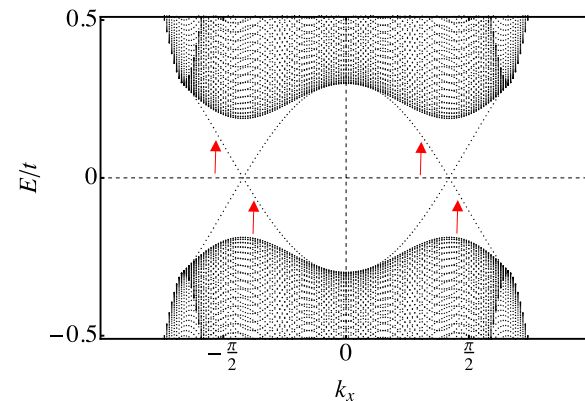
FIG. 3. (Color online) Low-energy dispersion of a one-band chiral d-wave model on a square lattice calculated using the same parameters used in Fig. 2. The arrows point to the chiral edge modes belonging to the same edge.
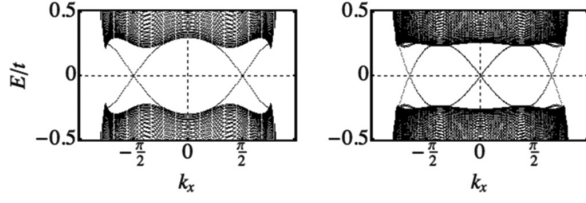
FIG. 4. Edge dispersion of the chiral d- and f-wave models on a triangular lattice with the same parameters used in Fig. 5.

continuum limit where the two components become degenerate. Outside the continuum limit, the two order-parameter components are not in general degenerate and $\Delta_{01} \neq \Delta_{02}$. As with d wave on a square lattice, we tune the interactions such that $\Delta_{01} \simeq \Delta_{02}$. In Fig. 5 we plot the edge currents of the chiral d- and f-wave models on a triangular lattice with an edge along one side of the triangles. For comparison, we also plot the edge current of a chiral p-wave superconductor, with $\Delta_{\mathbf{k}} = \Delta_0\{\sin(\sqrt{3}k_y/2)\cos(k_x/2) + \frac{i}{\sqrt{3}}[\sin k_x + \cos(\sqrt{3}k_y/2)\sin(k_x/2)]\}$. As with d wave, the two order-parameter components are degenerate on a triangular lattice. While the p- and d-wave models do not yield vanishing edge currents, the local edge current for the chiral f-wave state oscillates rapidly about zero, integrating to a small value, $J \simeq 0.017t$, much smaller than the corresponding value ($J \simeq 0.15t$) for p wave and about half the size of the value ($J \simeq 0.036t$) for d wave. As with our chiral d-wave results on a square lattice, we interpret this result as meaning that the edge current vanishes in the weak-coupling limit for chiral f wave on a triangular lattice.

Even though the edge current for chiral d wave on a triangular lattice is nonzero, it is smaller than that for p wave. Moreover, consistent with our semiclassical analysis and also Ref. [18], it vanishes in the weak-coupling, continuum limit, as μ approaches the bottom of the band.
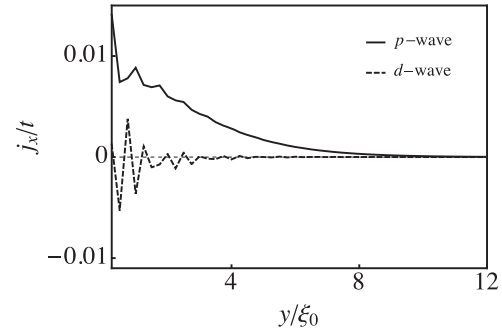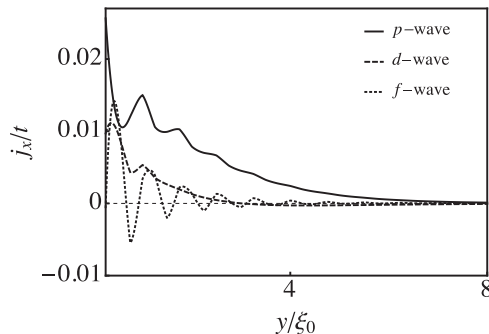

FIG. 5. Spatial dependence of the local edge current $j_x(y)$ for chiral p-, d-, and f-wave order parameters on a triangular lattice with hopping t. Calculations are done using $\mu = 0$ and $\Delta_0 \approx 0.2t$ ($\xi_0 \equiv t/\Delta_0 \approx 5$) in conjunction with the order parameters described in the text for a strip with the same size as that used for the square lattice calculations.

V. GINZBURG-LANDAU THEORY

We now seek insight into our BdG results from Ginzburg-Landau (GL) theory. The current arises from gradient terms in the GL free-energy density. For a system with two (complex) component order parameters ψ_1 and ψ_2, ignoring the possibility of an external potential, $A_0(\mathbf{r}) = 0$, the terms responsible for the current are [32]

$$f_{\mathrm{GL}} = k_3(\partial_x \psi_1^* \partial_y \psi_2 + \text{c.c.}) + k_4(\partial_y \psi_1^* \partial_x \psi_2 + \text{c.c.}) + \cdots,$$
(16)

where the ellipsis denotes higher-order terms. Making contact with our microscopic results, the complex order parameter is

$$[\psi_1(\mathbf{r}), \psi_2(\mathbf{r})] \equiv [\Delta_{01}(\mathbf{r}), i\,\Delta_{02}(\mathbf{r})]\exp[i\theta(\mathbf{r})],$$
(17)

where $\theta(\mathbf{r})$ is the U(1) phase and $\Delta_{01}(\mathbf{r})$ and $\Delta_{02}(\mathbf{r})$ are the purely real, spatially varying amplitudes, reducing to the bulk values Δ_{01} and Δ_{02} away from an external potential and far from the edge.

We emphasize that even though the notation of (16) is usually reserved for systems with tetragonal symmetry (see, e.g., Table VII in Ref. [32]), one can always construct an expression of the form given by (16) and it is valid for systems with arbitrary lattice symmetry. Adopting the notation in Ref. [32] for instance, our k_3 and k_4 are equal to K_3 and K_4 for a tetragonal lattice; for a hexagonal lattice, terms of the form (16) also arise however one instead has $k_3 = K_1 - K_3$ and $k_4 = -K_2 + K_3$. Moreover, to leading order in the gap amplitudes Δ_0, k_3 and k_4 are equal [33].

Using (17), the μ component of the current (where it appears as a Cartesian index, $\mu, \nu = 1, 2$ denote the x, y axes) is

$$j_\mu = \frac{\partial f_{\mathrm{GL}}}{\partial(\partial_\mu \theta)} = k_3 \epsilon_{\mu\nu}(\Delta_{0\mu}\partial_\nu\Delta_{0\nu} - \Delta_{0\nu}\partial_\nu\Delta_{0\mu}),$$
(18)

where $\epsilon_{\mu\nu}$ is the 2D Levi-Civita symbol. Hence, a vanishing edge current along one of the crystalline axes is associated with the vanishing of the k_3 GL coefficient.

As in Ref. [33], the GL expression (18) serves as an alternative and more phenomenological description of the BdG current. Although (18) is only rigorously valid close to T_c and does not give the exact current at low temperatures, it has been well established that GL theory provides a reliable qualitative description of the current in BdG calculations [31,33,34], and this is also confirmed here.

The gradient terms (16) in the GL free energy density lead to the following microscopic expression for k_3:

$$k_3 = k_4 = \left.\frac{\partial^2}{\partial q_x q_y}\Gamma_{12}^{-1}(\mathbf{q},0)\right|_{T=T_c},$$
(19)

where

$$\Gamma_{\alpha\beta}^{-1}(\mathbf{q},0) = -\sum_{\mathbf{k}} \frac{h_\alpha(\mathbf{k})h_\beta(\mathbf{k})(1 - f_{\mathbf{k}} - f_{\mathbf{k}-\mathbf{q}})}{\xi_{\mathbf{k}} + \xi_{\mathbf{k}-\mathbf{q}}} + \frac{\delta_{\alpha\beta}}{g}$$
(20)

is the inverse of the static particle-particle vertex function in the α-β Cooper pair channel. $h_\alpha(\mathbf{k})$ are the dimensionless form factors that arise in the order-parameter components, $\vec{\Delta}_{\mathbf{k}} = [\Delta_{01}h_1(\mathbf{k}), i\Delta_{02}h_2(\mathbf{k})]$, and also the attractive interaction $V_\alpha(\mathbf{k},\mathbf{k}') = -gh_\alpha(\mathbf{k})h_\alpha(\mathbf{k}')$ in the relevant channel;

$f_{\mathbf{k}} = [\exp(\beta\xi_{\mathbf{k}}) + 1]^{-1}$ is the Fermi occupation. Applying (19) to (20) gives

$$k_3 = \sum_{\mathbf{k}} \frac{h_1(\mathbf{k})h_2(\mathbf{k})}{8\xi_{\mathbf{k}}^3} \left\{ v_x v_y \left[\beta_c XY\xi_{\mathbf{k}}^2 + Y\xi_{\mathbf{k}} - 2X \right] \right.$$
$$\left. + \left(\partial_{k_x} v_y \right)\left[2X\xi_{\mathbf{k}} - Y\xi_{\mathbf{k}}^2 \right] \right\}. \quad (21)$$

Here, $v_i \equiv \partial_{k_i}\xi_{\mathbf{k}}$, $X \equiv \tanh(\beta_c \xi_{\mathbf{k}}/2)$, and $Y \equiv \beta_c \,\mathrm{sech}^2(\beta_c \xi_{\mathbf{k}}/2)$, with $\beta_c \equiv T_c^{-1}$.

Of all eigenstates of the z component of the angular momentum operator $\hat{L}_z$, (21) confirms that chiral p wave, with eigenvalue $m = 1$, is special. Using the continuum-limit form (1), $h_1(\mathbf{k}) = \cos m\theta$ and $h_2 = \sin m\theta$. Using $v_x \propto k\cos\theta$ and $v_y \propto k\sin\theta$, k_3 can be written as

$$k_3 = I(\mu, T_c) \int_0^{2\pi} d\theta \sin\theta\cos\theta\sin m\theta\cos m\theta, \quad (22)$$

where $I(\mu, T)$ is an integral over the radial part of $\mathbf{k}$. This shows explicitly that k_3 vanishes in the continuum limit for all m except 1 [35], in agreement with our semiclassical BdG results in Sec. II, showing that the edge current vanishes for all $m \neq 1$.

Moving away from the continuum limit, (21) remains valid for lattice systems using the appropriate forms for h_1, h_2, and $\xi_{\mathbf{k}}$. The condition for k_3 to vanish becomes more complicated than the continuum result (22), however. More generally, noting that the integrand in (21) is strongly peaked about the Fermi surface and that the second line vanishes under particle-hole symmetry, GL theory predicts that the edge along a crystalline axis vanishes when

$$k_3 \propto \langle h_1(\mathbf{k})h_2(\mathbf{k})v_x(\mathbf{k})v_y(\mathbf{k})\rangle_{\mathrm{FS}} \quad (23)$$

does. Here $\langle\cdots\rangle_{\mathrm{FS}}$ denotes an integral over the Fermi surface.

For a $d_{x^2-y^2} + id_{xy}$ order parameter on a square lattice, $h_1 = \cos k_x - \cos k_y$, $h_2 = \sin k_x \sin k_y$, and (23) vanishes by symmetry. Turning to a triangular lattice, aligning one of the symmetry axes with the x axis, $v_x = \partial_{k_x}\xi_{\mathbf{k}}$ and $v_y = \partial_{k_y}\xi_{\mathbf{k}}$ with $\xi_{\mathbf{k}} = -2t[2\cos(\sqrt{3}k_y/2)\cos(k_x/2) + \cos k_x]$. Using the same forms for the order parameters as we used in our numerical BdG calculations, we find that (23) vanishes for f wave, but not chiral p and d wave, consistent with our numerical BdG results.

Also consistent with our numerical results, the full GL coefficient (21) for chiral d wave is much smaller than that for chiral p wave, suggestive of a smaller current. In GL, this suppression is due to the multiple sign changes of the d-wave order parameter around the Fermi surface, leading to a partial cancellation. In the continuum limit, this partial cancellation becomes complete, tying into our continuum BdG results.

To make contact with the total angular momentum discussion in Sec. III and the "Chern-Simons-like" current (14), we now discuss the modifications to GL for the case where there is a spatially varying $A_0(\mathbf{r})$. A relevant discussion can be found in Ref. [33]. The disinterested reader may pass over this and proceed directly to the Discussion without losing continuity.

The presence of a spatially varying potential $A_0(\mathbf{r})$ leads to new gradient terms in the GL expansion of the form

$$f_{\mathrm{GL}} = c_{\alpha\beta}^{\mu\nu}[\psi_\alpha^*(\partial_\mu\psi_\beta)(\partial_\nu A_0) + \mathrm{c.c.}] + \cdots, \quad (24)$$

in addition to (16). Here, μ, ν denote Cartesian coordinates (e.g., x and y) while $\alpha, \beta = 1,2$ denote the components of the order parameter. The real-valuedness of the free energy in conjunction with U(1) gauge symmetry requires $c_{\alpha\beta}^{\mu\nu} \equiv c^{\mu\nu}\epsilon_{\alpha\beta}$, where $\epsilon_{\alpha\beta}$ is again the 2D Levi-Civita symbol. The current arising from this is

$$j_\mu = \frac{\partial f_{\mathrm{GL}}}{\partial(\partial_\mu\theta)} = -2c^{\mu\nu}\Delta_{01}\Delta_{02}(\partial_\nu A_0). \quad (25)$$

Equation (24) leads to the following microscopic definition:

$$c^{\mu\nu} \equiv \frac{1}{2\Delta_{01}\Delta_{02}} \lim_{\mathbf{q}\to 0} \frac{\partial\chi_{0\mu}(\mathbf{q})}{i\partial q_\nu}\bigg|_{\Delta_{01}=\Delta_{02}=0}. \quad (26)$$

Here $\chi_{0\mu} \equiv (2\beta)^{-1}\sum_{\mathbf{k},\omega_n} v_\mu(\mathbf{k})\mathrm{tr}[\hat{G}_0(\mathbf{k}+\frac{\mathbf{q}}{2}, i\omega_n)\hat{\tau}_3\hat{G}_0(\mathbf{k}-\frac{\mathbf{q}}{2}, i\omega_n)]$ is the static current-charge correlator per spin, where $\hat{G}_0(\mathbf{k}, i\omega_n)$ is the appropriate matrix Nambu-Gorkov Green's function (as a function of the Matsubara frequency ω_n) and $\hat{\tau}_3$ is the Pauli spin matrix. This correlation function is readily evaluated at all temperatures:

$$\lim_{\mathbf{q}\to 0} \frac{\partial\chi_{0\mu}(\mathbf{q})}{i\partial q_\nu} = \Delta_{01}\Delta_{02}\sum_{\mathbf{k}} \frac{v_\mu(\mathbf{k})}{4E_{\mathbf{k}}^3}\tanh(\beta E_{\mathbf{k}}/2)$$
$$\times \left[h_2(\partial_{k_\nu}h_1) - h_1(\partial_{k_\nu}h_2) \right], \quad (27)$$

where $E_{\mathbf{k}} \equiv \sqrt{\xi_{\mathbf{k}}^2 + |\Delta_{\mathbf{k}}|^2}$ is the bulk BCS quasiparticles dispersion.

Using (2), (27), and $\partial\chi_{0\mu}/\partial q_\nu = -\partial\chi_{0\nu}/\partial q_\mu$, one sees that at $T = 0$, modulo terms $\mathcal{O}(\Delta_0^2/E_F^2)$ that vanish in the weak-coupling limit, the Chern number is given by

$$\frac{C}{8\pi} = \lim_{\mathbf{q}\to 0} \frac{\partial\chi_{0\mu}(\mathbf{q})}{2i\partial q_\nu}\epsilon_{\nu\mu}. \quad (28)$$

Combining this result with (25) and (26) gives the result (14) for the $T = 0$ current.

At $T = T_c$, (26) and (27) give

$$c^{\mu\nu} = \sum_{\mathbf{k}} \frac{v_\mu(\mathbf{k})}{4\xi_{\mathbf{k}}^3}\tanh(\beta_c\xi_{\mathbf{k}}/2)\left[h_2(\partial_{k_\nu}h_1) - h_1(\partial_{k_\nu}h_2) \right]. \quad (29)$$

In conjunction with (25), this shows that the "Chern-Simons" current (14) at $T = 0$ smoothly evolves into a contribution $\propto c^{\mu\nu}\Delta_{01}(T)\Delta_{02}(T)$ near T_c. The momentum-space integrand involved with $c^{\mu\nu}$ has the same structure as that for the Chern number in the weak-coupling limit and as a result, $c^{\mu\nu}$ will not vanish as long as the Chern number does not. Moreover, in the soft edge limit, the two components of order parameter have the same spatial variation and the contribution to the current from (18) vanishes. In this limit, the current is given by (25) and does not vanish for any nonzero m. It is only in the sharp edge case, where $A_0 = 0$ in the superconductor, that (23) provides the condition for the edge current to vanish.

VI. DISCUSSION

Using semiclassical Bogoliubov–de Gennes (BdG), we have shown that the edge current for any chiral superconductor

TABLE I. Order-parameter (OP) and lattice symmetries and their relation to the existence of an integrated current. By "degenerate," we mean that the two order-parameter components transform with the same two-dimensional irreducible representation; details are given in the text. For chiral states in the continuum, *all* states with $m > 1$ have vanishing edge currents.

OP symmetry; lattice	Integrated current?	Degenerate?
p wave; continuum	yes	yes
d wave; continuum	no	yes
p wave; square	yes	yes
d wave; square	no	no
p wave; triangle	yes	yes
d wave; triangle	yes	yes
f wave; triangle	no	no

other than p wave vanishes exactly in the weak-coupling, continuum limit. Using numerical BdG and Ginzburg-Landau (GL) calculations, this result was generalized to a variety of lattice models. Specifically, we find nonzero integrated currents for $p_x + ip_y$ on square and triangular lattices, and $d_{x^2-y^2} + id_{xy}$ on a triangular lattice. We find very small integrated currents (which vanish in the limit $\Delta_0/E_F \to 0$, neglecting the possible growth of subdominant order parameters near the surface) for $d_{x^2-y^2} + id_{xy}$ on a square lattice, and $f_{x(x^2-3y^2)} + if_{y(3x^2-y^2)}$ on a triangular lattice. Noting that our zero-temperature BdG results are in complete agreement with GL on the matter of which systems we have studied exhibit edge currents, we expect that the vanishing of the Fermi-surface integral (23) gives a simple condition for the edge current to vanish in both continuum and lattice systems. Although we have not explored mixed states such as chiral $d_{xy} + is$ which are not eigenstates of $\hat{L}_z$, (23) also shows that this state will give rise to a nonvanishing edge current in the continuum, as expected from semiclassical BdG analyses [16,17].

For the combinations of superconducting states and lattices that have been studied, the existence of an edge current for a particular state coincides with the order-parameter components both transforming like basis functions of the same 2D irreducible representation of the lattice symmetry group (see Table I). On the square lattice, for instance, p_x and p_y form a basis for the 2D representation E, whereas d_{xy} and $d_{x^2-y^2}$ are bases for two different representations, B_1 and B_2. Generally one would expect chiral states to be energetically favorable only when the two components are degenerate or nearly degenerate, and our calculations suggest they will generally have nonzero currents under such conditions, albeit reduced currents for angular momenta greater than 1.

In the remainder of this concluding section, we discuss possible implications of our results for some candidate chiral superconductors.

After superfluid ^{3}He-A, the most studied candidate chiral superconductor to date is unquestionably Sr_2RuO_4 [6–8]. While μSR [36] and Kerr effect [37] measurements are strongly suggestive of spontaneous time-reversal symmetry breaking below T_c, as noted in the Introduction, superconducting quantum interference device magnetometry measurements have not seen evidence for edge currents [9]. Away from the clean-edge limit explored in the present paper, disorder [12],

gap anisotropy [13], and other edge effects [5,31,34,38] can have pronounced effects on the edge current, reducing them significantly. Here we speculate on another possibility, that Sr_2RuO_4 is a chiral superconductor, but not p wave. We emphasize that while we know of no microscopic reason why, e.g., chiral f-wave pairing should be favored on a square lattice such as that for Sr_2RuO_4 (emphasizing that the order-parameter components are not expected to be degenerate), this scenario would not necessarily be incompatible with the above experiments.

There exist some early proposals for chiral f-wave states such as $(k_x^2 - k_y^2)(k_x + ik_y)$, $k_x k_y (k_x + ik_y)$, and $k_z^2(k_x + ik_y)$ in Sr_2RuO_4 [39–42]. These correspond to $m = 1$, however, and hence, are expected to give rise to substantial edge currents. On the other hand, the 3D chiral $f_{z(x+iy)^2}$ state would exhibit the same (vanishing) edge current properties as a $d_{x^2-y^2} + id_{xy}$ state on a square lattice, although as noted before, the components are not expected to be degenerate on such a lattice.

The vanishing of the edge current for such a state need not be incompatible with μSR experiments, generally interpreted in terms of spontaneous edge currents at domain walls separating regions of opposite chirality [36], as well as around impurities, including the muons themselves. The irregular structure of the domain walls as well as the local nature of perturbing impurities means that some local currents would likely arise along irregular edges. As much has been seen in BdG studies of chiral $d + id$-wave [43] and $d + is$ [44] superconductors. In Appendix B, we show how to extend the GL theory presented here to describe edge currents along noncrystalline axes. For situations where the edge current vanishes along a crystalline axis, it does not vanish along other edges.

Another major piece of evidence in favor of time-reversal symmetry-breaking superconductivity in Sr_2RuO_4 is the appearance of a Kerr effect below T_c [37] (also seen in UPt$_3$ [20]). In continuum systems, similar to our results for the edge current, this effect vanishes for all chiral states except for chiral p wave [45]. Away from the continuum limit, however, an intrinsic Kerr effect arises from multiband transitions [46,47]. Although we cannot make any definitive statement about whether multiband chiral f-wave superconductivity on a square lattice would allow for a Kerr effect without a specific model, we note that the Fermi-surface integral (23) involved with the edge current is quite different than that involved in the intrinsic Kerr effect [47].

Some other candidate chiral superconductors that have recently attracted interest are UPt$_3$ [19], Na$_x$CoO$_2 \cdot y$H$_2$O [29], and SrPtAs [30], all of which are conjectured to be either chiral d-wave or f-wave superconductors with an in-plane chiral d-wave component. Without detailed knowledge about the structure of the order parameters, we again cannot draw any firm conclusions about the edge currents for these candidate gap symmetries. Our results suggest that one would expect such states to exhibit edge currents, albeit reduced from that of chiral p-wave pairing.

Note added. As this paper was being prepared for submission, a preprint [48] appeared which has some overlap. Focussing on the problem of the total angular momentum in the continuum limit, the authors of Ref. [48] find that the total angular momentum vanishes to order Δ_0/E_F in the weak-coupling BCS limit for all states with $m > 1$, consistent

with our results. They also extend these results to the BEC limit of the crossover, where they derive the result given by (12) for all m. These results have also been commented on by Volovik [49].

APPENDIX A: DIRAC EQUATION

In this section, we show how to map the semiclassical limit of the BdG equations (3) and (4) onto the one-dimensional twisted-mass Dirac equation [4] and use its solution to derive (8) and (9).

Substituting (4) into (3) and making the usual weak-coupling and semiclassical approximations [$\mu = E_F, \partial_y^2 a_\sigma(y) \ll k_F \partial_y a_\sigma(y), \partial_y^2 b_\sigma(y) \ll k_F \partial_y b_\sigma(y)$], the BdG equation reduces to the two one-dimensional Dirac equations

$$\begin{pmatrix} -i\sigma\,\partial_x & \Delta_0 e^{im\theta} \\ \Delta_0 e^{-im\theta} & i\sigma\,\partial_x \end{pmatrix} \hat{\Psi}_\sigma = E\hat{\Psi}_\sigma, \qquad (A1)$$

where, as before, $\hat{\Psi}_\sigma^\dagger \equiv [a_\sigma, b_\sigma]$, $\sigma = \pm$, and we have defined

$$x \equiv y/\hbar v_F \sin\theta, \qquad (A2)$$

with $v_F \equiv \hbar k_F/m^*$. Taking the complex conjugate of the $\sigma = -$ Dirac equation, these two equations can be combined into a single "twisted mass" Dirac equation,

$$\begin{pmatrix} -i\,\partial_x & \Delta_0 e^{i\phi(x)} \\ \Delta_0 e^{-i\phi(x)} & i\,\partial_x \end{pmatrix} \bar{\Psi} = E\bar{\Psi}, \qquad (A3)$$

for the composite spinor $\bar{\Psi} \equiv \Theta(-x)\hat{\Psi}_-(x) + \Theta(x)\hat{\Psi}_+(x)$, where

$$\phi(x) = -\Theta(-x)m\theta + \Theta(x)m\theta. \qquad (A4)$$

The two-dimensional edge problem has thus been mapped onto a one-dimensional problem where the phase of the order parameter is twisted across a domain at $x = 0$ from $\phi_L = -m\theta$ on the left-hand side to $\phi_R = m\theta$ on the right. The boundary condition $\hat{\Psi}_+(y = 0) = \hat{\Psi}_-(y = 0)$ in the original two-dimensional problem gets mapped onto the condition that $\bar{\Psi}(x)$ is continuous across $x = 0$. The integrated quasiparticle density $\sum_\sigma \hat{\Psi}_\sigma^\dagger \hat{\Psi}_\sigma$ needed to calculate the edge current is given by the "charge" $Q_m \equiv \sum_n \int_{-\infty}^{\infty} dx |\chi_n(x)|^2$ accumulated in the vicinity of the domain wall, where χ_n are the eigenstates of (A3) for a given magnetic quantum number m.

The solution of (A3) is discussed at length in Ref. [4]. The only difference in our case is that the phase is twisted between $-m\theta$ and $m\theta$ instead of between $-\theta$ and θ. This difference manifests itself in two ways. First, everywhere in the appendix of Ref. [4] where $\Phi \equiv \phi_L - \phi_R$ appears, we replace this with $-2m\theta$. Second, for the calculation of the edge state properties, the mismatch between the $\sin\theta$ factor that arises when mapping back to the original y coordinate [cf. (A2)] and the $\sin m\theta, \cos m\theta$ factors that arise in the solutions of (A3)

and (A4) leads to piecewise constraints when $m \neq 1$. (A3), for instance, supports a bound-state solution [4]

$$\chi_0(x > 0/x < 0) \propto \begin{bmatrix} E^{(0)} \pm i\kappa + \Delta_0 \\ E^{(0)} \mp i\kappa + \Delta_0 \end{bmatrix} e^{\mp\kappa x}, \qquad (A5)$$

with $\kappa = \Delta_0 \sin m\theta$. Using (A2) and (A5), boundedness in the original y space means that $\kappa/\sin\theta = \Delta_0(\sin m\theta/\sin\theta)$ must be positive for all θ. This constraint ($\sin m\theta/\sin\theta > 0$) plus continuity [$\chi_0(0^+) = \chi_0(0^-)$] leads to the result (8).

Turning to the continuum bulk states, the charge Q_m is calculated in exactly the same way as in Ref. [4] with the replacement $\Phi \equiv -2m\theta$ in, e.g., their Eq. (A13). The same considerations that lead to Eq. (A16) in Ref. [4] yield (9).

APPENDIX B: GINZBURG-LANDAU THEORY FOR EDGES NOT ALIGNED WITH THE CRYSTALLINE AXES

Here we generalize the GL expression (21) to allow for the possibility of currents along edges that are not parallel with crystalline axes. Implicit in the appearance of k_3 in the GL free energy density (16) is that it describes the energy cost associated with a spontaneous current [U(1) phase] along the y axis and spatial modulation of the amplitude of the order parameter along x (and vice versa), as would happen if there was an edge parallel to the y axis (x axis). One can generalize the definition of k_3 to allow for arbitrary orientation of the amplitude gradient, with the edge and resulting current perpendicular to this: $k_3(\phi) \equiv \partial^2 \Gamma_{12}^{-1}(\mathbf{q}, 0)/\partial q_x' \partial q_y'$, where $\mathbf{q}' \equiv [q_x', q_y']$ is rotated by ϕ with respect to $\mathbf{q}$. This leads to

$$k_3(\phi) \equiv \sin\phi \cos\phi \left[\frac{\partial^2 \Gamma_{12}^{-1}}{\partial q_x^2} - \frac{\partial^2 \Gamma_{12}^{-1}}{\partial q_y^2} \right]$$
$$+ (\cos^2\phi - \sin^2\phi) \frac{\partial^2 \Gamma_{12}^{-1}}{\partial q_x \partial q_y}. \qquad (B1)$$

This describes the current along an edge oriented by an angle ϕ with respect to a crystalline axis.

In the vicinity of an edge that is not parallel with a crystalline axis, we expect the order parameter to reorient itself to lower gradient energies, meaning that the h_1 and h_2 that enter this expression will be different. For an edge not along an axis of symmetry of the crystal, an additional calculation would be required to compute the resulting order parameter. Otherwise, symmetry and energetic arguments can be used to infer the correct form. As an example, a $\sin k_x + i \sin k_y$ order parameter on a cubic lattice will become $\sin k_x \cos k_y - \cos k_x \sin k_y + i(\sin k_x \cos k_y + \cos k_x \sin k_y)$ in the vicinity of the [11] edge; that is, it will simply be rotated in momentum space by $\pi/4$. Likewise, assuming that the $d_{x^2-y^2} + i d_{xy}$ order parameter on a cubic lattice is rotated by $\pi/4$ gives $h_1 = \sin k_x \sin k_y$ and $h_2 = (\sin k_x \cos k_y)^2 - (\cos k_x \sin k_y)^2$. The second line in (B1) vanishes for $\phi = \pi/4$ while the first line involves a Fermi-surface average of $h_1(\mathbf{k})h_2(\mathbf{k})(v_x^2 - v_y^2)$, which also vanishes. Thus, the generalized GL expression (B1) predicts a vanishing edge current along the [11] edge as well as the [01] edge for a $d_{x^2-y^2} + i d_{xy}$ order parameter on a square lattice. We have also used (B1) to confirm that $s + i d_{x^2-y^2}$ on a square lattice supports a current along [11], even though there is none along [01] [17].

[1] M. Ishikawa, Prog. Theor. Phys. **57**, 1836 (1977).

[2] N. D. Mermin and P. Muzikar, Phys. Rev. B **21**, 980 (1980).

[3] T. Kita, J. Phys. Soc. Jpn. **67**, 216 (1998).

[4] M. Stone and R. Roy, Phys. Rev. B **69**, 184511 (2004).

[5] J. A. Sauls, Phys. Rev. B **84**, 214509 (2011).

[6] A. P. Mackenzie and Y. Maeno, Rev. Mod. Phys. **75**, 657 (2003).

[7] Y. Maeno, S. Kittaka, T. Nomura, S. Yonezawa, and K. Ishida, J. Phys. Soc. Jpn. **81**, 011009 (2012).

[8] C. Kallin, Rep. Prog. Phys. **75**, 042501 (2012).

[9] J. R. Kirtley, C. Kallin, C. W. Hicks, E.-A. Kim, Y. Liu, K. A. Moler, Y. Maeno, and K. D. Nelson, Phys. Rev. B **76**, 014526 (2007).

[10] P. J. Curran, S. J. Bending, W. M. Desoky, A. S. Gibbs, S. L. Lee, and A. P. Mackenzie, Phys. Rev. B **89**, 144504 (2014).

[11] C. Kallin and J. Berlinsky, J. Phys.: Condens. Matter **21**, 164210 (2009).

[12] P. E. C. Ashby and C. Kallin, Phys. Rev. B **79**, 224509 (2009).

[13] W. Huang, S. Lederer, E. Taylor, and C. Kallin, arXiv:1412.4592.

[14] M. Stone and I. Anduaga, Ann. Phys. **323**, 2 (2008).

[15] M. Matsumoto and H. Shiba, J. Phys. Soc. Jpn. **64**, 4867 (1995).

[16] D. Rainer, H. Burkhardt, M. Fogelström, and J. A. Sauls, J. Phys. Chem. Solids **59**, 2040 (1998).

[17] B. Horovitz and A. Golub, Phys. Rev. B **68**, 214503 (2003).

[18] B. Braunecker, P. A. Lee, and Z. Wang, Phys. Rev. Lett. **95**, 017004 (2005).

[19] R. Joynt and L. Taillefer, Rev. Mod. Phys. **74**, 235 (2002).

[20] E. R. Schemm, W. J. Gannon, C. M. Wishne, W. P. Halperin, and A. Kapitulnik, Science **345**, 190 (2014).

[21] G. E. Volovik, JETP **67**, 1804 (1988).

[22] J. Goryo and K. Ishikawa, Phys. Lett. A **246**, 549 (1998).

[23] G. E. Volovik, JETP Lett. **70**, 609 (1999).

[24] For a charged chiral superconductor, screening effects reduce the angular momentum by an amount $\gtrsim \lambda/R$, where λ is the penetration depth and R is the radius of the disk.

[25] A. J. Leggett, in *Modern Trends in the Theory of Condensed Matter*, edited by A. Pekalski and R. Przystawa (Springer-Verlag, Berlin, 1980).

[26] Y. Jiang, D-X. Yao, E. W. Carlson, H.-D. Chen, and J. P. Hu, Phys. Rev. B **77**, 235420 (2008).

[27] R. Nandkishore, L. S. Levitov, and A. V. Chubukov, Nat. Phys. **8**, 158 (2012).

[28] A. M. Black-Schaffer, Phys. Rev. Lett. **109**, 197001 (2012).

[29] M. L. Kiesel, C. Platt, W. Hanke, and R. Thomale, Phys. Rev. Lett. **111**, 097001 (2013).

[30] M. H. Fischer, T. Neupert, C. Platt, A. P. Schnyder, W. Hanke, J. Goryo, R. Thomale, and M. Sigrist, Phys. Rev. B **89**, 020509(R) (2014).

[31] S. Lederer, W. Huang, E. Taylor, S. Raghu, and C. Kallin, Phys. Rev. B **90**, 134521 (2014)

[32] M. Sigrist and K. Ueda, Rev. Mod. Phys. **63**, 239 (1991).

[33] A. Furusaki, M. Matsumoto, and M. Sigrist, Phys. Rev. B **64**, 054514 (2001).

[34] A. Bouhon and M. Sigrist, arXiv:1409.1516.

[35] Sauls [J. A. Sauls, Adv. Phys. **43**, 113 (1994)] also finds that k_3 vanishes in the continuum for the chiral $k_z[(k_x^2 - k_y^2) \pm 2ik_xk_y]$ state.

[36] G. M. Luke, Y. Fudamoto, K. M. Kojima, M. I. Larkin, J. Merrin, B. Nachumi, Y. J. Uemura, Y. Maeno, Z. Q. Mao, Y. Mori, H. Nakamura, and M. Sigrist, Nature (London) **394**, 558 (1998).

[37] J. Xia, Y. Maeno, P. T. Beyersdorf, M. M. Fejer, and A. Kapitulnik, Phys. Rev. Lett. **97**, 167002 (2006).

[38] Y. Imai, K. Wakabayashi, and M. Sigrist, Phys. Rev. B **85**, 174532 (2012).

[39] Y. Hasegawa, K. Machida, and M. Ozaki, J. Phys. Soc. Jpn. **69**, 336 (2000).

[40] M. J. Graf and A. V. Balatsky, Phys. Rev. B **62**, 9697 (2000).

[41] H. Won and K. Maki, Europhys. Lett. **52**, 427 (2000).

[42] T. Dahm, H. Won, and K. Maki, arXiv:cond-mat/0006301.

[43] M. J. Graf, A. V. Balatsky, and J. A. Sauls, Phys. Rev. B **61**, 3255 (2000).

[44] W.-C. Lee, S.-C. Zhang, and C. Wu, Phys. Rev. Lett. **102**, 217002 (2009).

[45] J. Goryo, Phys. Rev. B **78**, 060501(R) (2008).

[46] K. I. Wysokiński, J. F. Annett, and B. L. Györffy, Phys. Rev. Lett. **108**, 077004 (2012).

[47] E. Taylor and C. Kallin, Phys. Rev. Lett. **108**, 157001 (2012).

[48] Y. Tada, W. Nie, and M. Oshikawa, arXiv:1409.7459.

[49] G. E. Volovik, arXiv:1409.8638.

Chapter 4

Non-topological nature of the edge current

4.1 Preface

The non-topological nature of the edge current is already implied in the previous chapter, where the integrated current at the sharp edge of a non-p-wave chiral superfluid vanishes, instead of being determined by the Chern number, i.e. the orbital angular momentum of the Cooper pairs. Similarly, the edge current of a chiral p-wave model on a general lattice also does not appear to be directly related to a topological invariant (Fig.4.1).

However, in the limit of a soft edge which can be described by a spatially varying potential A_0 and where the carrier density varies smoothly over large distances, the edge current can be derived from the Chern-Simons-like action[56, 97, 98, 59, 48] $\mathcal{L} = -\frac{m}{4\pi}\varepsilon^{0\mu\nu}A_\mu\partial_\nu A_0$, which gives (up to a correction of the order Δ^2/E_F^2 due to particle non-conservation),

$$j_\mu = -\frac{m}{4\pi}\varepsilon^{0\mu\nu}\partial_\nu A_0 \; . \tag{4.1}$$

Hence, the integrated edge current $J = \frac{mE_f}{4\pi} = \frac{mn_0}{4m^*}$ where n_0 is the bulk carrier density and m^* is the carrier effective mass, is "topological" (see publication). Moreover, there exist special chiral p-wave models where the edge current *coincides* with a "topological" value irrespective of how the edge potential is deformed (soft, hard, or intermediate). One example is the con-

tinuum chiral p-wave superfluid. There, the integrated edge current is always given by $J \sim \frac{n_0}{4}$.

Remarkably, in a disk geometry with N particles, the angular momentum carried by such a current coincides with what is intuitively expected of a superfluid with $N/2$ Cooper pairs each carrying $L_z = \hbar$. Another example is the simple p-wave model on a square lattice with only nearest neighbour pairing and nearest neighbour hopping, as can be seen in the inset of fig.4.1.

This work is an attempt to provide some insight into why the edge current in a chiral superconductor is generically non-topological and why it coincides with the topological value in some special scenarios. As a corollary, we see that the lack of topological protection suggests a means to reconcile the chiral p-wave order and the absence of edge current in Sr_2RuO_4— gap anisotropy. Note in support of the spectral flow argument given in the publication, Appendix C derives the expression for the total integrated current in terms of the so-called spectral asymmetry.
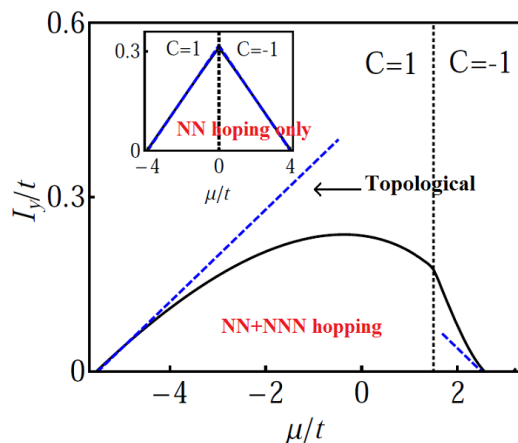
Figure 4.1: Integrated edge current as a function of chemical potential for a simple chiral p-wave model on a square lattice, with $\Delta_k = \Delta_0(\sin k_x + i \sin k_y)$ with $\Delta_0 = 0.2t$. The single particle tight-binding dispersion takes the form: $\xi_k = -2t(\cos k_x + \cos k_y) - 4t' \cos k_x \cos k_y - \mu$. For the model with only nearest neighbor (NN) hopping, $t' = 0$, while for the model with both NN and NNN hoppings, $t' = 0.375t$. The black solid lines are the numerical BdG results in the presence of sharp edge conditions, and the blue dashed lines are predictions derived from the Chern-Simons-like action for soft edge limits. The Chern numbers in the respective regimes of chemical potentials are as indicated.

4.2 Publication

Nontopological nature of the edge current in a chiral *p*-wave superconductor

Wen Huang,[1] Samuel Lederer,[2] Edward Taylor,[1] and Catherine Kallin[1,3]

[1]*Department of Physics and Astronomy, McMaster University, Hamilton, Ontario, Canada L8S 4M1*
[2]*Department of Physics, Stanford University, Stanford, California 94305, USA*
[3]*Canadian Institute for Advanced Research, Toronto, Ontario, Canada M5G 1Z8*
(Received 29 December 2014; published 12 March 2015)

The edges of time-reversal symmetry breaking topological superconductors support chiral Majorana bound states as well as spontaneous charge currents. The Majorana modes are a robust, topological property, but the charge currents are nontopological—and therefore sensitive to microscopic details—even if we neglect Meissner screening. We give insight into the nontopological nature of edge currents in chiral *p*-wave superconductors using a variety of theoretical techniques, including lattice Bogoliubov–de Gennes equations, the quasiclassical approximation, and the gradient expansion, and we describe those special cases in which edge currents do have a topological character. While edge currents are not quantized, they are generically large, but they can be substantially reduced for a sufficiently anisotropic gap function, a scenario of possible relevance for the putative chiral *p*-wave superconductor Sr_2RuO_4.

I. INTRODUCTION

Time-reversal symmetry breaking topological superconductors support branches of chiral Majorana bound states at their edges [1]. The number of these branches is insensitive to perturbations such as weak disorder, and it is equal to a Chern number, a topological invariant that is determined by the Fermi surface topology and the chirality of the order parameter. Quantum Hall systems support both topologically protected edge states and topologically protected *quantized* edge currents, with the conductance equal to fundamental constants multiplied by a Chern number [2]. Even though the number of topological edge modes is given by a Chern number in both these systems, the edge current of a topological superconductor is not topologically protected or quantized. This fact is clear from Bogoliubov–de Gennes (BdG) calculations [3–5] of topological chiral *p*-wave superconductors that reveal nonuniversal behavior dependent on microscopic details. This nonuniversal behavior is present even without taking into account the effects of Meissner screening (which we neglect here), which forces the total current to vanish (though the local currents should still yield observable magnetic signals [6,7]). One reason to study this issue is that the lack of topological protection of edge currents in chiral *p*-wave superconductors is crucial to any attempt to reconcile the null result of precision magnetometry experiments on the putative chiral *p*-wave superconductor Sr_2RuO_4 [8–11] with straightforward theoretical predictions [6].

In this work, we provide insight into the nontopological nature of edge currents in chiral *p*-wave superconductors using a variety of theoretical techniques, including lattice Bogoliubov–de Gennes equations, the quasiclassical approximation, a gradient expansion of the effective action, and spectral flow arguments. We begin by examining the circumstances under which topology *does* straightforwardly govern edge currents: (i) the coupling is weak, so that $\Delta_0 \ll E_F$ (assumed throughout this paper), and (ii) a spatially varying site energy $A_0(\mathbf{r})$ (equivalent to a static, unscreened scalar potential) drives the density to zero at the edge over a distance L much longer than the coherence length ξ_0. [We will refer to condition (ii) as

the *soft edge* limit.] Under these circumstances, the gradient expansion gives [12–15]

$$\boldsymbol{j}(\mathbf{r}) = -\frac{C}{4\pi}(\hat{\mathbf{z}} \times \boldsymbol{\nabla})A_0(\mathbf{r}) \tag{1}$$

for the current density, where C is the Chern number and we use units where the electron charge $e = \hbar = 1$ throughout. Apart from a factor of one-half, this is also the current density in quantum Hall systems, both in fractional quantum Hall systems where the Chern-Simons action was first derived in a condensed-matter context [16,17], as well as integer quantum Hall systems. In the quantum Hall context, (1) implies a quantized, topological value for the Hall conductance.

Contrary to the above assumptions, the edges of actual superconducting crystals are atomically sharp: the density at the edge vanishes over an atomic scale $k_F^{-1} \ll \xi_0$. This explicitly invalidates the systematic gradient expansion in powers of ξ_0/L. Even within the gradient expansion, there are subleading corrections to (1) whose importance grows as L is diminished; one such correction is discussed in Sec. IV. That said, despite the fact that (1) fails to even approximately describe the current *density* in the sharp edge limit, there are special models with sharp edges for which the *integrated* current (which is roughly proportional to the strength of the magnetic signal expected in experiment) coincides with the prediction of (1). These special models include all continuum models (for which the integrated current can be calculated using a one-dimensional Dirac equation [12,18]), as well as certain lattice models with restricted hopping matrix elements. We analyze these special models in Sec. V, using the "spectral flow" [19] properties of the BdG eigenvalues, to show that the integrated current remains equal to its "topological value" [i.e., the one inferred from the Chern-Simons expression (1)] as the edge is deformed from soft to sharp.

Outside of these special models, the integrated edge current generically evolves to a nontopological value (i.e., one unrelated to the Chern number) as we adiabatically deform a soft edge into a sharp one. While it remains generically substantial, there is nothing to prevent it from being small, and it can be tuned through zero by varying the band and/or gap

structure. For example, in a model with an anisotropic p-wave order parameter consistent with next-nearest-neighbor (NNN) pairing [20] on the γ band of Sr_2RuO_4, the integrated edge current vanishes at a filling fraction close to the experimental value (see Fig. 2). Although reliant on the fine-tuning of parameters, this result might be important for reconciling chiral p-wave superconductivity in Sr_2RuO_4 [21–24] with the null results of experiments designed to measure the expected magnetic fields [8–11].

II. TOPOLOGICAL PROPERTIES IN THE CONTINUUM LIMIT

The topological properties of a two-dimensional chiral p-wave superfluid are characterized by the Chern number

$$C = \frac{1}{4\pi} \int d^2k \, \hat{h} \cdot \left(\partial_{k_x}\hat{h} \times \partial_{k_y}\hat{h} \right). \quad (2)$$

Here $\vec{h} = \{\text{Re}[\Delta_0(\mathbf{k})], -\text{Im}[\Delta_0(\mathbf{k})], \xi(\mathbf{k})\}$ and $\hat{h} = \vec{h}/|\vec{h}|$. $\Delta_0(\mathbf{k})$ is the complex chiral order parameter and $\xi(\mathbf{k}) \equiv \epsilon(\mathbf{k}) - \mu$, with $\epsilon(\mathbf{k})$ the single-particle dispersion. For a chiral p-wave order parameter $\Delta_0(\mathbf{k}) = \Delta_0(k_x \pm ik_y)/k_F$ appropriate for continuum systems, the Chern number is ± 1. For lattice models, it depends not just on the chirality or winding of the order parameter, but also the topology of the Fermi surface, but it always takes an integer value.

One manifestation of a nonzero Chern number is a quantized value of the "static" Hall conductivity [12–15,25]: $\tilde{\sigma}_{xy} \equiv \lim_{\mathbf{q} \to 0} \lim_{\omega \to 0} \sigma_{xy}(\omega, \mathbf{q}) = C/4\pi + O[(\Delta_0/E_F)^2]$ in the weak-coupling limit, a result that follows from (1) (which we derive in Sec. IV). Note that in a continuum system, reversing the order of limits to evaluate the standard dc Hall conductivity, $\sigma_{xy} \equiv \lim_{\omega \to 0} \lim_{\mathbf{q} \to 0} \sigma_{xy}(\mathbf{q}, \omega)$, gives zero [25]. This noncommutativity of limits arises from a subtlety in the effective action (12), which we will discuss later on.

Closely related to this static quantum Hall effect is the fact that a long-wavelength density perturbation of a chiral p-wave superfluid will give rise to a quantized current. With $C = 1$ and $A_0(\mathbf{r})$ determining the local carrier density $n(\mathbf{r})$ according to $\nabla A_0(\mathbf{r}) = \pi \nabla n(\mathbf{r})/m$, (1) reduces to the well-known expression for the current in a chiral superfluid due to Mermin and Muzikar [26]:

$$\mathbf{j} = \frac{1}{4m}(\hat{\mathbf{z}} \times \nabla n). \quad (3)$$

Using this result to evaluate the edge current, assuming that the density evolves *slowly* from zero at $x = -\infty$ to its bulk value n_0 at $x = +\infty$, the integrated current is

$$I_y = \frac{C}{4m} \int_{-\infty}^{-\infty} dx \, \partial_x n(x) = \frac{n_0 C}{4m}. \quad (4)$$

Remarkably, this result agrees with calculations of the edge current in a Galilean invariant chiral p-wave superfluid by Stone and Roy [12] (using BdG) and Sauls [18] (using the quasiclassical approximation). This is surprising because these results are obtained for a sharp edge, whereas (1) is obtained from a gradient expansion of the action and should only be strictly valid in the soft-edge limit.

III. MODEL AND BDG RESULTS

We now turn to BdG calculations of the edge current for a range of one-band lattice models of chiral p-wave superconductivity. For simplicity, we consider spinless fermions on a two-dimensional square lattice (we will multiply our results for the current by 2 to compensate):

$$H = -\sum_{\mathbf{r},\mathbf{r}'} t_{\mathbf{r},\mathbf{r}'} c_{\mathbf{r}}^\dagger c_{\mathbf{r}'} - \mu \sum_{\mathbf{r}} c_{\mathbf{r}}^\dagger c_{\mathbf{r}} - \sum_{\mathbf{r},\mathbf{r}'} g_{\mathbf{r},\mathbf{r}'} c_{\mathbf{r}}^\dagger c_{\mathbf{r}'}^\dagger c_{\mathbf{r}'} c_{\mathbf{r}}. \quad (5)$$

Here $\mathbf{r},\mathbf{r}'$ denote the lattice positions, and $t \equiv t_{\mathbf{r},\mathbf{r}\pm\hat{x}} = t_{\mathbf{r},\mathbf{r}\pm\hat{y}}$ and $t' \equiv t_{\mathbf{r},\mathbf{r}\pm(\hat{x}\pm\hat{y})}$ are the nearest- (NN) and next-nearest-neighbor (NNN) hopping parameters. Decoupling the interaction term by introducing the two-component order parameter (Δ_x, Δ_y), the pairing term in the Hamiltonian is

$$H_\Delta = \sum_{\mathbf{r},\mathbf{s}} [\Delta_x(\mathbf{r},\mathbf{s}) + \Delta_y(\mathbf{r},\mathbf{s})] c_{\mathbf{r}-\mathbf{s}/2}^\dagger c_{\mathbf{r}+\mathbf{s}/2}^\dagger + \text{H.c.} \quad (6)$$

We select the chiral p-wave channel by taking a relative phase of $\pi/2$ between Δ_x and Δ_y, and by assuming Δ_x and Δ_y transform, respectively, under the p_x and p_y representation of the square lattice point group. Assuming that pairing occurs in a single lattice harmonic, $\Delta_\alpha(\mathbf{r},\mathbf{s}) \equiv \eta_\alpha(\mathbf{r})\Delta_{0,\alpha}(\mathbf{s})$ can be written as a separable function of the center-of-mass $\mathbf{r}$ and relative $\mathbf{s}$ coordinates, where $\eta_\alpha(\mathbf{r})$ is the dimensionless amplitude, equal to unity in the bulk. As is well known, this model supports chiral Majorana modes at the edges of the superconductor. Modulo a sign factor, the number of such chiral modes per edge is given by (2), where now

$$\xi(\mathbf{k}) = -2t(\cos k_x + \cos k_y) - 4t'\cos k_x \cos k_y - \mu \quad (7)$$

and

$$\Delta_0(\mathbf{k}) = \Delta_{0,x}(\mathbf{k}) + \Delta_{0,y}(\mathbf{k}), \quad (8)$$

where $\Delta_{0,\alpha}(\mathbf{k})$ is the Fourier transform of $\Delta_{0,\alpha}(\mathbf{s})$. For the simplest case of NN pairing, $\Delta_0(\mathbf{k}) = \Delta_0(\sin k_x \pm i \sin k_y)$.

To calculate the edge current in this model, we perform BdG calculations in a cylindrical geometry: periodic boundary conditions are taken in the y direction, and open boundary conditions in x. The current operator for the link from site i to site j is

$$\hat{J}_{i,j} = id_{ij}t_{i,j}[c_i^\dagger c_j - c_j^\dagger c_{i,}], \quad (9)$$

where d_{ij} is the bond length connecting i and j. (Here, in addition to $\hbar = 1$, we set $e = 1$; the unit cell length a is also set to unity so that $d_{ij} = 1$ for NN sites and $d_{ij} = \sqrt{2}$ for NNN sites.) Our primary results for the edge currents will concern the total current I_y flowing through one-half of the cylindrical system along the y direction. Let the cylinder be N_x sites wide and N_y sites in circumference (in all our calculations, we use $N_x = N_y$). Then

$$I_y = \sum_{n=1}^{N_x/2} \left\langle \hat{J}_{n\hat{x},n\hat{x}+\hat{y}} + \frac{1}{\sqrt{2}} \hat{J}_{n\hat{x},n\hat{x}+\hat{x}+\hat{y}} \right\rangle, \quad (10)$$

where the two terms in the sum are for NN and NNN links.

The mean-field Hamiltonian comprised of the single-particle terms of (5) and the pairing contribution (6) is diagonalized, and self-consistency is enforced by iterating the gap equation. Figure 1 shows the integrated edge current
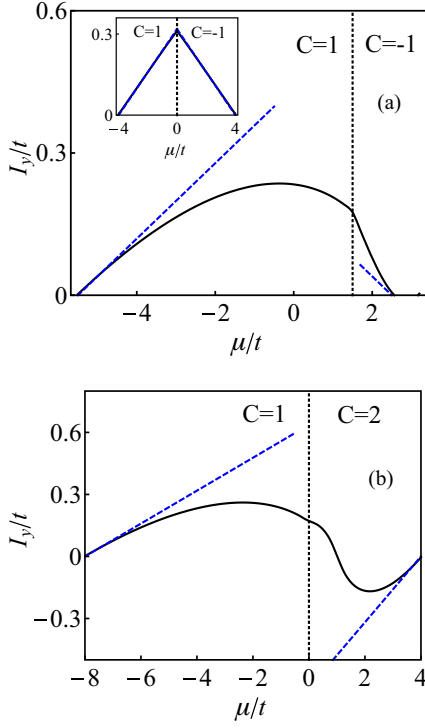
FIG. 1. (Color online) The integrated edge current calculated from $T = 0$ BdG (solid curves) as a function of the chemical potential over the entire bandwidth for (a) $t' = (3/8)t$ (inset, $t' = 0$) and (b) $t' = t$. $\Delta_0 = 0.2t$ for all plots; this requires varying the interaction g as the chemical potential is varied. In the inset of (a), for instance, g/t is varied from 11.2 at $\mu = -4t$ to 3.25 at $\mu = 0$. Calculations are carried out for $N_x = N_y = 300$ lattice sites. The "topological current" obtained from 1, with details given in Appendix A, is also shown (dashed lines) and coincides with the BdG result for $t' = 0$. Regions of μ with different Chern numbers are separated by a dotted vertical line.

as a function of the chemical potential for different values of the NNN hopping t'. We also show the "topological" (soft-edge limit) expressions for the integrated currents near the continuum limit at the top and bottom of the band obtained from (1) using the Chern numbers for these models (although this topological expression is not always uniquely defined, as we discuss in Appendix A). Apart from a coincidence in the case in which $t' = 0$ [shown in the inset of Fig. 1 and elaborated on in Sec. V], these topological values differ considerably from the BdG results, explicitly demonstrating the nontopological nature of the edge current.

Figure 2 compares the integrated current as a function of chemical potential for models with chiral p-wave order parameters of dramatically different anisotropy: the NN pairing case, $\Delta_0(\mathbf{k}) = \Delta_0(\sin k_x + i \sin k_y)$, and the NNN pairing case, $\Delta_0(\mathbf{k}) = \Delta_0(\sin k_x \cos k_y + i \sin k_y \cos k_x)$. For comparison, we also show a suitably defined topological expression which, away from the top and bottom of the band, fails to even qualitatively track the current in the case of NNN pairing. For parameters appropriate for Sr$_2$RuO$_4$, $\mu \sim 1.4t$
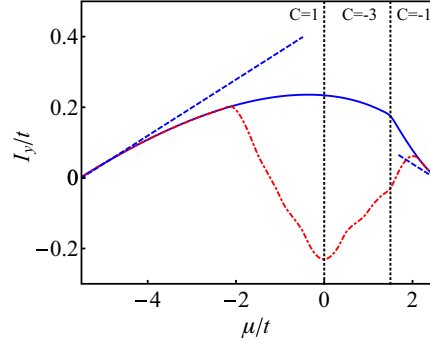
FIG. 2. (Color online) The effect of order parameter anisotropy on the edge current. The integrated edge current for two different order parameters is shown for $t' = 3t/8$: $\Delta_0(\mathbf{k}) = \Delta_0(\sin k_x + i \sin k_y)$ [solid curve; same as in Fig. 1(a)] and $\Delta_0(\mathbf{k}) = \Delta_0(\sin k_x \cos k_y + i \sin k_y \cos k_x)$ (red dot-dashed curve). The Chern number in the latter case is equal to 1 for $-5.5t \leqslant \mu < 0$, -3 for $0 < \mu < 1.5t$, and -1 for $1.5t < \mu < 2.5t$. The topological current value is shown by the blue dashed curves and coincides for the two order parameters.

[27], the current obtained for NNN pairing is significantly reduced compared to that for NN pairing.

All our numerical BdG results are well approximated by the expression

$$ I_y = \frac{1}{(2\pi)^d} \oint_{FS} \frac{d^{d-1}\mathbf{k}}{|\mathbf{v}|} v_x v_y \tan^{-1}\left(\frac{\Delta_{0,x}}{\Delta_{0,y}}\right), \quad (11) $$

which is derived in detail using the quasiclassical approximation in Appendix B. Here the subscript "FS" denotes an integral over the Fermi surface, $v_\mu \equiv \partial_{k_\mu} \xi(\mathbf{k})$, $|\mathbf{v}| \equiv \sqrt{v_x^2 + v_y^2}$, and $\Delta_{0,x}(\mathbf{k})$ and $\Delta_{0,y}(\mathbf{k})$ are the momentum-dependent order parameter components [cf. (8)]. This result confirms that the edge current is generically equal to the Fermi energy times a number of order 1 and fundamental constants. However, there can be substantial cancellations in the integral of (11) if the order parameter components have "accidental" sign changes around the Fermi surface, as occurs for the anisotropic gap shown in Fig. 2 at sufficiently large carrier density. For certain non-p-wave chiral order parameters such as $d_{xy} + i d_{x^2-y^2}$ on a square lattice, symmetry requires this cancellation to be complete and the current vanishes identically within a quasiclassical approximation [28,34].

IV. GRADIENT EXPANSION OF THE BCS ACTION FOR A CHIRAL p-WAVE SUPERCONDUCTOR

To complement our BdG results, we now turn to a gradient expansion of the mean-field BCS action for a chiral p-wave superconductor. Previous authors [12,14,15] have used such an expansion of the action with respect to gradients of the scalar $A_0(\mathbf{r})$ potential to understand the edge current. A vector potential $\mathbf{A}(\mathbf{r})$ is also included to generate an expression for the current from the action, taking it to be zero after this is done. At $T = 0$, and in the weak-coupling limit, the leading-order terms that give rise to a spontaneous current in this gradient

expansion are (see Appendix C)

$$\mathcal{L}_{\text{eff}} = -\frac{C}{4\pi}\epsilon_{0\mu\nu}A_\mu\partial_\nu A_0, \tag{12}$$

where implicit summation over the Cartesian indices μ, ν is assumed. C is the Chern number defined in (2), and $\epsilon_{\lambda\mu\nu}$ is the Levi-Civita symbol corresponding to space-time indices $(0,1,2) = (\tau, x, y)$. Equation (12) resembles the Chern-Simons term, which arises in the effective theory of the fractional quantum Hall effect [16,17]. Unlike in that theory, the "Chern-Simons-like" action (12) lacks the time derivative $-(C/4\pi)\epsilon_{\mu 0\nu}A_\mu\partial_0 A_\nu$ [12]. The absence of this only affects dynamic properties such as the Hall response discussed earlier and not static ones such as the edge current, and hence it is not responsible for the nontopological nature of the edge current. Applying $\boldsymbol{j} = \delta\mathcal{L}_{\text{eff}}/\delta\mathbf{A}|_{\mathbf{A}=0}$ to (12) gives the result (1) for the current.

The gradient expansion leading to (12) is strictly valid only when $A_0(\mathbf{r})$ varies on length scales much longer than the superconducting coherence length. This is the opposite limit to a sharp crystalline edge, where the density varies over an atomic scale $k_F^{-1} \ll \xi_0$, so the gradient expansion formally breaks down. As one moves away from the soft-edge limit, there will be gradient corrections involving A_0 beyond (12). In addition, one expects the order parameter amplitudes η_x and η_y to vary in space differently in response to the presence of an edge [29]. Including such textures in the gradient expansion of the BCS action leads to a term

$$\mathcal{L}_\Delta = \gamma[A_y\partial_x + A_x\partial_y](\eta_y - \eta_x), \tag{13}$$

where

$$\gamma \equiv \int \frac{d^2\mathbf{k}}{(2\pi)^2} \frac{v_x v_y \text{Im}[\Delta_{0,x}^*(\mathbf{k})\Delta_{0,y}(\mathbf{k})]}{2E_\mathbf{k}^3}, \tag{14}$$

with $E_\mathbf{k} = \sqrt{\xi^2(\mathbf{k}) + |\Delta_0(\mathbf{k})|^2}$. Equation (13) gives rise to an additional, nontopological contribution

$$j_{\Delta,i}(\mathbf{r}) \equiv \gamma\epsilon_{ij}\partial_j[\eta_i(\mathbf{r}) - \eta_j(\mathbf{r})] \tag{15}$$

to the edge current.

Equation (15) is the zero-temperature analog of the usual Ginzburg-Landau expression (see, e.g., Ref. [30]) for the current in the absence of an explicit potential $A_0(\mathbf{r})$. [For $A_0(\mathbf{r}) \neq 0$, there is also an analog of the Chern-Simons term at $T = T_c$ [28].] While the expansion involving gradients of A_0 breaks down completely in the sharp-edge limit [31], (13) remains qualitatively valid since the order parameter textures vary over the coherence length, putting this term at the edge of the domain of validity of our gradient expansion. The same calculation that yields γ at $T = 0$ gives the GL coefficient $k_3 = k_4$ at $T \simeq T_c$ [28]. At $T = 0$, in the continuum limit, it reduces to $\gamma = \mu/8\pi \simeq n/8m$, showing that this contribution to the edge current is generically substantial. Indeed, the γ coefficient bears a qualitative resemblance to the quasiclassical expression (11) for the current. Calculating the integrated current that results from (15) using (14) and self-consistent values of $\eta_x(\mathbf{r}), \eta_y(\mathbf{r})$ from BdG calculations, the result is in qualitative agreement with numerical BdG calculations for all lattice structures and gap anisotropies studied.
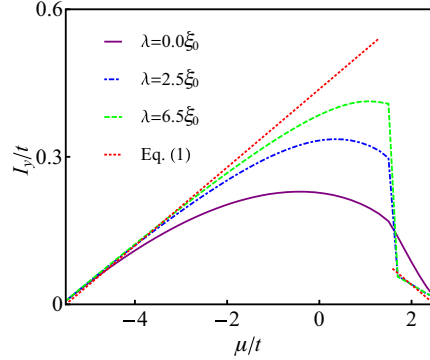
FIG. 3. (Color online) Plots of the integrated edge current from BdG for $t' = 3t/8$ [see also Fig. 1(b)] with an edge at $x = 0$ and an edge potential $A_0(x) = (\mu + 5.5t)[1 - \tanh(x/\lambda)]$ for $\mu < 1.5t$ and $A_0(x) = (\mu - 2.5t)[1 - \tanh(x/\lambda)]$ for $\mu > 1.5t$. As the edge becomes progressively softer (λ/ξ_0 increasing), the BdG results approach the topological value (A3) obtained from (1). All results should coincide near the bottom ($\mu = -5.5t$) and top ($\mu = 2.5t$) of the band. The van Hove singularity at $\mu = 1.5t$ pushes the region of agreement near the top of the band to values of μ very close to $2.5t$. For $\lambda = 6.5\xi_0$, the current does not vanish at the top of the band since we had to use a large value of the order parameter, $\Delta_0 = 0.4t$, to keep the coherence length small.

V. TOPOLOGICAL AND NONTOPOLOGICAL ASPECTS OF THE EDGE CURRENT

The existence of nontopological gradient corrections to the current density means that the integrated edge current will generically evolve from a topological to a nontopological value as the edge is deformed from soft to sharp. This evolution is shown in Fig. 3 for BdG results for a range of edge widths, using the $t' = 3t/8$ lattice model, which are compared to the current predicted by (1).

While the current *density* is never topological near the atomically sharp edges of superconducting crystals, as noted in Sec. III, there do exist special models of chiral p-wave superconductivity for which the *integrated* current at an atomically sharp edge agrees exactly with the "topological" result (1), valid for a soft edge. One such model is the simple case of NN hopping and pairing on the square lattice with an edge along the y direction, the results for which are shown in the inset of Fig. 1(a). In that case, the integrated current is actually independent of the length scale over which the density vanishes at the edge (unlike the case shown in Fig. 3), so it maintains its topological value as we deform a soft edge into a sharp one.

To understand this curious result, we begin by noting a property of the energy spectrum. For the cylindrical geometry considered in Sec. III (open boundary conditions along x, periodic along y), the single-particle energy levels are enumerated by the quasimomentum k_y as well as an eigenvalue j associated with the choice of potential or boundary conditions implemented along x. The usual particle-hole redundancy of the BdG equations is reflected as follows: for each value of j

and k_y, there exists a $\bar{j}$ satisfying

$$E(k_y, j) = -E(-k_y, \bar{j}). \tag{16}$$

This relation allows us to write the integrated current for the cylindrical geometry with NN hopping as

$$I_y = -\frac{1}{4\pi} \int dk_y v_y(k_y) \eta(k_y), \tag{17}$$

where $v_y = 2t \sin k_y$ is the velocity and

$$\eta(k_y) \equiv \sum_j \text{sgn}(E(k_y, j)) \tag{18}$$

is the *spectral asymmetry* [32]. This result—valid for both soft and sharp boundary conditions along x—shows that the only way the *total* integrated edge current (i.e., for a cylinder of width $2L$, the integrated current between $-L$ and $+L$) I_y can change as one or both edges are adiabatically deformed is if there is *spectral flow* of the eigenvalues across zero energy. That is, the total current only changes if unoccupied states [$E(k_y, j) > 0$] evolve to occupied ones [$E(k_y, j) < 0$] or vice versa.

Spectral flow was invoked by Volovik [19] (see also Stone and Gaitan [32]) to argue that the angular momentum of a disk of N superfluid $^3\text{He} - A$ atoms would be equal to $N/2$ in the weak-coupling BCS limit as long as there is no spectral flow as the chemical potential is tuned from large and negative (the so-called "BEC limit" [26,33], where this value for the angular momentum is evident) to the Fermi energy in the BCS limit. The absence of spectral flow in a disk geometry through this BCS-BEC crossover has been confirmed recently for continuum chiral p-wave superfluids in Ref. [34].

We consider instead the related crossover from a soft to a sharp edge in a cylinder geometry, amounting to an evolution of the *local* chemical potential $\mu - A_0(\mathbf{r})$. Specifically, consider the situation in which both boundaries, one at $x \ll 0$ and the other at $x \gg 0$, are initially soft, such that the integrated currents between $(-L, 0)$ and $(0, L)$ are both topological, given by $\pm (C/4\pi)\mu(0)$, where $\mu(0)$ is the bulk chemical potential at $x = 0$. These two currents are equal in magnitude but opposite in sign such that the total integrated current I_y over $(-L, L)$ is zero. Now imagine deforming one of the edges, say the one in the domain $x > 0$, into a sharp one. Since the integrated current over $(-L, 0)$ remains unchanged (the two edges are *very* far apart), the integrated current at the sharp edge will remain equal to its soft-edge value if and only if the total current remains equal to zero. That is, spectral flow as an edge is deformed is required in order for the integrated current at a sharp edge to be different from that at a soft one. In turn, since the total integrated current is initially zero, the spectral asymmetry $\eta(k_y)$ must evolve to a nonzero value.

In Fig. 4, we compare the spectral flows of the BdG spectrum for NN hopping but with order parameters corresponding to NN and NNN pairing as the edge is evolved from soft to sharp. Consistent with the results in Ref. [34], there is no spectral flow for NN pairing for the smoothly varying edge potentials that we consider. This is related to the symmetry protection of the $k_y = 0$ crossing of the chiral edge branch. Particle hole redundancy (16) is incompatible with any continuous shift up or down in energy, as would be required to
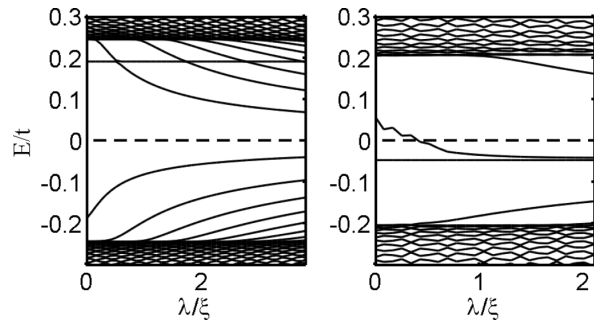
FIG. 4. Spectral flow plots showing the evolution of BdG eigenvalues for $E_{k_y=-0.29\pi}^{(j)}$, $\Delta(\mathbf{k}) = \Delta_0(\sin k_x + i \sin k_y)$ (left) and $E_{k_y=-0.26\pi}^{(j)}$, $\Delta(\mathbf{k}) = \Delta_0(\sin k_x \cos k_y + i \sin k_y \cos k_x)$ (right) for NN-only hopping and $\mu = -t$ as the edge width λ is evolved.

have spectral flow, of the edge modes near $E = 0$ and $k_y = 0$. In the finite strip geometry studied here, the two lowest energy $k_y = 0$ edge modes are separated by a finite gap [which scales as $\exp(-L/\xi_0)$], and so it is clear that one cannot have spectral flow at $k_y = 0$ [34]. However, the symmetry (16) ensures no spectral flow even in the thermodynamic limit where this gap closes. By contrast, zero crossings away from $k_y = 0$ do not individually satisfy (16), but come in pairs with the same chirality, such that the pair of edge modes satisfy (16). In this case, one can continuously shift the states up or down in energy while satisfying (16), so spectral flow is allowed.

The absence of spectral flow for the case of NN pairing explains why the edge current retains its topological value: analogous to the constancy of the angular momentum of a chiral p-wave superfluid through the BCS-BEC crossover, the integrated edge current does not change as the edge is deformed, and it remains equal to the topological value inferred from the gradient expansion. The absence of spectral flow also explains why a continuum chiral p-wave superfluid in a disk with sharp edges [12,18,34] has the same total angular momentum $N/2$ as one confined to a harmonic trap, where the density vanishes slowly [35].

In contrast, for the case of NNN pairing, shown in the lower panel of Fig. 4, there are zeros in the excitation spectrum at momenta $k_y \neq 0, \pi$, giving rise to spectral flow under edge deformation. These zeros arise not only from the additional chiral edge branches that open up when the Chern number changes, but even for lower filling fractions, as the single Majorana branch at zero momentum bends over and crosses $E = 0$ elsewhere as well. For the spectral flow shown in Fig. 4, there is a single Majorana branch ($C = 1$) and the spectral flow is due entirely to this additional zero crossing of this branch. In Fig. 5(a), we show the dispersion for the case in which one edge is sharp while the other is soft. Consistent with the spectral flow shown in Fig. 4, the Majorana branch for the soft edge with a single zero crossing at $k_y = 0$ evolves into one with additional zero crossings at the sharp edge. As with non-p-wave superfluids [34], these zeros at $k_y \neq 0, \pi$ provide channels for spectral flow, and hence a nonzero spectral asymmetry [see Fig. 5(b)] and nontopological value of the integrated current moving to the sharp-edge limit.
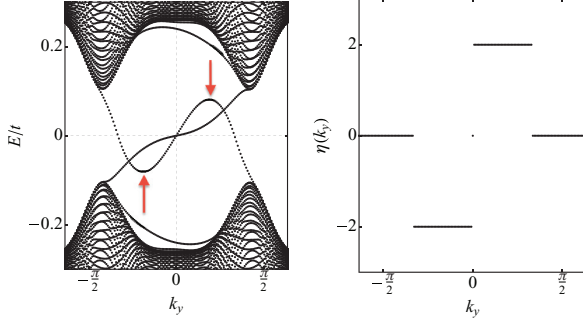
FIG. 5. (Color online) Dispersion (left) and spectral asymmetry (right) for the NNN-pairing model $\Delta(\mathbf{k}) = \Delta_0(\sin k_x \cos k_y + i \sin k_y \cos k_x)$ for NN-only hopping at $\mu = -t$ where one edge is sharp and the other is soft. Left: arrows point to the Majorana branch at the sharp edge. Unlike the soft-edge branch, which only crosses zero at $k_y = 0$, the sharp-edge branch has an additional zero crossing away from $k_y = 0$, as expected from the spectral flow shown in Fig. 4. This extra zero crossing gives rise to the nonzero spectral asymmetry shown in the right panel.

Introducing NNN hopping, the integrated edge current can be written as a sum of (17) and another component I'_y involving the NNN velocity operator $v'_y \equiv 4t' \sin k_y f(a)$, where a is some quantum number appropriate for the potential or boundary conditions implemented along x, and f reduces to $\cos k_x$ in the sharp-edge limit. As the edge is deformed, $f(a)$ and hence I'_y will evolve even without spectral flow across zero energy, although the component described by (17) will remain constant without it.

VI. DISCUSSION

In this paper, we have reconciled the nonuniversal and nontopological nature of the edge currents in chiral p-wave superconductors, as inferred from BdG calculations [3,4,6,36], with naive expectations for a topological value based on the leading-order Chern-Simons term in a gradient expansion of the action [13,15]. While the integrated edge current is always dictated by a Chern number in the soft edge limit in which the density varies over a length scale much longer than the coherence length—as would happen, for instance, in a chiral p-wave atomic gas superfluid confined to a harmonic trap [35]—nontopological gradient corrections to the current can arise outside this limit. Using numerical BdG and quasiclassical calculations of lattice p-wave superconductors, we have investigated the evolution of the integrated edge current as the edge is evolved from soft to sharp. Symmetry-allowed physics such as next-nearest-neighbor hopping and gap anisotropy lead to evolution away from the topological value.

In the special cases—certain lattice models with restricted hopping as well as the continuum limit of all models—where the integrated current is found to be topological when the edge is sharp, we have shown how this result follows from the soft-edge topological value by invoking the spectral flow of the BdG eigenvalues as the edge is deformed. In general, however, the nontopological nature of the edge current in a topological superconductor means that the edge current is

sensitive to effects such as band structure [3–6] and gap anisotropy, as well as to disorder and pair-breaking surface effects [30]. Even for a topologically trivial superconductor with zero Chern number, such as would arise in the putative chiral p-wave superconductor Sr_2RuO_4 were pairing only to arise on the quasi-one-dimensional α and β bands [37], the edge current is generically substantial [3,4,36].

On the other hand, the nontopological nature of the edge current means that circumstances could arise in Sr_2RuO_4 [4], in which the total edge current arising from all three bands is strongly suppressed compared to predictions based on continuum systems [6,7]. For instance, even with a fixed band structure, gap anisotropy can reduce the edge current substantially below naive expectations. Large-gap anisotropy has been predicted from weak-coupling renormalization-group calculations [37–39]. Note that the reduction in current due to gap anisotropy discussed here is present in the clean limit and is unrelated to the disorder effect suggested in Ref. [38], although disorder near the surface or interface can further reduce the current. If a sufficiently anisotropic gap is present in Sr_2RuO_4, this reduction, along with some interface effect [4,20,36,40], may reconcile theory with experiment.

APPENDIX A: TOPOLOGICAL EXPRESSIONS FOR THE EDGE CURRENT IN LATTICE MODELS

Integrating (1) gives $I_y = C(\mu)[A_0(x_{\text{edge}}) - A_0(\text{bulk})]/4\pi$ for the integrated edge current where the location x_{edge} of the edge is determined by the point where the effective local chemical potential $\mu - A_0(x)$ equals its "vacuum value" μ_{vac}. Assuming that A_0 is zero in the bulk, this result can thus be written as

$$I_y = C(\mu)[\mu - \mu_{\text{vac}}]/4\pi. \tag{A1}$$

The value of μ_{vac} depends on whether the Fermi surface (FS) is hole- or electronlike. In the former case, it corresponds to the value of the chemical potential at the top of the band, whereas in the latter case, it is the chemical potential at the bottom of the band. For the model with no NNN hopping, $\mu_{\text{vac}} = -4t$ in the bottom half of the band ($\mu < 0$) and $4t$ in the top half ($\mu > 0$), and (A1) reduces to

$$I_y = \frac{1}{4\pi}(4t - |\mu|). \tag{A2}$$

For $t' \neq 0$, the topological expression fails to describe the current at intermediate μ, and so we restrict our attention to μ near the bottom and top of the band. For $t' = 3t/8$, there is a van Hove singularity at $\mu = 1.5t$ where the FS changes from being electronlike to holelike. This change is accompanied

by a change in the Chern number from $C = 1$ to -1. For the electronlike FS, the bottom of the band is $\mu_{\text{vac}} = -5.5t$. For the holelike FS, the top of the band is $\mu_{\text{vac}} = 2.5t$. Thus, using (A1),

$$I_y = \begin{cases} \frac{1}{4\pi}(5.5t + \mu) & \text{for } \mu \text{ near band bottom.} \\ \frac{1}{4\pi}(2.5t - \mu) & \text{for } \mu \text{ near band top.} \end{cases} \quad \text{(A3)}$$

For $t' = t$ and $\mu < 0$, there is an electronlike FS with $C = 1$ and $\mu_{\text{vac}} = -8t$. For $\mu > t$, there are two hole pockets, each with $C = 1$ for a total Chern number of 2, and $\mu_{\text{vac}} = 4t$. Hence,

$$I_y = \begin{cases} \frac{1}{4\pi}(8t + \mu) & \text{for } \mu \text{ near band bottom.} \\ \frac{2}{4\pi}(\mu - 4t) & \text{for } \mu \text{ near band top.} \end{cases} \quad \text{(A4)}$$

APPENDIX B: QUASICLASSICAL EXPRESSION FOR THE EDGE CURRENT

In this section, we extend the calculation of the integrated edge current in Ref. [18] to an arbitrary band structure and either two or three spatial dimensions. We consider a single-band problem on a lattice, near an edge or (surface) parallel to a reflection plane of the bulk band structure. In three dimensions, we further assume a symmetry of the superconducting state under reflection through a horizontal plane. For triplet order parameters, we assume a fixed **d**-vector axis, which we take to be **z**, so that the spin structure is trivial for both triplet and singlet cases. We assume a chiral order parameter $\Delta_x(\vec{p}) + i\Delta_y(\vec{p})$, where $\Delta_{x,y}$ are real and $\vec{p}$ represents a momentum vector on the Fermi surface (FS). Furthermore, we neglect the texture of the order parameter in the vicinity of the edge, and so we take $\Delta_{x,y}$ to equal their uniform bulk values. Note that the presence of a sharp edge formally invalidates the quasiclassical approximation, which is valid only on length scales much greater than k_F^{-1}, so the edge physics is incorporated here as a phenomenological boundary condition. Form the quasiclassical propagator,

$$\widehat{\mathcal{G}}(\vec{r}, \vec{p}; i\omega_n) = \begin{pmatrix} g(\vec{r}, \vec{p}; i\omega_n) & f(\vec{r}, \vec{p}; i\omega_n) \\ f^*(\vec{r}, \vec{p}; i\omega_n) & -g(\vec{r}, \vec{p}; i\omega_n) \end{pmatrix}. \quad \text{(B1)}$$

This object is essentially the Nambu propagator integrated with respect to relative momentum. It depends on the center-of-mass position $\vec{r}$, the Fermi surface momentum $\vec{p}$, and the Matsubara frequency $\omega_n \equiv (2n + 1)\pi T$. $\widehat{\mathcal{G}}$ obeys the Eilenberger equation:

$$i\vec{v} \cdot \nabla_{\vec{r}}\widehat{\mathcal{G}} = -[\widehat{\mathcal{H}}, \widehat{\mathcal{G}}], \quad \text{where} \quad \text{(B2)}$$

$$\widehat{\mathcal{H}} = \begin{pmatrix} i\omega_n & \Delta_x(\vec{p}) - i\Delta_y(\vec{p}) \\ -\Delta_x(\vec{p}) - i\Delta_y(\vec{p}) & -i\omega_n \end{pmatrix} \quad \text{(B3)}$$

and $\vec{v}$ is the Fermi velocity at momentum $\vec{p}$ (with $\vec{p}$ on the Fermi surface). $\widehat{\mathcal{G}}$ is taken to obey the normalization condition

$$(\widehat{\mathcal{G}})^2 = -\pi^2. \quad \text{(B4)}$$

If we decompose $\widehat{\mathcal{G}}$ into Pauli matrices according to

$$\widehat{\mathcal{G}} = g\widehat{\tau}_3 + if_2\widehat{\tau}_1 - if_1\widehat{\tau}_2, \quad \text{(B5)}$$

and form the column vector

$$|\mathcal{G}\rangle = \begin{pmatrix} f_1 \\ f_2 \\ g \end{pmatrix}, \quad \text{(B6)}$$

then $|\mathcal{G}\rangle$ obeys the (vector) differential equation

$$\frac{1}{2}\vec{v} \cdot \nabla_{\vec{r}}|\mathcal{G}\rangle = \widehat{M}|\mathcal{G}\rangle, \quad \text{where} \quad \text{(B7)}$$

$$\widehat{M} = \begin{pmatrix} 0 & i\omega_n & \Delta_y \\ -i\omega_n & 0 & -\Delta_x \\ \Delta_y & -\Delta_x & 0 \end{pmatrix}. \quad \text{(B8)}$$

Solutions to (B7) are exponential in position, with the decay length determined by the eigenvalues of $\widehat{M}$. Since $\widehat{M}$ is Hermitian these are real, and they have eigenvectors

$$|0; \vec{p}\rangle = \frac{1}{\lambda}\begin{pmatrix} -\Delta_x \\ -\Delta_y \\ i\omega_n \end{pmatrix} \quad \text{(B9)}$$

for eigenvalue 0, where $\lambda = \sqrt{\omega_n^2 + \Delta_x^2 + \Delta_y^2}$, and

$$|\pm; \vec{p}\rangle = \frac{1}{\sqrt{2}\lambda\lambda_1}\begin{pmatrix} \pm i\omega_n\lambda - \Delta_x\Delta_y \\ \lambda_1^2 \\ i\omega_n\Delta_y \mp \lambda\Delta_x \end{pmatrix} \quad \text{(B10)}$$

for eigenvalues $\pm\lambda$, where $\lambda_1 = \sqrt{\omega_n^2 + \Delta_x^2}$. We now assume the edge is along $x = 0$, with the superconductor in the region $x > 0$, and we use translation invariance along y to write down the generic solution of (B7):

$$|\mathcal{G}(x, \vec{p})\rangle = C_0|0; \vec{p}\rangle + C_+ \exp\left(\frac{2\lambda}{v_x}x\right)|+; \vec{p}\rangle$$
$$+ C_- \exp\left(-\frac{2\lambda}{v_x}x\right)|-; \vec{p}\rangle. \quad \text{(B11)}$$

We must exclude solutions that explode as $x \to +\infty$. If we define $s \equiv \text{sgn}(v_x)$, then

$$|\mathcal{G}(x, \vec{p})\rangle = C_0|0; \vec{p}\rangle + C_{-s}\exp\left(-\frac{2\lambda}{|v_x|}x\right)|-s; \vec{p}\rangle. \quad \text{(B12)}$$

The normalization condition fixes $C_0 = -\pi$. C_{-s} is determined by boundary conditions at $x = 0$, namely that $|\mathcal{G}(0, \vec{p})\rangle = |\mathcal{G}(0, \underline{\vec{p}})\rangle$, where $\underline{\vec{p}}$ is the specular reflection of $\vec{p}$, i.e., $\underline{\vec{p}} = (-p_x, p_y)$. Applying this condition yields

$$C_{-s} = \frac{\sqrt{2}\pi\Delta_x\lambda_1}{i\omega_n\lambda s + \Delta_x\Delta_y}. \quad \text{(B13)}$$

The current density is computed from the normal part of the propagator according to

$$\vec{J}(\vec{r}) = \frac{2T}{(2\pi)^d}\sum_{i\omega_n}\oint_{\text{FS}}\frac{d\vec{p}}{|\vec{v}|}\vec{v} \times g(\vec{r}, \vec{p}; i\omega_n), \quad \text{(B14)}$$

where d is the spatial dimension. The current flows solely in the y direction and depends only on x:

$$J_y(x) = \frac{2T}{(2\pi)^d}\sum_{i\omega_n}\oint_{\text{FS}}\frac{d\vec{p}}{|\vec{v}|}v_y \times g(x, \vec{p}; i\omega_n). \quad \text{(B15)}$$

Our solution for the normal part of the propagator can be written

$$g(x, \vec{p}; i\omega_n) = -\pi \frac{i\omega_n}{\lambda} + \pi \frac{\Delta_x}{\lambda} \frac{i\omega_n \Delta_x - \lambda s \Delta_y}{(i\omega_n)^2 - \Delta_y^2}$$
$$\times \exp\left(-\frac{2\lambda}{|v_x|}x\right). \quad (B16)$$

The only part of the above whose contribution to the current density does not vanish by symmetry is

$$\tilde{g}(x, \vec{p}; i\omega_n) = \pi \frac{s\Delta_x \Delta_y}{\omega_n^2 + \Delta_y^2} \exp\left(-\frac{2\lambda}{|v_x|}x\right). \quad (B17)$$

We compute the integrated current

$$I_y = \int_0^\infty dx \, J_y(x)$$
$$= \frac{2T}{(2\pi)^d} \int_0^\infty dx \sum_{i\omega_n} \oint_{\text{FS}} \frac{d\vec{p}}{|\vec{v}|} v_y \times \tilde{g}(x, \vec{p}; i\omega_n)$$
$$= \frac{1}{2(2\pi)^d} \oint_{\text{FS}} \frac{d\vec{p}}{|\vec{v}|} v_x v_y \Delta_x \Delta_y 2\pi T \sum_{i\omega_n} \frac{1}{\lambda} \frac{1}{\omega_n^2 + \Delta_y^2}. \quad (B18)$$

In the zero-temperature limit, the Matsubara sum becomes an integral: $2\pi T \sum_{i\omega_n} \to \int d\omega$,

$$I_y = \frac{1}{2(2\pi)^d} \oint_{\text{FS}} \frac{d\vec{p}}{|\vec{v}|} v_x v_y \Delta_x \Delta_y$$
$$\times \int_{-\infty}^\infty d\omega \frac{1}{\sqrt{\omega^2 + \Delta_x^2 + \Delta_y^2}} \frac{1}{\omega^2 + \Delta_y^2}. \quad (B19)$$

The integral has a closed-form solution:

$$\int_{-\infty}^\infty d\omega \frac{1}{\sqrt{\omega^2 + \Delta_x^2 + \Delta_y^2}} \frac{1}{\omega^2 + \Delta_y^2}$$
$$= \frac{2}{|\Delta_x||\Delta_y|} \tan^{-1}\left(\frac{|\Delta_x|}{|\Delta_y|}\right) \quad (B20)$$

yielding

$$I_y = \frac{1}{(2\pi)^d} \oint_{\text{FS}} \frac{d\vec{p}}{|\vec{v}|} v_x v_y \tan^{-1}\left(\frac{\Delta_x}{\Delta_y}\right). \quad (B21)$$

Equation (B21) is the main result. It shows that the edge current, unless prohibited by symmetry, is generically equal to the Fermi energy times a number of order 1 and fundamental constants.

Up until now we have taken the order parameter to be chiral, but we assumed nothing about its symmetry and very little about the point group symmetry. We now specialize to a tetragonal point group and consider various possible chiral order parameters. For an order parameter of symmetry $d_{xy} + id_{x^2-y^2}$, the total current of Eq. (B21) vanishes by symmetry. The total current also vanishes by symmetry (under reflection $y \to -y$) for a $d_{x^2-y^2} + is$ order parameter, though the analysis above does not directly apply in that case.

When $\Delta_{x,y}$ corresponds to a two-dimensional representation of the tetragonal point group (i.e., the order parameter has either $p_x + ip_y$ or $d_{xz} + id_{yz}$ symmetry), there is a useful

simplification of (B21). Under a 90° rotation in the $k_x k_y$ plane,

$$\Delta_x \to \Delta_y, \quad \Delta_y \to -\Delta_x, \quad v_x \to v_y, \quad v_y \to -v_x.$$
$$v_x v_y \tan^{-1}\left(\frac{\Delta_x}{\Delta_y}\right) \to v_x v_y \tan^{-1}\left(\frac{\Delta_y}{\Delta_x}\right)$$
$$= v_x v_y \left[\frac{\pi}{2}\text{sgn}(\Delta_x \Delta_y) - \tan^{-1}\left(\frac{\Delta_x}{\Delta_y}\right)\right].$$

Accordingly, the relative magnitudes of $\Delta_{x,y}$ are unimportant, and the zero-temperature current is determined only by the sign structure of the order parameter components on the Fermi surface:

$$I_y = \frac{\pi}{4(2\pi)^d} \oint_{\text{FS}} \frac{d\vec{p}}{|\vec{v}|} v_x v_y \text{sgn}(\Delta_x \Delta_y). \quad (B22)$$

In the absence of "accidental" zeros of either order parameter component, the dependence on $\Delta_{x,y}$ drops out entirely, except for the overall chirality $\eta = \text{sgn}(v_x v_y \Delta_x \Delta_y)$:

$$I_y = \frac{\pi \eta}{4(2\pi)^d} \oint_{\text{FS}} \frac{d\vec{p}}{|\vec{v}|} |v_x v_y|. \quad (B23)$$

For the special case of a two-dimensional system in which the dispersion relation separates according to $\epsilon(k) = \epsilon_x(k_x) + \epsilon_y(k_y)$, this simplifies to

$$I_y = \frac{\pi\eta}{(2\pi)^2} \int_{\text{first quadrant}} dp_y v_y = \frac{\eta}{4\pi} \int_0^\mu d(\epsilon_y) = \frac{\eta\mu}{4\pi}, \quad (B24)$$

which coincides with the result gleaned from the gradient expansion, with η equal to the Chern number.

APPENDIX C: GRADIENT EXPANSION OF THE MEAN-FIELD BCS ACTION FOR A CHIRAL p-WAVE SUPERCONDUCTOR

The effective Euclidean Bose action for a superconductor has the usual form [41,42]

$$S_{\text{eff}} = -\int d^{2+1}x \int d^{2+1}x' \frac{|\Delta(x,x')|^2}{V(\mathbf{r},\mathbf{r}')} - \text{Tr}\ln \hat{\boldsymbol{G}}^{-1}, \quad (C1)$$

where $V(\mathbf{r},\mathbf{r}')$ is the attractive effective interaction that supports p-wave superconductivity and $x = (\mathbf{r},\tau)$, where $\tau \equiv it$ is the Wick-rotated imaginary time variable. Consistent with mean-field BdG, we will deal with the mean-field, "saddle-point" value of this action by ignoring fluctuations of the phase of the order parameter. The inverse of the mean-field 2×2 matrix Nambu-Gorkov Green's

function is thus ($\hbar = e = c = 1$)

$$\hat{G}^{-1}(x,x') = \begin{pmatrix} \left[-\partial_\tau - \frac{(-i\nabla+\mathbf{A})^2}{2m} + \mu + A_0\right]\delta(x-x') & \Delta(\mathbf{r},\mathbf{r}')\delta(\tau-\tau') \\ \Delta^*(\mathbf{r}',\mathbf{r})\delta(\tau-\tau') & \left[-\partial_\tau + \frac{(i\nabla+\mathbf{A})^2}{2m} - \mu - A_0\right]\delta(x-x') \end{pmatrix},$$

where the minimal coupling scheme $\partial_\tau \to \partial_\tau - A_0$, $\nabla \to \nabla + i\mathbf{A}$ has been used.

We now expand (C1) in gradients of the static potential

$$A_0(\mathbf{r}) = A_0 \sin \mathbf{Q} \cdot \mathbf{r} \qquad (C2)$$

as well as gradients of the order parameter amplitudes

$$\Delta_\alpha(x,x') = \Delta_{0,\alpha}(\mathbf{r}-\mathbf{r}')\eta_\alpha\left(\frac{\mathbf{r}+\mathbf{r}'}{2}\right)\delta(\tau-\tau') \qquad (C3)$$

with

$$\eta_\alpha(\mathbf{r}) = 1 + \lambda_\alpha \sin \mathbf{Q} \cdot \mathbf{r}. \qquad (C4)$$

Here $\Delta_{0,\alpha}$ are the complex mean-field order parameter components for $\alpha = x,y$ (only dependent on the relative coordinate $\mathbf{r} - \mathbf{r}'$) and η_α is the corresponding amplitude, equal to unity in the absence of an external potential. A gradient expansion need not be applied to the vector potential $\mathbf{A}(\mathbf{r})$ since this will be set to zero at the end of the calculation of the current and we can simply treat it as small, retaining only terms in the action that are linear in $\mathbf{A}$.

Fourier transforming (C1) to Matsubara frequency/momentum space $k \equiv (\mathbf{k},i\omega_n)$, the logarithm is expanded as

$$\text{Tr}\ln[\hat{G}(k,k')^{-1}] = \text{Tr}\ln\left[\hat{G}_0^{-1}\right] + \text{Tr}[(\hat{G}_0\hat{\Sigma})] + \frac{1}{2}\text{Tr}[(\hat{G}_0\hat{\Sigma})^2] + \cdots, \qquad (C5)$$

where ($\hat{\tau}_\alpha$ are Pauli matrices)

$$\hat{G}_0^{-1}(k) = i\omega_n - \xi(\mathbf{k})\hat{\tau}_3 + \text{Re}\Delta_0(\mathbf{k})\hat{\tau}_1 - \text{Im}\Delta_0(\mathbf{k})\hat{\tau}_2, \qquad (C6)$$

$$\hat{\Sigma}(k,k') = -\frac{1}{m}\sum_\mathbf{q} \mathbf{A}(\mathbf{q}) \cdot (\mathbf{k} - \mathbf{q}/2)\delta_{\mathbf{k'},\mathbf{k}-\mathbf{q}} + \left\{\left[\frac{A_0}{2i}\hat{\tau}_3 \right.\right.$$
$$\left.+ \frac{\lambda_\alpha}{2i}[\text{Re}\Delta_\alpha(\mathbf{k}-\mathbf{Q}/2)\hat{\tau}_1 - \text{Im}\Delta_\alpha(\mathbf{k}-\mathbf{Q}/2)\hat{\tau}_2]\right]$$
$$\left. \times \delta_{\mathbf{k'},\mathbf{k}-\mathbf{Q}} - (\mathbf{Q} \to -\mathbf{Q})\right\}, \qquad (C7)$$

and the trace is performed over frequency and momentum variables in addition to Nambu indices. $\hat{\Sigma} = 0$ when $\mathbf{Q} = \mathbf{0}$ and $\mathbf{A} = \mathbf{0}$, and consequently (C5) constitutes a perturbative expansion in powers of $\mathbf{Q}$ and $\mathbf{A}$.

Using (C6) and (C7) in (C5), the leading-order gradients terms in the action [given by the second term on the right-hand side of (C5) and discarding terms of order $\mathbf{A}^2$] are (from hereon in, we reserve μ and ν to denote Cartesian components x,y)

$$S^{(2)} = \frac{A_0 A_\mu(\mathbf{Q})}{2i}\chi_{0\mu}(\mathbf{Q}) + \frac{\lambda_\mu A_\nu(\mathbf{Q})}{2i}\chi_{\Delta_\mu\nu}(\mathbf{Q}) - (\mathbf{Q} \to -\mathbf{Q}). \qquad (C8)$$

Here we only show the gradient terms involving the vector potential $\mathbf{A}$ since only these contribute to the current. The following *static* correlation functions have been defined [$k \equiv (\omega_n,\mathbf{k})$ and $q \equiv (0,\mathbf{Q})$, where ω_n is a Fermi-Matsubara frequency and the external Bose-Matsubara frequency is zero]:

$$\chi_{0\mu}(\mathbf{Q}) \equiv \frac{1}{\beta}\sum_k v_\mu(\mathbf{k})\text{tr}\left[\hat{G}_0\left(k+\frac{q}{2}\right)\hat{\tau}_3\hat{G}_0\left(k-\frac{q}{2}\right)\right] \qquad (C9)$$

is the density-current correlation function, and, taking $\Delta_x(\mathbf{k})$ and $\Delta_y(\mathbf{k})$ to be purely real and imaginary, respectively,

$$\chi_{\Delta_x\nu}(\mathbf{Q}) \equiv \frac{1}{\beta}\sum_k \Delta_x(\mathbf{k})v_\nu(\mathbf{k})\text{tr}\left[\hat{G}_0\left(k+\frac{q}{2}\right)\hat{G}_0\left(k-\frac{q}{2}\right)\hat{\tau}_1\right],$$
$$\times \chi_{\Delta_y\nu}(\mathbf{Q})$$
$$\equiv -\frac{1}{\beta}\sum_k \Delta_y(\mathbf{k})v_\nu(\mathbf{k})\text{tr}\left[\hat{G}_0\left(k+\frac{q}{2}\right)\hat{G}_0\left(k-\frac{q}{2}\right)\hat{\tau}_2\right] \qquad (C10)$$

are the order parameter–current correlation functions. $v_\mu \equiv \partial_{k_\mu}\xi(\mathbf{k})$ is the bare velocity vertex.

Continuing with the gradient expansion, we expand the static correlation functions (C9) and (C10) in powers of $\mathbf{Q}$. At $T = 0$,

$$\chi_{0y}(\mathbf{Q}) = -iQ_x\sum_\mathbf{k} \frac{v_y\Delta_y(\partial_{k_x}\Delta_x)}{2E_\mathbf{k}^3} + O(\mathbf{Q}^3), \quad (C11)$$

$$\chi_{0x}(\mathbf{Q}) = iQ_y\sum_\mathbf{k} \frac{v_y\Delta_y(\partial_{k_x}\Delta_x)}{2E_\mathbf{k}^3} + O(\mathbf{Q}^3), \quad (C12)$$

$$\chi_{\Delta_x\mu}(\mathbf{Q}) = -iQ_\nu\sum_\mathbf{k} \frac{v_\mu\Delta_x}{2E_\mathbf{k}^3}\left[v_\nu\Delta_y - \xi(\partial_{k_\nu}\Delta_y)\right] + O(\mathbf{Q}^3), \qquad (C13)$$

and

$$\chi_{\Delta_y\mu}(\mathbf{Q}) = iQ_\nu\sum_\mathbf{k} \frac{v_\mu\Delta_y}{2E_\mathbf{k}^3}\left[v_\nu\Delta_x - \xi(\partial_{k_\nu}\Delta_x)\right] + O(\mathbf{Q}^3). \qquad (C14)$$

The first terms in the square brackets in (C11) and (C12) are both equal to the Chern number modulo particle-hole corrections:

$$\sum_\mathbf{k} \frac{v_y\Delta_y(\partial_{k_x}\Delta_x)}{2E_\mathbf{k}^3} = \sum_\mathbf{k} \frac{v_x\Delta_x(\partial_{k_y}\Delta_y)}{2E_\mathbf{k}^3}$$
$$= \frac{C}{4\pi} + O\left(\Delta_0^2/E_F^2\right). \qquad (C15)$$

Note that this is the static Hall conductivity $\tilde{\sigma}_{xy}$ defined in Sec. II. Turning to (C13) and (C14), the first term in square brackets is the γ coefficient, also shown in (14). The second term in both expressions is $O(\Delta_0^2/E_F^2)$ and is related to the difference in the Ginzburg-Landau coefficients k_3 and k_4 [30], which can also be obtained from the order parameter–current

correlation function (C10), albeit in the limit $T \to T_c$ instead of $T = 0$.

Using the long-wavelength limiting values (C11)–(C15) in (C8) and Fourier-transforming back to real space gives the Chern-Simons action (12) plus the amplitude contribution (13).

The generalization of the above results to lattice models is straightforward. As long as the coherence length ξ_0 is much longer than $k_F^{-1} \sim a$, where a is the lattice spacing, the

hydrodynamic Lagrangian retains the same form as (12), with only a few minor modifications to the coefficients. For a single-band model, one can simply use the expressions (C11)–(C15) for the hydrodynamic coefficients using values appropriate for a lattice model, e.g., (7) and (8) instead of $\xi(\mathbf{k}) = \mathbf{k}^2/2m - \mu$ and $\Delta_0(\mathbf{k}) = \Delta_0(k_x + ik_y)/k_F$. For multiband models, one must go back and evaluate the correlation functions (C9) and (C10) using the appropriate higher-dimensional matrix Green's functions.

[1] C. W. J. Beenakker, Annu. Rev. Condens. Matter **4**, 113 (2013).

[2] Q. Niu, D. J. Thouless, and Y.-S. Wu, Phys. Rev. B **31**, 3372 (1985).

[3] Y. Imai, K. Wakabayashi, and M. Sigrist, Phys. Rev. B **88**, 144503 (2013).

[4] S. Lederer, W. Huang, E. Taylor, S. Raghu, and C. Kallin, Phys. Rev. B **90**, 134521 (2014).

[5] Y. Imai, K. Wakabayashi, and M. Sigrist, J. Phys. Soc. Jpn. **83**, 124712 (2014).

[6] M. Matsumoto and M. Sigrist, J. Phys. Soc. Jpn. **68**, 994 (1999).

[7] A. Furusaki, M. Matsumoto, and M. Sigrist, Phys. Rev. B **64**, 054514 (2001).

[8] J. R. Kirtley, C. Kallin, C. W. Hicks, E.-A. Kim, Y. Liu, K. A. Moler, Y. Maeno, and K. D. Nelson, Phys. Rev. B **76**, 014526 (2007).

[9] C. W. Hicks, J. R. Kirtley, T. M. Lippman, N. C. Koshnick, M. E. Huber, Y. Maeno, W. M. Yuhasz, M. B. Maple, and K. A. Moler, Phys. Rev. B **81**, 214501 (2010).

[10] J. Jang, D. G. Ferguson, V. Vakaryuk, R. Budakian, S. B. Chung, P. M. Goldbart, and Y. Maeno, Science **331**, 186 (2011).

[11] P. J. Curran, S. J. Bending, W. M. Desoky, A. S. Gibbs, S. L. Lee, and A. P. Mackenzie, Phys. Rev. B **89**, 144504 (2014).

[12] M. Stone and R. Roy, Phys. Rev. B **69**, 184511 (2004).

[13] G. E. Volovik, JETP **67**, 1804 (1988).

[14] G. E. Volovik, JETP **55**, 368 (1992).

[15] J. Goryo and K. Ishikawa, Phys. Lett. A **246**, 549 (1998).

[16] S. M. Girvin and A. H. MacDonald, Phys. Rev. Lett. **58**, 1252 (1987).

[17] S. C. Zhang, T. H. Hansson, and S. Kivelson, Phys. Rev. Lett. **62**, 82 (1989).

[18] J. A. Sauls, Phys. Rev. B **84**, 214509 (2011).

[19] G. E. Volovik, JETP **61**, 958 (1995).

[20] T. Scaffidi and S. H. Simon, arXiv:1410.6073.

[21] A. P. Mackenzie and Y. Maeno, Rev. Mod. Phys. **75**, 657 (2003).

[22] C. Kallin and A. J. Berlinsky, J. Phys.: Condens. Matter **21**, 164210 (2009).

[23] C. Kallin, Rep. Prog. Phys. **75**, 042501 (2012).

[24] Y. Maeno, S. Kittaka, T. Nomura, S. Yonezawa, and K. Ishida, J. Phys. Soc. Jpn. **81**, 011009 (2012).

[25] R. Roy and C. Kallin, Phys. Rev. B **77**, 174513 (2008).

[26] N. D. Mermin and P. Muzikar, Phys. Rev. B **21**, 980 (1980).

[27] A. Damascelli, D. H. Lu, K. M. Shen, N. P. Armitage, F. Ronning, D. L. Feng, C. Kim, Z.-X. Shen, T. Kimura, Y. Tokura, Z. Q. Mao, and Y. Maeno, Phys. Rev. Lett. **85**, 5194 (2000).

[28] W. Huang, E. Taylor, and C. Kallin, Phys. Rev. B **90**, 224519 (2014).

[29] V. Ambegaokar, P. G. de Gennes, and D. Rainer, Phys. Rev. A **9**, 2676 (1974).

[30] P. E. C. Ashby and C. Kallin, Phys. Rev. B **79**, 224509 (2009).

[31] In the sharp-edge limit, the short-distance physics of A_0 is implicitly incorporated as phenomenological boundary conditions on the order parameter identical to those employed in Ginzburg-Landau calculations.

[32] M. Stone and F. Gaitan, Ann. Phys. (NY) **178**, 89 (1987).

[33] A. J. Leggett, in *Modern Trends in the Theory of Condensed Matter*, Lecture Notes in Physics Vol. 115 (Springer, Berlin, 1980), p. 13.

[34] Y. Tada, W. Nie, and M. Oshikawa, arXiv:1409.7459.

[35] M. Stone and I. Anduaga, Ann. Phys. (NY) **323**, 2 (2008).

[36] Y. Imai, K. Wakabayashi, and M. Sigrist, Phys. Rev. B **85**, 174532 (2012).

[37] S. Raghu, A. Kapitulnik, and S. A. Kivelson, Phys. Rev. Lett. **105**, 136401 (2010).

[38] Q.-H. Wang, C. Platt, Y. Yang, C. Honerkamp, F. C. Zhang, W. Hanke, T. Rice, and R. Thomale, Europhys. Lett. **104**, 17013 (2013).

[39] T. Scaffidi, J. C. Romers, and S. H. Simon, Phys. Rev. B **89**, 220510 (2014).

[40] A. Bouhon and M. Sigrist, Phys. Rev. B **90**, 220511(R) (2014).

[41] V. N. Popov, *Functional Integrals and Collective Excitations* (Cambridge University Press, Cambridge, 1987).

[42] I. J. R. Aitchison, P. Ao, D. J. Thouless, and X.-M. Zhu, Phys. Rev. B **51**, 6531 (1995).

Chapter 5

Suppression of edge currents in Sr_2RuO_4 by surface disorder

5.1 Preface We now present a calculation of the edge current in a multi-band chiral p-wave model of Sr_2RuO_4. This work was originally motivated by a weak coupling RG analysis which suggested dominant superconductivity on the two quasi-1D bands.[73] In the proposed microscopic model, the chiral p-wave pairings on the two-bands are characterized by opposite Chern numbers, which render the ground state topologically trivial. This was conjectured to lead to vanishing edge current, thus explaining the experimental null results.[60, 61, 62]

However, as we have seen in the preceding chapters, edge current is generically unrelated to the underlying topological properties, and can also arise in a topologically trivial but TRSB superconductor. Indeed, Imai *et al.*[67] have shown that simple two-band models of Sr_2RuO_4 also exhibit substantial edge current.

Here, we carry out systematic self-consistent BdG calculations for the one-band (γ) and two-band (α&β) chiral p-wave models of Sr_2RuO_4. In agreement with the previous studies, we also found a non-vanishing edge current in our two-band model. More importantly, we

examine the scenarios with sufficiently strong surface disorder to result in a metallic surface region. Combined with lattice effects, this results in a substantial suppression of the edge current. Our numerical results are qualitatively consistent with the Ginzburg-Landau theories. In addition, due to the abundance of low-energy edge states in the two-band model, the total edge current is more rapidly suppressed in that model as the temperature increases.

This study has subsequently been substantiated by another work,[66] which uses a more realistic anisotropic chiral p-wave superconducting gaps obtained from a microscopic weak coupling calculation.[77]

5.2 Publication

Suppression of spontaneous currents in Sr$_2$RuO$_4$ by surface disorder

Samuel Lederer,[1] Wen Huang,[2] Edward Taylor,[2] Srinivas Raghu,[1,3] and Catherine Kallin[2,4]

[1]*Department of Physics, Stanford University, Stanford, California, 94305, USA*

[2]*Department of Physics and Astronomy, McMaster University, Hamilton, Ontario, L8S 4M1, Canada*

[3]*SLAC National Accelerator Laboratory, 2575 Sand Hill Road, Menlo Park, California 94025, USA*

[4]*Canadian Institute for Advanced Research, Toronto, Ontario M5G 1Z8, Canada*

A major challenge to the chiral *p*-wave hypothesis for the pairing symmetry of the unconventional superconductor Sr$_2$RuO$_4$ is the null result of sensitive scanning magnetometry experiments designed to detect the expected spontaneous charge currents. Motivated by junction tunneling conductance measurements, which indicate the quenching of superconductivity at the surfaces of even high-purity samples, we examine the spontaneous currents in a chiral *p*-wave superconductor near a normal metal/superconductor interface using the lattice Bogoliubov-de Gennes equations and Ginzburg-Landau theory, and find that the edge current is suppressed by more than an order of magnitude compared to previous estimates. These calculations demonstrate that interface details can have a quantitatively meaningful effect on the expectations for magnetometry experiments.

I. INTRODUCTION

Strontium Ruthenate, Sr$_2$RuO$_4$, is an unconventional superconductor ($T_c = 1.5$ K) [1] for which there exists substantial evidence for odd-parity pairing [2–5] as well as for the spontaneous breaking of time reversal symmetry below T_c [6–8]. These observations lead naturally to the conclusion that the pairing symmetry is chiral *p* wave ($p_x \pm i p_y$), a two-dimensional analog of the A phase of superfluid ^{3}He. Though this is the leading phenomenological hypothesis, it is seemingly contradicted by several experiments. Prominent among these are high-resolution scanning magnetometry measurements [9–11], which image magnetic fields across several μm of sample (including the sample edge) and see no sign of the expected spontaneous currents.

The presence of spontaneous, persistent charge currents at edges and domain walls is a robust consequence of time-reversal symmetry breaking superconductivity. However, the magnitude of these currents is determined by microscopic details—they are neither quantized nor universal. The reason that the null result of the scanning magnetometry experiments poses such a challenge to the chiral *p*-wave hypothesis is quantitative—spontaneous currents of size comparable to theoretical estimates [12–16] would give a magnetic signal more than two orders of magnitude greater than the experimental resolution. Magnetometry measurements on mesoscopic samples [5] also see no signs of these currents.

In this paper, we calculate the spontaneous surface currents for a family of models consistent with the phenomenology of superconductivity in Sr$_2$RuO$_4$. Motivated by *a*-axis tunneling experiments [17], we employ a different interface condition than previous studies, modeling the surface region as a normal metal layer adjoining the superconducting bulk. We find that, compared to previous estimates, the expected magnetic signal from edge currents is reduced by over an order of magnitude. These calculations demonstrate that interface details can have a quantitatively meaningful effect on the expectations for magnetometry experiments.

II. SURFACE IMPERFECTION

The assumption of specular surface scattering as employed in Refs. [12–16] requires an atomically smooth surface. *ab* faces of Sr$_2$RuO$_4$ can be cleaved, but *ac* and *bc* faces are typically polished to a smoothness of several *nm* [9], on the order of ten lattice constants. In *a*-axis junction tunneling conductance measurements, signatures of superconductivity at the surface are present only at the sub-1% level on top of a substantial smooth background [17], as shown in Fig. 2 of that reference. Accordingly, the best indication from experiment is that the edge regions of large crystals are metallic [18], with a superconducting gap developing only further into the sample. (It has not been established whether a metallic region is present near the etched edges of Ref. [11].)

The scenario of a metallic edge is plausible given the fragility of unconventional superconductivity to elastic scattering (i.e., the inapplicability of Anderson's theorem to a sign-changing order parameter), which has been explicitly verified for this material [19]. Rough or pair-breaking surface effects have been shown [20,21] to sharply reduce the superconducting order parameter at the surface, although not to meaningfully alter the surface density of states. Accordingly, the observation of metallic behavior suggests that there is a higher density of defects near the surface (presumably introduced during crystal growth or preparation procedures), leading to a reduced mean free path and the quenching of superconductivity near the surface.

To facilitate calculations, we do not directly treat a rough surface or defects in the surface region, but rather adopt a model consisting of a clean interface between vacuum and a metallic region, which in turn has a clean interface with the superconducting bulk. The metallic region is arranged by setting appropriate coupling constants to zero in lattice Bogoliubov de-Gennes Hamiltonians. This introduces artifacts which will be discussed in Sec. VII. We focus narrowly on spontaneous currents here, though a calculation of quantities such as the tunneling conductance (to compare with Ref. [17]) within a more realistic model will be important in evaluating the consistency of the present scenario with experiment.

III. MODEL HAMILTONIANS

We consider spinless fermions on a 2D square lattice corresponding to the RuO$_2$ plane, and work in a cylinder geometry: periodic boundary conditions are taken in the y direction, and open boundary conditions in x. We will consider two different Bogoliubov-de-Gennes Hamiltonians:

$$H_\gamma = - \sum_{i,j} T_{ij}^z c_{z,i}^\dagger c_{z,j}$$
$$+ \sum_i \left[\Delta_x^\gamma(i) c_{z,i}^\dagger c_{z,i+\hat{x}}^\dagger + \Delta_y^\gamma(i) c_{z,i}^\dagger c_{z,i+\hat{y}}^\dagger + \text{H.c.} \right],$$
$$(1)$$

$$H_{\alpha\beta} = - \sum_{i,j} \sum_{\eta=x,y} T_{ij}^\eta c_{\eta,i}^\dagger c_{\eta,j}$$
$$- t' \sum_i \sum_{s=\pm1} s [c_{x,i}^\dagger c_{y,i+\hat{x}+s\hat{y}} + \text{H.c.}]$$
$$+ \sum_i \sum_{s=\pm1} \left[\Delta_x^{\alpha\beta}(i) c_{x,i}^\dagger c_{x,i+\hat{x}+s\hat{y}}^\dagger \right.$$
$$\left. + s \Delta_y^{\alpha\beta}(i) c_{y,i}^\dagger c_{y,i+\hat{x}+s\hat{y}}^\dagger + \text{H.c.} \right],$$
$$(2)$$

where H_γ is a minimal Hamiltonian for chiral p-wave superconductivity on the γ band of Sr$_2$RuO$_4$, which arises principally from Ru 4d d_{xy} orbitals (represented by the index z on fermion operators), for which we include the tight binding matrix elements $t_z \equiv T_{i,i\pm\hat{x}}^z = T_{i,i\pm\hat{y}}^z$, $t_z' \equiv T_{i,i\pm\hat{x}\pm\hat{y}}^z$, $\mu_z \equiv T_{i,i}^z$. $H_{\alpha\beta}$ corresponds to the quasi-one-dimensional α and β bands, which arise principally from the d_{xz} and d_{yz} orbitals (fermion indices x and y respectively), with tight binding matrix elements $t \equiv T_{i,i\pm\hat{x}}^x = T_{i,i\pm\hat{y}}^y$, $t_\perp \equiv T_{i,i\pm\hat{y}}^x = T_{i,i\pm\hat{x}}^y$, $\mu \equiv T_{i,i}^x = T_{i,i}^y$. For this model, there is also an important next-nearest-neighbor orbital hybridization matrix element t', whose presence is crucial for establishing a chiral superconducting gap. We take values $\{t,t_\perp,t',\mu,t_z,t_z',\mu_z\} = \{1,0.1,0.1,1,0.8,0.3,1.15\}$, which are consistent with the Fermi surface measured in ARPES [22] and the quasiparticle effective masses measured in quantum oscillations [23].

Nearest-neighbor pairing for the d_{xy} orbital and next-nearest neighbor pairing for the d_{xz} and d_{yz} orbitals represent the lowest lattice harmonics consistent with a weak-coupling analysis [24], which predicts a fully gapped d_{xy} orbital and "accidental" nodes on d_{xz} and d_{yz} that are lifted to parametrically deep gap minima in the presence of orbital mixing t'. Calculations are performed with the self-consistency conditions $\Delta_x^\gamma(i) = -g_\gamma(i)\langle c_{z,i+\hat{x}}c_{z,i}\rangle$, $\Delta_y^\gamma(i) = -g_\gamma(i)\langle c_{z,i+\hat{y}}c_{z,i}\rangle$, $\Delta_x^{\alpha\beta}(i) = -g_{\alpha\beta}(i)\langle c_{x,i+\hat{x}+\hat{y}}c_{x,i}\rangle$, $\Delta_y^{\alpha\beta}(i) = -g_{\alpha\beta}(i)\langle c_{y,i+\hat{x}+\hat{y}}c_{y,i}\rangle$ with attractive interactions $g_{\alpha\beta}(i)$ and $g_\gamma(i)$, which are allowed to vary along the x direction. We model the metallic edge region adjoining the superconducting bulk by setting $g_{\alpha\beta}$ and g_γ to zero in a region of width N_m sites, and nonzero and uniform in a region of width N_s sites, with value chosen to yield the desired bulk values of $\Delta^{\alpha\beta}$ and Δ^γ. In this model, superconductivity arises independently on the quasi-two-dimensional γ band and on the quasi-one-dimensional α and β bands (i.e., there is no inter-band proximity effect) and our estimate for the Sr$_2$RuO$_4$ edge current will be the sum of contributions from H_γ and

$H_{\alpha\beta}$. The consequences of this artificial assumption will be considered in Sec. VII.

The current operator for the link from site i to site j can be derived from the lattice version of the equation of continuity and the Heisenberg equation of motion. It has an intraorbital part

$$\hat{J}_{i,j}^\eta = i T_{i,j}^\eta [c_{\eta,i}^\dagger c_{\eta,j} - \text{H.c.}],$$
$$(3)$$

where $\eta = x,y,z$ is the orbital index. For the model of the α and β bands, there is also an inter-orbital part for the current between next-nearest neighbors

$$\hat{J}_{i,i+s_1\hat{x}+s_2\hat{y}}^{xy} = it's_1s_2[c_{x,i}^\dagger c_{y,i+s_1\hat{x}+s_2\hat{y}}$$
$$+ c_{y,i}^\dagger c_{x,i+s_1\hat{x}+s_2\hat{y}} - \text{H.c.}],$$
$$(4)$$

where $s_1,s_2 = \pm1$.

We neglect the effect of screening, whose effects have been explored elsewhere [12,13,20]. Accordingly, our figure of merit for edge currents will be the total amount of current I flowing through the metal region and half of the superconducting bulk, i.e.,

$$I = \sum_{n=1}^{N_m+N_s/2} \langle \hat{J}_{n\hat{x},n\hat{x}+\hat{y}} + \hat{J}_{n\hat{x},n\hat{x}+\hat{x}+\hat{y}} \rangle,$$
$$(5)$$

where the two terms in the sum are for nearest neighbor and next-nearest neighbor links, including intra- and interorbital contributions as appropriate, and the angle brackets represent a thermal average. Note that only net currents in the $\hat{y}$ direction are allowed by continuity in the cylinder geometry.

IV. GINZBURG LANDAU THEORY

Ginzburg-Landau theory represents an approximate solution to the BdG equations that becomes exact in the limit $T - T_c \to 0^-$, but provides valuable intuition even at low temperatures. The expression for the free energy can be found in the literature [25]:

$$F = r(|\psi_x|^2 + |\psi_y|^2) + K_1(|\partial_x\psi_x|^2 + |\partial_y\psi_y|^2)$$
$$+ K_2(|\partial_y\psi_x|^2 + |\partial_x\psi_y|^2)$$
$$+ K_3([\partial_x\psi_x]^*[\partial_y\psi_y] + [\partial_y\psi_x]^*[\partial_x\psi_y] + \text{c.c.})$$
$$+ \text{higher order terms.}$$
$$(6)$$

For our purposes, we need not treat quartic terms or those with more than two derivatives. The equations for the order parameter fields must be supplemented by appropriate conditions for a boundary at fixed x:

$$\psi_x = 0 \quad \text{and} \quad \partial_x\psi_y = 0 \quad \text{for an insulating boundary,}$$
$$(7)$$

$$\partial_x\psi_x = \frac{\psi_x}{b_x} \quad \text{and} \quad \partial_x\psi_y = \frac{\psi_y}{b_y} \quad \text{for a metallic boundary.}$$
$$(8)$$

The conditions for an insulating boundary follow from the fact that specular scattering is fully pair-breaking for ψ_x (which is by construction odd under $x \to -x$) [26]. The conditions

for a metallic boundary involve phenomenological parameters $b_{x,y}$, which capture the fact that a metal interface is partially pair-breaking for both components [27].

We continue to ignore screening, and focus on the spontaneous current (i.e., the current which exists in the absence of phase gradients imposed by an external field):

$$J_{\text{spont}} \propto -i K_3 (\psi_y [\partial_x \psi_x]^* + \psi_x [\partial_x \psi_y]^* - \text{c.c.})$$
$$\propto K_3 (|\psi_y|\partial_x|\psi_x| - |\psi_x|\partial_x|\psi_y|). \quad (9)$$

In these expressions, we have implemented translation symmetry in the y direction and assumed a uniform relative phase factor of i between ψ_x and ψ_y (i.e., positive chirality). Here the coefficients K_1 and K_2 determine the coherence lengths of the two order parameter components, the intercomponent gradient coupling K_3 sets the scale of the currents, and $r \propto T - T_c$ is the usual parameter that tunes through the critical point. The coefficients can be treated as phenomenological parameters or computed directly from the microscopic Hamiltonians given above.

V. BDG RESULTS

As previously mentioned, our estimate for the edge current in Sr$_2$RuO$_4$ is the sum of contributions due to the quasi-2D γ band and the quasi-1D α, β bands; we initially plot and discuss these contributions separately. Values of net current are given in units of $I_0 \equiv 0.073 et/\hbar$, which is the net current due to the γ band with an insulating interface ($N_m = 0$) at $T = 0.2T_c$, in the weak-coupling limit $\Delta_0^\gamma \to 0^+$. I_0 is approximately equal to the value of the total current per spin in a quasiclassical approximation (such as the Matsumoto-Sigrist prediction [12] used in Refs. [9,10]) when screening is neglected. If our model predicts a current I and screening alters our predictions in the same way as it does the quasiclassical Matsumoto-Sigrist results, then our prediction of a magnetic signal (such as the peak flux) is equal to the Matsumoto-Sigrist prediction times I/I_0.

Plots of the current and both components of the order parameter as a function of distance from the edge are shown in Fig. 1. Figure 2 shows the current contributions from the quasi-2D and quasi-1D bands versus temperature for several choices of N_m. Data points near T_c are not included due to computational cost. Figures 3 show the current contributions as a function of the bulk order parameter (Δ^γ and $\Delta^{\alpha\beta}$ respectively), with fixed values of T/T_c and N_m/ξ, where ξ is the superconducting coherence length. Before considering the effect of the normal-metal region, we note basic results for a clean insulator (or vacuum) / superconductor (IS) interface ($N_m = 0$). In that case, compared to the contribution from H_γ, the net current from $H_{\alpha\beta}$ is reduced by a factor of approximately three at zero temperature and six at the experimental temperature of $0.2T_c$.

Turning to the results for a normal metal / superconductor (NS) interface (i.e., $N_m \neq 0$), one feature of the $I - T$ curves for different values of N_m is that they all coincide at zero temperature and at sufficiently high temperature, differing only in an intermediate crossover region. This follows from the proximity effect: while the superconducting gap $\Delta(i) \equiv -g\langle cc \rangle$ is zero in the metal (where $g = 0$), pair correlations
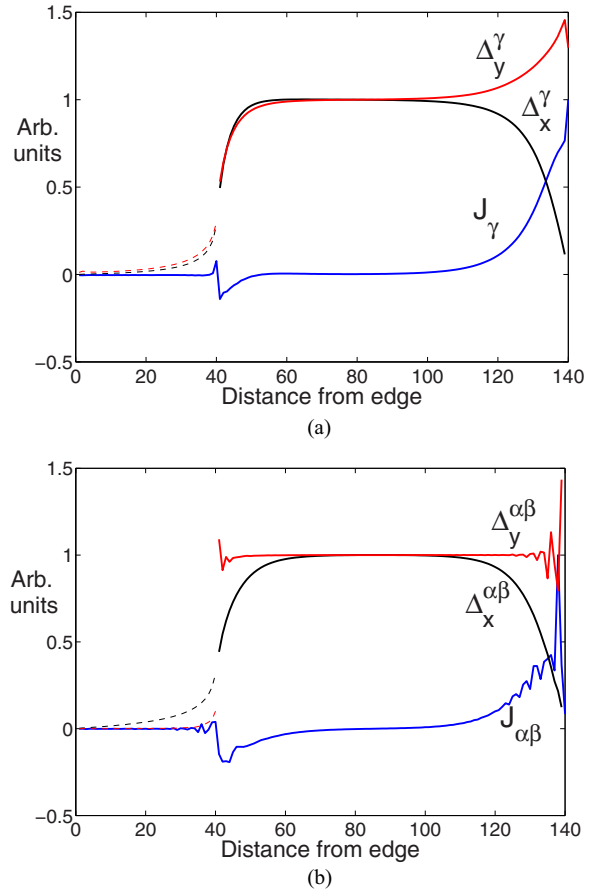
FIG. 1. (Color online) Current and the two components of the order parameter as a function of position for (a) H_γ and (b) $H_{\alpha\beta}$. The first 40 sites are the metallic region, in which the gap vanishes, and clean interfaces with vacuum are present at positions 0 and 140. Pair correlations in the metallic region are shown in dashed lines. The bulk order parameter values are $\Delta_0^{\alpha\beta} = \Delta_0^\gamma = 0.05t$, $T = 0.2T_c$

$\langle cc \rangle$ do penetrate. The length scale for this penetration is set by v_F/T, (where v_F is the Fermi velocity), and thus diverges at zero temperature, so that the width of the metallic region is effectively zero. By contrast, at temperatures such that $v_F/T < N_m$, pairing correlations decay to zero before the edge is encountered, so that the metallic region is effectively infinite. In both cases, an increase in N_m should have a negligible effect on the currents, consistent with the calculation.

For $v_F/T < N_m$, there is a pronounced suppression of the current in both the one and quasi-1D cases compared with the current without a metallic region ($N_m = 0$). The amount of this suppression depends on the size of the pairing gap. For Sr$_2$RuO$_4$, the pairing gap is on the order of $10^{-3}t$, so that extrapolation to the weak-coupling limit $\Delta_0 \to 0^+$ is necessary for a quantitative estimate. For a model including all three bands in this weak-coupling limit, we find a suppression of approximately twenty compared to the initial Matsumoto-Sigrist predictions.

FIG. 2. (Color online) Contributions to the current near a metallic edge region from (a) the γ band and (b) the α,β bands vs temperature for several values of N_m, the thickness of this metallic edge region abutting the superconducting bulk. The superconducting bulk is of width $N_s = 100$ sites, and currents are quoted in units of I_0, which is essentially the Matsumoto-Sigrist result [12] in the absence of screening. The bulk order parameter values are $\Delta_0^{\alpha\beta} = \Delta_0^\gamma = 0.05t$. For the current from α,β there are finite size effects associated with near-nodal quasiparticles, which render the results at very low temperature less well behaved. We have verified that the zero-temperature current values in the thermodynamic limit are within 15% of those shown here.

VI. QUALITATIVE EXPLANATION FROM GINZBURG-LANDAU THEORY

The results of the previous section can be summarized as follows: (1) the contribution from the α,β bands is several times smaller than that of the γ band for the IS geometry; (2) both contributions are substantially suppressed in the NS geometry; and (3) the suppression due to the NS geometry is considerably larger for the γ band than for the α,β bands. Ginzburg-Landau theory, though it is not quantitatively valid at low temperatures, can nonetheless qualitatively explain each of these results.

(1) With a conventional insulating interface, the scale of spontaneous currents is set by the coefficient K_3. In the quasi-2D model, this is a number of order one, whereas in the quasi-1D model, it vanishes in the limit of zero interorbital mixing t'. Since $t' = 0.1t$, it follows that $K_3^{\alpha\beta}$ is substantially smaller than
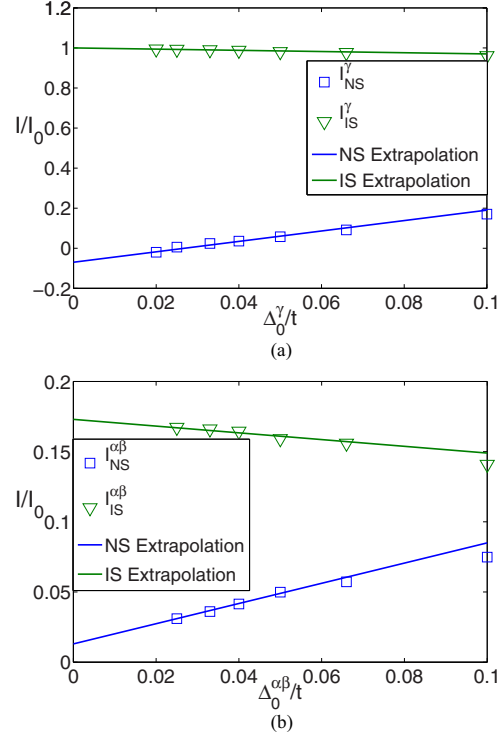
FIG. 3. (Color online) Extrapolation of current contributions of (a) the γ band and (b) the α,β bands to the weak-coupling limit $\Delta_0^{\alpha\beta}, \Delta_0^\gamma \to 0^+$ for the both insulator/superconductor (IS) 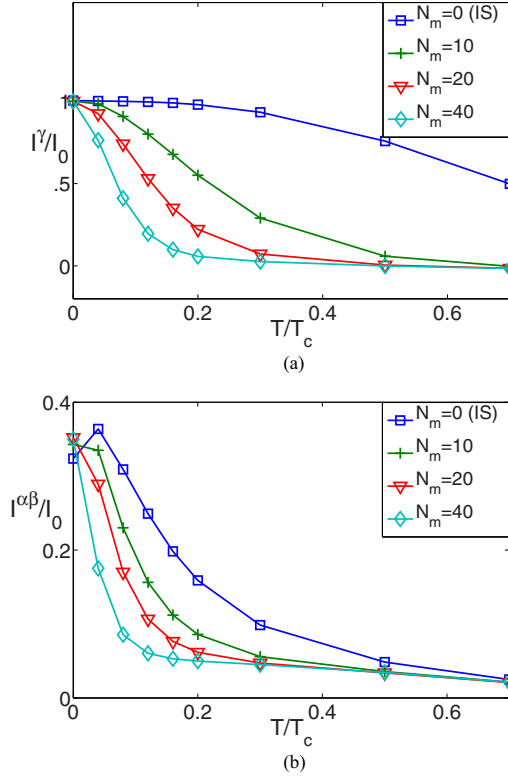and normal metal/superconductor (NS) interfaces. Currents are quoted in units of I_0, which is essentially the Matsumoto-Sigrist result [12] in the absence of screening. As the bulk gap is reduced, the temperature is reduced and the length scales N_m, N_s are increased in order to fix the values $T/T_c = 0.2$, $N_m/\xi \approx 4$, $N_s/\xi \approx 12$. The metallic boundary leads to suppression of over an order of magnitude in both the quasi-1D and quasi-2D cases.

K_3^γ and similarly for the currents. A microscopic calculation gives $K_3^{\alpha\beta} \approx 0.02 K_3^\gamma$.

(2) The suppression in current in the NS geometry can be viewed as a consequence of the different boundary conditions on the order parameter. The boundary values of of $|\psi_x|$ and $|\psi_y|$ are respectively increased and decreased compared to the insulating case. At a fixed distance from the edge, $|\psi_x|$ and $\partial_x|\psi_y|$ are larger, while $|\psi_y|$ and $\partial_x|\psi_x|$ are smaller than their corresponding values for the insulating boundary. Equation (9) for the current shows that this yields a numerical (though not parametric) reduction in the current for any choice of G-L coefficients.

(3) The tremendous suppression of the current in the quasi-2D NS model is a lattice effect. For the fine-tuned case $K_1 = K_2$, one can show that $b_x = b_y$ and the two components of the order parameter heal away from the metal in precisely the same way, leading to a vanishing current in lowest-order G-L theory [20]. For a quadratic dispersion and an order parameter $k_x + ik_y$, as is often used to describe the γ band [12–14,16], the coefficients satisfy $K_1 = 3K_2$. However, for a

lattice-compatible order parameter $\sin k_x + i \sin k_y$ as treated here and for an appropriate tight-binding band structure for the γ band, $K_1 = 0.71 K_2$. The large suppression of the γ band current due to the NS geometry can be roughly identified with the proximity of this result to the fine-tuned case $K_1 = K_2$.

VII. DISCUSSION

Superconductivity on the quasi-1D bands was previously conjectured [24] to lead to dramatically reduced edge currents compared to a quasi-2D scenario due to trivial topology (i.e., the Chern numbers of the two bands add to zero, yielding no net chiral edge modes). The results shown above for the IS interface show a substantial reduction (by a factor between three and six), but nonetheless of order one, falsifying the initial conjecture and illustrating the tenuous connection between topology and edge currents in chiral p-wave superconductors (this topic will be treated in depth in a forthcoming paper).

Even if the quasi-1D bands had vastly reduced currents in the IS case, the contribution from the γ band would generically be large, even if it were not the "dominant" band. The neglect of the current contribution from the subdominant band(s) is only justified if the experimental temperature exceeds the subdominant gap scale. However, thermodynamic evidence shows that the gaps on all bands are at least comparable to $T_c = 1.5$ K ≈ 0.13 meV [28]. At low temperatures, the edge currents should then correspond to the sum of contributions from the quasi-1D and quasi-2D bands, with the weak-coupling limit taken for both $\Delta^{\alpha\beta}$ and Δ^γ. At low temperatures and with a clean interface, the generic scale of edge currents is "of order one" regardless of microscopic mechanism details such as the identity of the dominant band(s).

Though there does not seem to be any physical reason for a parametric suppression of edge currents, we find a meaningful quantitative reduction of over an order of magnitude compared to previous estimates by considering the effect of surface imperfection. Within a model of a clean metal of width $\sim 4\xi_0$ abutting a clean superconductor, with $T = 0.2T_c$, the total current from all three bands is suppressed by a factor of more than twenty in the weak-coupling limit compared to the result for the γ band and an IS interface. Within our model, there is essentially no suppression in the limit of sufficiently low temperatures and/or narrow metallic regions, where superconducting correlations induced by the proximity effect extend all the way to the edge. This is an artifact of our model, however, which does not treat surface roughness or disorder directly. For example, pair-breaking and diffuse scattering effects are known to reduce the zero-temperature current [20,21].

The calculations presented here are not expected to be quantitatively correct for the actual superconducting gap structure and surface physics of Sr_2RuO_4. Our model of spinless fermions entirely neglects spin-orbit coupling (SOC), which has been proposed to qualitatively affect pairing [29]. However, as far as the edge current is concerned, the primary effect of SOC is to modestly renormalize the band structure; hence, its explicit inclusion would not change any of our results substantially. A more serious unphysical assumption is the neglect of the interband proximity effect, without which superconductivity would generically arise at very different

temperatures on the γ and α/β bands. While interband proximity coupling would not change the additivity of the current contributions from the different bands, it would alter the length scale over which the various order parameter components heal away from an interface. The resulting currents could be reduced or increased compared to our results, depending on microscopic details.

These defects notwithstanding, the model treated above illustrates that substantial reductions in magnetic signal can arise from interface effects. We now consider the consequences of a twenty-fold reduction for the interpretation of magnetometry experiments. Even with this reduction the magnetic signal at the edge would still be estimated to be several times the resolution of scanning magnetometry experiments, and should therefore be observable. However, if multiple domains of sufficiently small size are present in the sample and intersect the edge, the magnetic fields from spontaneous currents would be unobservable. Kirtley *et al.* [9] find that, to be consistent with the Matsumoto-Sigrist predictions [12], ab-plane domains below about 1.5 μm in size are necessary. To be consistent with a prediction twenty times smaller, the domains could be as large as perhaps 5 μm. However, the presence of multiple ab-plane domains within the sample would lead to spontaneous currents at the domain walls, which have not been treated here. Unless domain walls are pinned by crystal defects that, like a rough edge, lead to quenched superconductivity (an unlikely proposition), the suppression indicated in the foregoing calculations would not apply to the domain wall currents.

One scenario for the lack of an edge signal which would not imply a signal at interior domain boundaries is the c-axis stacking of planar domains of macroscopic horizontal extent and alternating chirality. The energetic cost of the domain boundaries would be small, due to the very weak dispersion of the electronic band structure along the c direction, and symmetry requires that no spontaneous current would flow at these boundaries. The measurements of Hicks *et al.* [10] place an upper bound of 20–400 nm on the height of such domains, depending on microscopic domain details, and again assuming Matsumoto-Sigrist predictions for edge currents [12] (similar bounds have not been estimated for the experimental geometries of Refs. [5,11]). Here, a twenty-fold reduction of expected edge currents for a single domain would revise upward the experimental bound on domain size, possibly reconciling the null result of scanning magnetometry experiments with the spontaneous time reversal symmetry breaking seen in Kerr effect measurements with mesoscopic spot size (~ 50 μm) and skin depth (~ 150 nm [30]).

We have shown that spontaneous currents in a chiral p-wave superconductor are highly sensitive to interface details, in particular that surface disorder leading to a micrometer-thickness metallic surface region can cause a suppression of more than an order of magnitude compared to naive estimates. We propose that a scenario of c-axis domain stacking, along with surface disorder, might resolve the seeming disagreement between scanning magnetometry and Kerr probes, and further suggest that the edge of a crystal fractured in vacuum might host a much lower defect density and potentially lead to observable edge currents.

[1] A. Mackenzie and Y. Maeno, Rev. Mod. Phys. **75**, 657 (2003).

[2] K. Ishida, H. Mukuda, Y. Kitaoka, K. Asayama, Z. Q. Mao, Y. Mori, and Y. Maeno, Nature (London) **396**, 658 (1998).

[3] K. D. Nelson, Z. Q. Mao, Y. Maeno, and Y. Liu, Science **306**, 1151 (2004).

[4] F. Kidwingira, J. D. Strand, D. J. Van Harlingen, and Y. Maeno, Science **314**, 1267 (2006).

[5] J. Jang, D. G. Ferguson, V. Vakaryuk, R. Budakian, S. B. Chung, P. M. Goldbart, and Y. Maeno, Science **331**, 186 (2011).

[6] G. M. Luke, Y. Fudamoto, K. M. Kojima, M. I. Larkin, J. Merrin, B. Nachumi, Y. J. Uemura, Y. Maeno, Z. Q. Mao, Y. Mori *et al.*, Nature (London) **394**, 558 (1998).

[7] G. M. Luke, Y. Fudamoto, K. M. Kojima, M. I. Larkin, B. Nachumi, Y. J. Uemura, J. E. Sonier, Y. Maeno, Z. Q. Mao, Y. Mori *et al.*, Physica B **289-290**, 373 (2000).

[8] J. Xia, Y. Maeno, P. T. Beyersdorf, M. M. Fejer, and A. Kapitulnik, Phys. Rev. Lett. **97**, 167002 (2006).

[9] J. R. Kirtley, C. Kallin, C. W. Hicks, E.-A. Kim, Y. Liu, K. A. Moler, Y. Maeno, and K. D. Nelson, Phys. Rev. B **76**, 014526 (2007).

[10] C. W. Hicks, J. R. Kirtley, T. M. Lippman, N. C. Koshnick, M. E. Huber, Y. Maeno, W. M. Yuhasz, M. B. Maple, and K. A. Moler, Phys. Rev. B **81**, 214501 (2010).

[11] P. J. Curran, S. J. Bending, W. M. Desoky, A. S. Gibbs, S. L. Lee, and A. P. Mackenzie, Phys. Rev. B **89**, 144504 (2014).

[12] M. Matsumoto and M. Sigrist, J. Phys. Soc. Jpn. **68**, 994 (1999).

[13] A. Furusaki, M. Matsumoto, and M. Sigrist, Phys. Rev. B **64**, 054514 (2001).

[14] M. Stone and R. Roy, Phys. Rev. B **69**, 184511 (2004).

[15] Y. Imai, K. Wakabayashi, and M. Sigrist, Phys. Rev. B **85**, 174532 (2012).

[16] J. A. Sauls, Phys. Rev. B **84**, 214509 (2011).

[17] S. Kashiwaya, H. Kashiwaya, H. Kambara, T. Furuta, H. Yaguchi, Y. Tanaka, and Y. Maeno, Phys. Rev. Lett. **107**, 077003 (2011).

[18] S. Kashiwaya (private communication).

[19] A. P. Mackenzie, R. K. W. Haselwimmer, A. W. Tyler, G. G. Lonzarich, Y. Mori, S. Nishizaki, and Y. Maeno, Phys. Rev. Lett. **80**, 161 (1998).

[20] P. E. C. Ashby and C. Kallin, Phys. Rev. B **79**, 224509 (2009).

[21] Y. Nagato, M. Yamamoto, and K. Nagai, J. Low Temp. Phys. **110**, 1135 (1998).

[22] A. Damascelli, D. H. Lu, K. M. Shen, N. P. Armitage, F. Ronning, D. L. Feng, C. Kim, Z.-X. Shen, T. Kimura, Y. Tokura, Z. Q. Mao, and Y. Maeno, Phys. Rev. Lett. **85**, 5194 (2000).

[23] C. Bergemann, A. P. Mackenzie, S. R. Julian, D. Forsythe, and E. Ohmichi, Adv. Phys. **52**, 639 (2003).

[24] S. Raghu, A. Kapitulnik, and S. A. Kivelson, Phys. Rev. Lett. **105**, 136401 (2010).

[25] M. Sigrist and K. Ueda, Rev. Mod. Phys. **63**, 239 (1991).

[26] V. Ambegaokar, P. DeGennes, and D. Rainer, Phys. Rev. A **9**, 2676 (1974).

[27] P. de Gennes, *Superconductivity of Metals and Alloys* (Benjamin, New York, 1966).

[28] I. A. Firmo, S. Lederer, C. Lupien, A. P. Mackenzie, J. C. Davis, and S. A. Kivelson, Phys. Rev. B **88**, 134521 (2013).

[29] C. Veenstra, Z.-H. Zhu, M. Raichle, B. Ludbrook, a. Nicolaou, B. Slomski, G. Landolt, S. Kittaka, Y. Maeno, J. Dil *et al.*, Phys. Rev. Lett. **112**, 127002 (2014).

[30] A. Kapitulnik (private communication).

Chapter 6

Leggett modes and multi-band superconductivity

6.1 Preface Multi-band superconductors exhibit physical properties that are not available in single-band superconductors. In the latter, Cooper pairing is driven by interactions that scatter pairs of electrons within the band. However, in a multi-band system, Cooper pair scattering exists not only within the individual bands, but also in general between the bands. In an unconventional superconductor, non-vanishing inter-band interactions may originate from direct Coulomb interactions between the multiple bands (oribtals), and may also derive from higher order scattering processes associated with spin and/or charge density wave fluctuations. In this chapter, we examine the multi-band nature of the superconductivity in Sr_2RuO_4, and discuss several potentially novel aspects related to it.

6.1.1 Leggett modes In each superconducting channel, the effective interactions between the bands mediate effective Josephson-like couplings between the superconducting order parameters on the bands. In Sr_2RuO_4, due to the disparate dimensional characters of the α/β- and γ-bands, it is expected that the Cooper pairing scattering amplitude between the two sets

of bands will be significantly smaller than that within each subset[99]. This naturally leads to weak inter-band Josephson couplings between the order parameters on the two sets of bands.

In the ground state, the system stabilizes a three-band order parameter configuration which minimizes the intra-band and inter-band interactions. Here, an order parameter configuration denotes the relative magnitudes and signs of the superconducting gaps on the three bands. In the presence of perturbing electromagnetic fields or at finite temperatures, the relative magnitudes and phases of the band gaps may fluctuate and form coherent collective modes. These modes were first discussed by Leggett[100] (thus termed Leggett modes), and their excitation gaps (masses) are determined by the effective inter-band Josephson couplings. In Sr_2RuO_4, a relatively low-energy Leggett mode may emerge due to the weaker Josephson coupling, corresponding to relative phase oscillations between the γ and the other two bands. In principle, this Leggett mode can be probed by optical experiments, such as Raman spectroscopy.

6.1.2 Comparable gaps on the bands The distinction between the two sets of bands also leads to another expectation, that superconductivity in this material is dominated by one subset of the bands.[99] This follows from two observations: 1) the γ-band Fermi surface is close to a van-Hove singularity, which promotes small wavevector spin density wave fluctuations[101] favorable for the development of p-wave superconductivity[76]; 2) the two quasi-nested 1D bands are associated with strong large wavevector spin density wave fluctuations[101] which may promote noticeable p-wave superconducting correlations on their own.[78] The qualitative differences between the two kinds of bands might lead one to believe that superconductivity is dominated by one kind of band or the other. However, given 1) and 2), it is possible that the microscopics may lead to the amplitude of the p-wave order parameter being comparable on the two sub-bands.

In fact, through a weak coupling renormalization group calculation[77] that is believed to be appropriate to Sr_2RuO_4, we find that the two sets of bands are characterized by comparable effective interactions in the Cooper channel. These interactions conspire with the relatively weaker interactions between the two sets of bands to drive comparable superconducting gaps on the three bands, as is compatible with specific heat measurements[79] and tunneling spectroscopic measurements.[80]

6.1.3 Novel multi-band TRSB pairing?   There is yet another possible novel phenomenon in a multi-band system, namely, a time-reversal symmetry breaking (TRSB) superconducting order which does not originate from chiral pairing [102]. This has been discussed in the context of $MgCNi_3$,[103] some three-band models of iron-based superconductors,[104, 105] and SrPtAs.[106] There, the frustrated interband interactions result in two degenerate or near degenerate configurations of order parameters on the bands, with distinct sets of relative gap amplitudes and phases. In such a scenario, a stable ground state may be realized in which the order parameter is composed of a complex linear superposition of the two configurations, thereby breaking time reversal symmetry. In relation to Sr_2RuO_4, this possibility would arise purely from the multi-band physics and be independent of the intrinsic TRSB associated with the putative chiral p-wave pairing within the individual bands. Note that the TRSB state generated by inter-band frustration requires two successive thermodynamic transitions if the two configurations are non-degenerate.

A closely related possibility is a multi-band helical state with TRSB. Helical pairing in a one-band system is intrinsically time-reversal invariant, analogous to the B-phase of ^{3}He. However, as discussed in the previous paragraph, a multi-band system may allow for a complex TRSB order parameter to develop out of the otherwise time-reversal-invariant helical

Cooper pairing on the individual bands. Such a state possesses no spontaneous edge current at its boundaries, and hence may be compatible with the puzzling absence [60, 61, 62] of the edge current, while being consistent with the strong evidence for spin-triplet odd-parity superconductivity.[19, 20, 21]

The novel TRSB helical state is also appealing due to the possible close competition between the chiral and helical pairings in Sr_2RuO_4. This is evident, e.g. from the invariance of spin susceptibility below T_c for all external field orientations in NMR Knight shift measurements.[19, 107] Remarkably, the in-plane $\hat{d}$-vector orientation inherent to the helical state naturally explains the experimental indications of Pauli limiting behavior: anomalous suppression of the in-plane upper critical field H_{c2}[108] and signatures of first order transitions for in-plane H_{c2}[109] at low temperatures. The Pauli limiting effect is expected to be absent in the chiral p-wave order. On the theory front, a weak coupling RG[77] found leading instability in the helical channel over a broad range of interaction parameters.

In our model for Sr_2RuO_4, however, the inter-band interactions turn out to be unfrustrated in both chiral and helical channels. Thus the complex multi-band order parameter seems unlikely to occur. However, given the difficulties in reconciling the expectations for chiral p-wave order and the few key experiments mentioned above, it may be helpful to study alternative forms of TRSB superconductivity which do not necessarily involved chiral p-wave pairing.

6.2 Publication

Leggett modes and multi-band superconductivity in Sr_2RuO_4

Wen Huang[1], Thomas Scaffidi[2], Manfred Sigrist[3], and Catherine Kallin[1,4]

[1]*Department of Physics and Astronomy, McMaster University, Hamilton, Ontario, L8S 4M1, Canada*
[2]*Rudolf Peierls Centre for Theoretical Physics, Oxford OX1 3NP, United Kingdom*
[3]*Institut für Theoretische Physik, ETH-Zürich, CH-8093 Zürich, Switzerland and*
[4]*Canadian Institute for Advanced Research, Toronto, Ontario M5G 1Z8, Canada*
(Dated: July 29, 2016)

Sr_2RuO_4 is a prototypical multi-band superconductor with three bands crossing the Fermi level. These bands exhibit distinct dimensional characteristics, with one quasi-2D γ-band and two quasi-1D α- and β-bands. This leads to the expectation that the superconductivity on the γ-band may be only weakly Josephson-coupled to that on the other two bands. Based on an explicit microscopic weak coupling calculation appropriate for Sr_2RuO_4, we study the collective Leggett modes associated with the relative phase oscillations between the bands and show that a relatively soft Leggett mode exists due to the comparatively weaker inter-band Josephson coupling. These calculations also provide insight into why the superconducting gap magnitudes may be comparable on all three bands, despite the noticeable differences between the γ and α/β bands. The analyses can be readily applied to other multi-band superconductors.

Multi-band superconductors possess physical properties that are not present in single-band superconductors. Depending on the nature of the interactions driving the Cooper pairing and the orbital character of the bands, the superconducting order parameter may not be dominated by one band with only much weaker induced superconductivity on the other bands. This is particularly so in multi-band systems with unconventional pairing symmetry, where the correlations underlying the superconductivity often involve electrons on different bands strongly interacting with each other. These inter-band interactions give rise to effective Josephson couplings between the superconducting order parameters of the different bands[1]. As a consequence, in the ground state, the multiple order parameters are locked in a configuration with a particular set of relative phases and magnitudes.

Under external perturbations or at finite temperatures, the relative phase between the multiple order parameters can fluctuate, costing a finite amount of energy that is determined by the inter-band couplings. These collective excitations are commonly referred to as Leggett modes.[1] They respond to electromagnetic fields in a peculiar manner, and are unlike the usual global U(1) phase fluctuations which are pushed up to the plasma frequency due to Coulomb interactions.[2]

The putative chiral p-wave superconductor Sr_2RuO_4[3–5] is a prototypical multi-band system, with three bands crossing the Fermi energy – two quasi one dimensional (1D) α/β-bands and one quasi two dimensional (2D) γ-band (Fig. 1).[9] The quasi-1D bands originate primarily from the hybridized $4d$ xz and yz-orbitals, while the γ-band is dominated by the xy-orbital. These orbitals are further mixed by spin-orbit coupling.[6–8]

The exact superconducting gap structure in this material is an ongoing debate.[9–11] In spite of this, a few things can be said regarding the effective interactions between the low energy fermions on the three Fermi surfaces. Firstly, the intra-band Cooper pair scattering on the quasi-1D bands may be markedly different from that on the quasi-2D band. This could lead to one set of bands or the other dominating the superconductivity, as was first pointed out by Agterberg et al.[12] However, as we will see, inter-band interactions make this
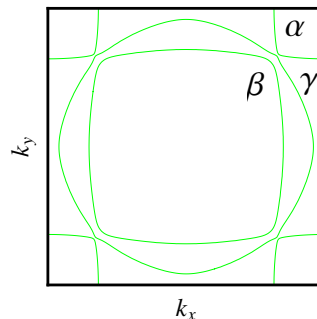
FIG. 1: The three Fermi surfaces of Sr_2RuO_4 in the $k_z = 0$ plane. The c-axis dispersion is small and is ignored in our calculations.

less likely. Secondly, due to the quasi-1D nature of the α/β-bands, the inter-band scattering between these two must be much stronger compared with that involving the γ-band. This naturally leads to a relatively weaker Josephson coupling between γ and α/β-bands.

There is some experimental evidence in favor of comparable superconductivity on all three bands of Sr_2RuO_4,[13,14] and theoretically, a weak-coupling renormalization group analysis by Scaffidi et al.[15] predicts comparable pairing strength on all of the bands in the parameter range believed to be appropriate to Sr_2RuO_4. However, this is an unresolved issue, and both experimental[16,17] and theoretical[18–24] indications exist in support of a state where one of the two sets of bands dominates.

Zhitomirsky and Rice[18] have studied the effects driven by the inter-band interactions in a simplified two-band model, using phenomenological estimates for the interactions. There, it was found that a reasonable amount of inter-band interaction is necessary to bind together the primary and the passive superconducting bands. In this work, we evaluate the effective inter-band interactions and Josephson couplings in Sr_2RuO_4 via explicit microscopic calculations following Scaffidi et al.[15] We will show that a relatively soft Leggett mode should be present because of the comparatively weaker

coupling between the quasi-2D γ- and quasi-1D α/β-bands. This detailed investigation into the inter-band interactions also helps to elucidate how the three bands may or may not support comparable Cooper pairing.

In a chiral p-wave superconductor, whether single-band or multi-band, additional phase modes may also arise in connection with the relative phase fluctuations between the two chiral components. These are referred to in literature as "clapping" modes.[25] While we do not study these modes in detail, we argue that some of their experimental signatures differ from the Leggett modes and the two types of collective modes may be distinguished.

Finally, although there is strong evidence for the time-reversal symmetry breaking (TRSB) chiral p-wave superconductivity in Sr_2RuO_4,[26–30] difficulties remain in reconciling the expectations for this order and a few key experiments, including the puzzling absence[31–34] (or smallness[35]) of spontaneous edge current (although recent years have seen numerous attempts to explain the absence of edge current[36–42]), the anomalous suppression of the in-plane upper critical field H_{c2}[43] and indications of a first order transition for in-plane H_{c2} at low temperatures[44] (see Ramires et al.[45] for a recent attempt to explain this). It is thus tempting to ask whether Sr_2RuO_4 could in fact support an alternative TRSB odd-parity superconducting order, made possible by the multi-band nature,[46] analogous to what has been discussed in the context of $MgCNi_3$,[47] some iron-based superconductors,[48–50] and $SrPtAs$.[52] There, TRSB is associated with a complex order parameter configuration on three or more bands. In relation to Sr_2RuO_4, a helical p-wave pairing with complex multi-band order parameter for example would seem consistent with the experiments mentioned above. Note that a one-band helical p-wave is intrinsically time-reversal invariant, in the sense that the spin up and down electrons form Cooper pairs of opposite orbital angular momenta.[25] However, in our model, we find that Sr_2RuO_4 lacks the ingredients favorable for the formation of this type of TRSB multi-band superconductivity.

The rest of the paper is organized as follows. We first formulate in Sec I a qualitative description of the multi-band superconductivity in Sr_2RuO_4, and then substantiate in Sec II with inputs obtained from microscopic weak coupling calculations. We then make specific analyses of the Leggett modes, along with a discussion of the experimental consequence in connection with Raman scattering in Sec III. Finally we examine the possibility of exotic TRSB multi-band chiral and helical pairings in Sec IV.

I. EFFECTIVE MODEL

As is clear from the above discussion, a study of the multi-band dynamics in Sr_2RuO_4 requires a knowledge of the Josephson couplings between the multiple order parameters on the three bands. We start here by introducing an effective model to qualitatively capture the main features of the inter-band couplings. Despite the lack of microscopic accuracy, this model is instructive for understanding the properties of the ground state and the collective phase modes.

The effective Hamiltonian may be written as,

$$
H = \sum_{\mu,\sigma} \int d\boldsymbol{r}\, \psi_{\mu,\sigma}^\dagger(\boldsymbol{r})(\frac{\hat{\boldsymbol{p}}^2}{2m_\mu} - \mu)\psi_{\mu,\sigma}(\boldsymbol{r})
$$
$$
+ \sum_{\substack{\mu,\nu \\ \sigma,\sigma'}} \int d\boldsymbol{r}\, \psi_{\mu,\sigma}^\dagger(\boldsymbol{r})\psi_{\mu,\sigma'}^\dagger(\boldsymbol{r}')V_{\sigma\sigma'}^{\mu\nu}(\boldsymbol{r}-\boldsymbol{r}')\psi_{\nu,\sigma'}(\boldsymbol{r}')\psi_{\nu,\sigma}(\boldsymbol{r}).
$$
(1)

Here $\mu = \alpha, \beta, \gamma$ are the band indices, m_μ is the effective mass for band-μ, and σ represent pseudospins which differ from the original spin indices due to spin-orbit coupling. The second term describes the *effective* electron-electron interactions between band-μ and band-ν in a particular *presumed* pairing channel (different channels are characterized by different effective interactions). These interactions presumably originate from Coulomb correlations and their associated particle-hole density-wave fluctuations.

Note that we are only considering intra- and inter-band interactions which scatter pairs of electrons, respectively, within a band and from one band to another. Effectively, this amounts to having no inter-band Cooper pairs. No particular forms are specified for the interactions $V^{\mu\nu}(\boldsymbol{r}-\boldsymbol{r}')$ at this point. However, it is assumed that such interactions lead to the highly anisotropic chiral p-wave pairing with comparable pairing amplitudes on all of the bands, as found in earlier calculations.[15] In particular, the inter-band interactions $V^{\alpha\gamma}$ and $V^{\beta\gamma}$ are considered weak compared to $V^{\alpha\beta}$ as well as to the intra-band interactions, while $V^{\alpha\beta}$ is relatively strong and may even exceed $V^{\alpha\alpha/\beta\beta}$ due to the quasi-1D nesting.[53] One may make a further simplifying approximation and set $V^{\alpha\alpha} \simeq V^{\beta\beta}$ on account of the similarity of the two 1D band structures.

As is elaborated in Appendix A, the eigenvectors of the interaction matrix $\hat{V}$ qualitatively approximate the possible order parameter configurations in the *presumed* pairing channel. In particular, the eigenstate with the most attractive eigenvalue corresponds to the most favorable configuration.

After a Hubbard-Stratonovich transformation in the Cooper channel using auxiliary fields Δ_μ (the superconducting order parameter) and integrating out the fermionic fields, the effective action becomes,

$$
S = \int d\tau d^2r \left(\sum_{\mu,\nu} \Delta_\mu^* \hat{\mathcal{V}}_{\mu\nu} \Delta_\nu - \sum_\mu \text{Tr} \ln G_\mu^{-1} \right), \quad (2)
$$

where the first term may be simplified to $(\hat{\Delta}^*)^T \hat{\mathcal{V}}\hat{\Delta}$ with $\hat{\Delta} = (\Delta_\alpha, \Delta_\beta, \Delta_\gamma)^T$ and $\hat{\mathcal{V}} = -\hat{V}^{-1}$, and the Gor'kov Green's function is given by

$$
\hat{G}_\nu^{-1} = -\begin{pmatrix} \partial_\tau - \frac{\nabla^2}{2m_\nu} - \mu_\nu & -\Delta_\nu \\ -\Delta_\nu^* & \partial_\tau + \frac{\nabla^2}{2m_\nu} + \mu_\nu \end{pmatrix}. \quad (3)
$$

In this action we have ignored the vector potential which is irrelevant to our discussion.

Particular attention is due for the coupling matrix $\hat{\mathcal{V}}$, whose off-diagonal elements describe inter-band Josephson couplings. Our expectation of much weaker $V^{\alpha\gamma}$ and $V^{\beta\gamma}$ compared to $V^{\alpha\beta}$ as well as the other interactions immediately

leads to interband couplings of similar nature. On these bases, we take,

$$\hat{\mathcal{V}} = \frac{1}{V_0} \begin{pmatrix} a_1 & \lambda & \eta_1 \\ \lambda & a_2 & \eta_2 \\ \eta_1 & \eta_2 & a_3 \end{pmatrix} . \tag{4}$$

with $|\eta_1|$, $|\eta_2| \ll |\lambda|$. Here V_0 sets the overall interaction energy scale, the quantities λ and η_1/η_2 describe respectively the inter-band α-β and γ-α/β Josephson couplings, while the a_i's are the intra-band couplings irrelevant to the rigidity of the relative phases between the bands. Noting the similarity between the quasi-1D bands, one may approximate $|\eta_1| \simeq |\eta_2| = \eta$.

The rigidity of the relative phase between the bands is determined by the inter-band couplings. Assuming the same order parameter amplitude on all bands, and setting $\lambda > 0$, $\eta_1 \sim \eta_2 = \eta < 0$ in light of our numerical results to be presented in the next section, our analyses follow the standard procedure[49,54] and are given in detail in Appendix B (see a more thorough derivation in Marciani et al.[51]). To simply quote the main conclusion: the system exhibits a relatively soft Leggett mode, with an excitation gap that is determined by the inter-band couplings η in the following way,

$$w_L = \sqrt{\frac{3|\eta|}{N_0 V_0}} \Delta_0 , \tag{5}$$

where for simplicity we have assumed similar density of states N_0 and gap amplitudes on all bands. This mode is a consequence of phase fluctuations on the γ-band with respect to the other two bands. In the limit of vanishing interaction between the two sets of bands, this mode becomes massless.

The particular set of inter-band couplings considered above is free of frustration (see Sec IV). On the other hand, a set of frustrated inter-band interactions not realized in our model of Sr$_2$RuO$_4$, such as one that would lead to $\lambda > 0$, $\eta_1 > 0$ and $\eta_2 < 0$, gives rise to an anomalously soft Leggett mode, as has been shown previously[49,54] (see Appendix B).

II. WEAK COUPLING CALCULATIONS

We now present a microscopic calculation of the interaction matrix $\hat{V}$ for Sr$_2$RuO$_4$. The first step is to obtain the effective band interactions using the microscopic Hamiltonian of the three Ru t_{2g} 4d-orbitals. This can be achieved following the weak coupling renormalization group calculations by Scaffidi et al.[15] of the effective interaction $V^{\mu\nu}(\mathbf{k}, \mathbf{p})$ associated with each Cooper pair scattering process on any pair of μ- and ν-band Fermi surfaces. For the sake of brevity, we refer to Ref. 15 for details and only sketch the calculations here.

Most crucially, the study starts with on-site Coulomb inter-

actions in the orbital basis,

$$\begin{aligned} H_{\text{int}} &= \sum_{i,a,s \neq s'} \frac{U}{2} n_{ias} n_{ias'} + \sum_{i,a \neq b,s,s'} \frac{U'}{2} n_{ias} n_{ibs'} \\ &+ \sum_{i,a \neq b,s,s'} \frac{J}{2} c^\dagger_{ias} c^\dagger_{ibs'} c_{ias'} c_{ibs} \\ &+ \sum_{i,a \neq b,s \neq s'} \frac{J'}{2} c^\dagger_{ias} c^\dagger_{ias'} c_{ibs'} c_{ibs} , \end{aligned} \tag{6}$$

where i is the site index, $a = xz, yz, xy$ is the orbital index, s denotes the spin, $n_{ias} \equiv c^\dagger_{ias} c_{ias}$, $U' = U - 2J$, and $J' = J$ where J is the Hund's coupling. Following Raghu et al.,[20] these interactions are treated perturbatively in the limit $U, J \ll W$ where W is the bandwidth. Thus J/U fully parameterizes the interactions in the model. Projecting all interactions to the Fermi level, $V^{\mu\nu}(\mathbf{k}, \mathbf{p})$ in the Cooper channel is then evaluated up to the one-loop level, as is appropriate in the weak coupling limit. Finally, the superconducting gap function is obtained by solving the linearized gap equation using $V^{\mu\nu}(\mathbf{k}, \mathbf{p})$.

For a range of interaction and tight-binding parameters thought to be appropriate for Sr$_2$RuO$_4$, an anisotropic chiral p-wave pairing emerges as the most attractive solution to the gap equation (although a helical pairing represents a close competitor, see also Sec IV). We denote this gap in the following form,

$$\hat{\Delta}_{\mathbf{k}} = \begin{pmatrix} \Delta_{0\alpha} \phi_\alpha(\mathbf{k}) \\ \Delta_{0\beta} \phi_\beta(\mathbf{k}) \\ \Delta_{0\gamma} \phi_\gamma(\mathbf{k}) \end{pmatrix} , \tag{7}$$

where $\phi_\mu(\mathbf{k})$ is the normalized form factor of the full anisotropic chiral p-wave gap function on band-μ, and the vector $\hat{\Delta} = (\Delta_{0\alpha}, \Delta_{0\beta}, \Delta_{0\gamma})^T$, with its elements indicating the relative phase and magnitude of the order parameters on the three bands, specifies the order parameter configuration. Note that these anisotropic pairing gaps in general lead to noticeably reduced edge current,[38,39,42] with strong further suppression when combined with surface disorder.[37,39] Similarly anisotropic gaps on the two quasi-1D bands have also been invoked to explain tunneling conductance along the c-axis.[14]

In Appendix A we formulate an approach to extract the effective intra- and inter-band interactions. Essentially, in analogy to Scalapino et al.[55] formulated for a one-band model, the integrated inter-band interaction is approximated by,

$$V^{\mu\nu} = \frac{\oint_{\mu FS} d\mathbf{k} \oint_{\nu FS} d\mathbf{p} \frac{\phi_\mu^*(\mathbf{k}) V^{\mu\nu}(\mathbf{k},\mathbf{p}) \phi_\nu(\mathbf{p})}{v_\mu(\mathbf{k}) v_\nu(\mathbf{p})}}{\left(\oint_{\mu FS} d\mathbf{k} \frac{|\phi_\mu(\mathbf{k})|^2}{v_\mu(\mathbf{k})} \right)^{\frac{1}{2}} \left(\oint_{\nu FS} d\mathbf{p} \frac{|\phi_\nu(\mathbf{p})|^2}{v_\nu(\mathbf{p})} \right)^{\frac{1}{2}}} , \tag{8}$$

where $v_\mu(\mathbf{k})$ is the μ-band Fermi velocity at Fermi wavevector $\mathbf{k}$. For the parameters $J/U = 0.06$, $\lambda_{\text{SOC}} = 0.1t$,[56] used in Scaffidi et al.[15] (t is the primary in-plane hoping intergral of the 1D orbitals), we obtain,

$$\hat{V} = V_0 \begin{pmatrix} 0.5206 & -1.2181 & -0.0635 \\ -1.2181 & 0.3427 & -0.0608 \\ -0.0635 & -0.0608 & -1.0000 \end{pmatrix} \tag{9}$$

where $V_0 > 0$ sets the overall interaction energy scale in the pairing channel under consideration. Most notable features of this matrix include: a rather strong interaction between the two quasi-1D bands, considerably weaker inter-band interactions between the quasi 1D and 2D bands, and comparable intra-band couplings on the two quasi-1D bands, all of which are roughly consistent with the qualitative observation in the previous section. We verify that these main features are generic for a broad range of interaction parameters (also see (12) in Sec IV), and for spin-orbit coupling smaller than $0.1t$. Note that in this calculation, $\lambda_{SOC} = 0.1t$ already represents a rather strong spin-orbit coupling[56] suggested by recent measurements.[6–8] The relative inter-band interactions between γ and the other two bands depends on λ_{SOC} and are weaker for smaller spin-orbit coupling.

Following Appendix A, solving the compact gap equation (A4) which is related to (9), we obtain two attractive solutions, with the leading one given by $\hat{\Delta} \sim (0.33, 0.31, 0.89)^T$,[57] i.e. comparable gap amplitudes on the three bands similar to what was originally obtained in Ref. 15. In this regard, the $\hat{V}$-matrix encapsulates crucial information about the multi-band character of the superconducting state in the pairing channel under consideration. The noticeable attractive interaction on the γ-band can be attributed to the proximity to the van Hove singularity on that band. Interestingly, the quasi-1D bands experience repulsive intra-band interactions which disfavor Cooper pairing. This is however compensated by a strong interaction induced by the pronounced incommensurate spin fluctuations between the two bands, which is even stronger than the intra-band interaction on γ, to make the pairing strengths on the two sets of bands comparable. In fact, over a wide parameter range ($0 < J/U < 0.3$) one finds comparable gap magnitudes on all bands.[15]

As an important remark, while the one-loop weak coupling calculations likely have captured reasonably well the structure of the interactions and hence the symmetry and structure of the gaps, they could potentially predict inaccurate relative gap amplitudes on the bands. For example, at finite interaction scale, due to the quasi-nesting, the inter-band interactions between the 1D bands can in principle be enhanced once higher order scattering processes, such as at the level of random phase approximation, are included. This would accordingly enhance the pairing on these two bands with respect to that on γ. Of course, higher order contributions could also enhance the effect of the van Hove singularity, which would have the opposite effect, but this may be mitigated somewhat by the fact that the odd-parity gap function must vanish at the van Hove point.

In addition, in contrast to the results found here and originally in Scaffidi *et al.*[15], two recent numerical functional renormalization group approaches[22,24] have reported dominant triplet superconductivity on one of the two sets of bands. However, the two predictions differ in an important manner. Wang *et al.*[22] argued that the small wavevector spin fluctuations associated with the γ-band van-Hove singularity dominates the superconducting correlation (see also alternative argument by Huo *et al.*[23]), while in Tsuchiizu *et al.*[24] superconductivity is driven primarily by the large wavevector spin fluc-

tuations associated with the quasi-1D bands. The latter study also found noticeable proximity induced superconductivity on the γ-band once spin-orbit coupling is included. While we cannot resolve the on-going debate with our calculations, it may not be ruled out that both the small and large wavevector spin fluctuations enter at low energies with similar strength, promoting comparable pairings on all bands, as is found in this work.

III. LEGGETT MODES AND THEIR DETECTION IN RAMAN SPECTROSCOPY

To analyze the collective phase modes, we turn to the Josephson coupling matrix $\hat{\mathcal{V}} = -\hat{V}^{-1}$ using (9),

$$\hat{\mathcal{V}} = \frac{1}{V_0} \begin{pmatrix} 0.2653 & 0.9302 & -0.0734 \\ 0.9302 & 0.4019 & -0.0835 \\ -0.0734 & -0.0835 & 1.0000 \end{pmatrix} . \quad (10)$$

The qualitative features of the inter-band couplings we discussed below (4) are reproduced. The excitation gap of the soft Leggett mode may now be obtained following Appendix B,

$$w_L \simeq \sqrt{\frac{0.08}{N_0 V_0}} \Delta_0 , \quad (11)$$

where we have used the relation $2.8\Delta_{0\alpha} \simeq 2.8\Delta_{0\beta} \simeq \Delta_{0\gamma} = \Delta_0$ obtained above. One may use a rough weak-coupling estimate $N_0 V_0 \simeq 0.2$. Thus the energy required to excite this mode ($\sim 0.64\Delta_0$) is lower than the $2\Delta_0$ needed to break a Cooper pair in a fully gapped isotropic superconductor. Nevertheless, due to the strong anisotropy of the superconducting gap structure, low-lying quasi-particles should also exist well below $2\Delta_0$. Furthermore, with weaker spin-orbit coupling, η_1 and η_2 decrease, thus the Leggett mode becomes softer accordingly. Finally, at constant $\Delta_{0\gamma}$, w_L increases (decreases) with increasing (decreasing) $\Delta_{0\alpha,\beta}$.

We now discuss the experimental consequences for the Leggett modes. These collective phase modes couple indirectly to external electromagnetic fields and hence can be excited by photons in optical probes, such as electronic Raman spectroscopy. The Raman response can be derived via standard linear response theory, and we refer to Refs 49,58–60 for details. Essentially, when the frequency difference between the appropriate incident and scattered photons matches the excitation gap of a collective mode, the Raman spectrum exhibits a sharp resonance, as has been observed in the multi-band MgB_2 superconductor[61]. Moreover, since the Leggett modes correspond only to the relative phase fluctuations between the bands and do not perturb the symmetry of the Cooper pair wavefunction within the individual bands, they couple only to the A_{1g} channel. Thus the Raman spectrum in the A_{1g} channel is a direct measurement of the properties of these phase modes. In realistic situations, the sharp resonances are broadened due to damping effects introduced by impurities and low energy quasi-particles in anisotropic superconductors[62].
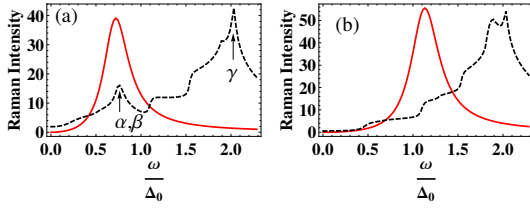
FIG. 2: Typical low-frequency electronic Raman response in
Sr_2RuO_4 in the A_{1g} channel in the cases of two different gap ra-
tios between the 1D and 2D bands: (a) $|\Delta_{0\gamma}| \simeq 2.8|\Delta_{0\alpha,\beta}|$, (b)
$|\Delta_{0\gamma}| \simeq |\Delta_{0\alpha,\beta}|$. The continuum contribution (black dashed), ex-
hibiting nonvanishing intensity below $\omega = 2\Delta_0$, is evaluated using
an anisotropic three-band chiral p-wave model. The gap anisotropy
resembles the one obtained in Ref. 15. A small imaginary part
$\tau = 0.004\Delta_0$ is used in the analytic continuation of the Raman
susceptibility for regularization. The Leggett mode contribution is
shown in red (solid). Here we have simplified the calculation by us-
ing a broadening of $\tau_L = 0.5\Delta_0$ to model the damping due to the
coupling with the low-lying quasi-particle states. This does not alter
the Leggett mode peak position[62].

In addition to the Leggett modes, there exists another
form of collective phase fluctuations in chiral superconduc-
tors – the so-called clapping modes[25]. These modes origi-
nate from relative phase oscillations between the two com-
ponents of the chiral order parameter (thus belonging to an-
gular momentum $2\hbar$ fluctuations) and are characterized by
an excitation gap $\sqrt{2}\Delta_0$ for a two dimensional isotropic chi-
ral p-wave superconductor.[63–66] The excitation energy may
become smaller for anisotropic superconductors.[66,67] Note
that by symmetry orthogonal order parameter components
from different bands do not couple, so that one can treat the
Leggett and clapping modes separately. In principle,
the clapping modes also manifest as resonances in optical
spectroscopies.[62,63,65,66] However, they do not couple to the
Raman A_{1g} channel,[65] thus distinguishing them from the
Leggett modes.

Following the derivations in Ref. 49, we plot in Fig 2 typi-
cal A_{1g} Raman response for a three-band chiral p-wave model
of Sr_2RuO_4 using (10). We have considered two different sce-
narios, one with smaller gap amplitude on the α and β-bands,
another with approximately equal gaps on all bands. In both
cases, the Leggett mode manifests as a peak in the spectra. In
the cases of sufficiently distinct gaps on the two sets of bands,
however, the Leggett mode peak can in principle overlap (as
in Fig.2 a), or even switch position with the continuum peak
associated with the smaller gap(s), thus potentially complicat-
ing the identification of the soft mode.

In summary, the existence of a low-frequency peak in the
A_{1g} channel of the Raman spectrum should be a character-
istic feature of the relatively soft Leggett mode in the multi-
band Sr_2RuO_4. However, some technical difficulties in Ra-
man spectroscopy, such as laser heating, must be overcome
in order to perform measurement at sub-Kelvin temperatures.
Furthermore, since the Leggett mode resides at sub-meV fre-
quency range, it may be obscured by the wings of the elastic

peak in the Raman spectrum.

IV. NEAR DEGENERATE ORDER PARAMETERS AND TRSB

Here we examine the possibility of TRSB multi-band pair-
ing. This has been predicted for some multi-band (three or
more bands) systems when there are two degenerate or near
degenerate order parameters, as can occur when the inter-band
interactions are frustrated.[46–50,52] In that case, the system may
pick a complex linear combination of the two near-degenerate
order parameters and, consequently, break time-reversal sym-
metry. Typically for there to be only a single transition with
the TRSB phase condensing at T_c, it requires fine tuning and
degenerate order parameters. But this phase may exist over
a range of parameters (for example as doping is varied), con-
densing at a second transition below T_c.

For the chiral channel of Sr_2RuO_4, the inter-band interac-
tions in (9) are unfrustrated, as they are all attractive, i.e. the
three band gaps can choose to have the same sign to simulta-
neously minimize the inter-band interactions. However, due
to the relatively weak interactions between γ and the other
two bands, the system might still permit two near degenerate
solutions, with $\Delta_{0\gamma}$ taking opposite signs with respect to the
other bands.

If two solutions are sufficiently close to degeneracy,
whether the two solutions would form a TRSB complex order
parameter can then be analyzed using an effective Ginzburg-
Landau theory (see Appendix C). Taking order parameter
fields Δ_1 and Δ_2 to denote the respective amplitudes of the
leading and subleading solutions, we find that the relative
phase between the two is determined by three quartic terms in
the free energy: $\beta'|\Delta_1|^2(\Delta_1^*\Delta_2 + \Delta_1\Delta_2^*)$, $\beta''|\Delta_2|^2(\Delta_1^*\Delta_2 +
\Delta_1\Delta_2^*)$, and $\beta(\Delta_1^*\Delta_2 + \Delta_1\Delta_2^*)^2$ ($\beta > 0$), the first two of
which favor a non-TRSB real superposition of the two fields,
while the last term promotes complex superposition. Since
Δ_1 dominates below T_c, the β' term is most significant. We
thus conclude that this type of complex multi-band order pa-
rameter is unlikely to develop in our system.

Another interesting possibility is a TRSB helical state.
However, we verify through our microscopic calculations that
the inter-band interactions in the helical channel are qualita-
tively similar to those of the chiral channel (thus our previ-
ous discussions of a relatively soft Leggett mode equally ap-
plies to the helical channel). For example, using $J/U = 0.08$,
$\lambda_{SOC} = 0.1t$, as in Ref. 15, we obtain for the helical channel,
similar to (9),

$$\hat{V} = V_0 \begin{pmatrix} 0.6185 & -1.6331 & -0.0635 \\ -1.6331 & 0.5193 & -0.0677 \\ -0.0635 & -0.0677 & -1.0000 \end{pmatrix}. \quad (12)$$

Thus the inter-band interactions are also unfrustrated. The
leading attractive order parameter has $\hat{\Delta} \sim (0.50, 0.65, 0.57)$,
i.e. comparable gap amplitudes on the thee bands as in the
chiral channel. Combined with the Ginzburg-Landau analysis,
we see that the TRSB multi-band pairing is equally unlikely
in this channel.

V. CONCLUSIONS

In this work we have focused on some novel aspects of Sr_2RuO_4 associated with the multi-band nature of the superconductivity in this material. Our qualitative and quantitative analyses yield a consistent description of the multi-band interactions and couplings between the three bands. In particular, in line with an earlier argument,[12] the distinct dimensional characters of the quasi-2D γ-band and the quasi-1D α/β-bands in general results in a rather weak coupling between the two sets of bands. Such a peculiar coupling scheme permits a relatively soft Leggett mode, which may be detected in optical probes such as Raman scattering, thereby providing a testing ground for understanding the nature of the multi-band unconventional superconductivity in Sr_2RuO_4.

In addition, our microscopically evaluated band interactions indicate comparable pairing interactions on the quasi-1D and 2D bands, although from quite different origins, thus clarifying the origin for Sr_2RuO_4 to exhibit comparable gaps on the three bands. We note this is compatible with specific heat measurements[13] and recent tunneling spectroscopy measurements.[14]

We also discussed the possibility of novel TRSB multi-band superconductivity, in both chiral and helical channels. However, Sr_2RuO_4 lacks the frustrated inter-band interactions favorable for the formation of the complex multi-band order parameter. Nevertheless, given the difficulties in reconciling chiral p-wave pairing[9–11,31] and the strict experimental upper bounds placed on the edge current,[32–35] as well as the indications of Pauli limiting effect in this material,[43,44] it might be instructive to investigate the possibility of alternative TRSB superconductivity which does not necessarily involve chiral p-wave pairing.

Finally, although our discussions are focused on Sr_2RuO_4, the analyses are suitable for studying the nature of multi-band superconductivity in other systems.

Appendix A: Gap equation and inter-band Josephson coupling

In the weak coupling renormalization group calculation presented in Scaffidi *et al.*,[15] the effective interaction $V^{\mu\nu}(\boldsymbol{k}, \boldsymbol{p})$ that scatters Cooper pairs is obtained by including all of the contributing diagrams up to the one-loop level. Here the wavevectors $\boldsymbol{k}$ and $\boldsymbol{p}$ are Fermi wavevector on band μ and ν, respectively. As will be further elaborated below, the "average" inter-band interaction *in a particular pairing channel* is a good measure of the strength of the inter-band Josephson coupling pertaining to that channel.

One can solve the linearized gap equation to obtain solutions belonging to different pairing channels,

$$\phi_\mu(\boldsymbol{k})\Delta_{0\mu} = -C \sum_{\nu=\alpha,\beta,\gamma} \oint_{\nu FS} \frac{d\boldsymbol{p}}{v_\nu(\boldsymbol{p})} V^{\mu\nu}(\boldsymbol{k},\boldsymbol{p})\phi_\nu(\boldsymbol{p})\Delta_{0\nu} .$$

(A1)

Here $C = \ln\frac{1.13W_D}{T_c}$, $\Delta_{0\mu}$ is the amplitude of the superconducting gap on band-μ, $\phi_\mu(\boldsymbol{k})$ is the normalized form factor characteristic of the symmetry and structure of the gap, and $v_\nu(\boldsymbol{p})$ is the Fermi velocity of band-ν. The most attractive eigen solution of (A1) corresponds to the leading superconducting instability with largest T_c.

The Josephson coupling between the bands in any particular pairing channel may be extracted through the following procedure. First multiply both sides of (A1) by $\frac{1}{v_\mu(\boldsymbol{k})}$, perform an integration over $\boldsymbol{k}$, and define the following quantities,

$$A_\mu = \oint_{\mu FS} d\boldsymbol{k} \frac{\phi_\mu^*(\boldsymbol{k})\phi_\mu(\boldsymbol{k})}{v_\mu(\boldsymbol{k})}$$

(A2)

$$V_0^{\mu\nu} = \oint_{\mu FS} d\boldsymbol{k} \oint_{\nu FS} d\boldsymbol{p}\frac{\phi_\mu^*(\boldsymbol{k})V^{\mu\nu}(\boldsymbol{k},\boldsymbol{p})\phi_\nu(\boldsymbol{p})}{v_\mu(\boldsymbol{k})v_\nu(\boldsymbol{p})}$$

(A3)

It is easy to show that $V_0^{\mu\nu} = (V_0^{\nu\mu})^*$. The gap equation (A1) can then be transformed into a simple matrix form,

$$\begin{pmatrix} A_\alpha\Delta_{0\alpha} \\ A_\beta\Delta_{0\beta} \\ A_\gamma\Delta_{0\gamma} \end{pmatrix} = -C \cdot \hat{V}_0 \begin{pmatrix} \Delta_{0\alpha} \\ \Delta_{0\beta} \\ \Delta_{0\gamma} \end{pmatrix},$$

(A4)

where,

$$\hat{V}_0 = \begin{pmatrix} V_0^{\alpha\alpha} & V_0^{\alpha\beta} & V_0^{\alpha\gamma} \\ V_0^{\beta\alpha} & V_0^{\beta\beta} & V_0^{\beta\gamma} \\ V_0^{\gamma\alpha} & V_0^{\gamma\beta} & V_0^{\gamma\gamma} \end{pmatrix}.$$

(A5)

Eq (A4) thus constitutes a set of compact gap equations where the form factors of the gap functions are integrated out. Note that all of the eigen solutions of this gap equation belong with the same underlying pairing channel specified by those form factors. In other words, the eigen solutions of (A4) only give the order parameter configurations (relative amplitudes and signs of the gaps) on the three bands, and the actual gap functions must necessarily contain the characteristic form factors.

We define the effective interactions between the bands as,

$$V^{\mu\nu} = \frac{V_0^{\mu\nu}}{\sqrt{A_\mu A_\nu}} . \tag{A6}$$

For a one-band system, this returns the effective interaction originally formulated in Ref. 55. Note that if we take a loose approximation $A_\alpha \simeq A_\beta \simeq A_\gamma = A_0$ (which is roughly correct for most of our numerical calculations), the eigen vectors of $\hat{V}_0$ (or $\hat{V}$) constitute the solutions to the gap equation.

In conjunction with the discussions below (2) in the main text, we obtain for the inter-band Josephson coupling, up to an overall constant of the order of the density of states,

$$\hat{\mathcal{V}} = -\hat{V}_0^{-1} . \tag{A7}$$

As a side remark, the relative signs of the $\Delta_{0\mu}$'s depend on the choice of gauge but the physics remains the same. For example, one can assign an arbitrary sign to the form factor of, say band-i, which according to (A3) results in a change in the signs of both V_0^{ij} and V_0^{ik} for $i \neq j$ and $i \neq k$. This yields sign changes in the corresponding Josephson couplings $\mathcal{V}^{ij}$ and $\mathcal{V}^{ik}$. However, neither the eigenvalues of (A4) nor the masses of the collective phase excitations are altered because of the sign change.

A gauge transformation cannot change the sign of *only* one of the three inter-band couplings. Thus one can classify the multi-band superconductivity based on the configuration of the signs of the inter-band Josephson couplings – a classification beyond the lattice point group symmetries.[54] For example, $\mathrm{sgn}[\mathcal{V}^{\alpha\beta}, \mathcal{V}^{\alpha\gamma}, \mathcal{V}^{\beta\gamma}] = [+ + -]$ is equivalent to $\mathrm{sgn}[\mathcal{V}^{\alpha\beta}, \mathcal{V}^{\alpha\gamma}, \mathcal{V}^{\beta\gamma}] = [+ - +]$, as the two can be transformed into one another by changing the sign of the form factor of the γ-band.

Appendix B: Leggett modes

Here, we analyze the effective model introduced in Sec I in detail and highlight the important features of the collective excitations associated with the relative phase fluctuations between the bands.

We ignore the generically massive order parameter amplitude modes. Making explicit the complex phases of the three gaps, $\Delta_l e^{i\theta_l}$ with $\Delta_l \equiv \Delta_{0l}$ positive real, we can then proceed to derive the dispersion relations for the phase modes, following the standard procedure[68]. After a gauge transformation, $(\psi_{l\sigma}, \psi_{l\bar\sigma}^\dagger)^T \to (e^{i\theta_l/2}\psi_{l\sigma}, e^{-i\theta_l/2}\psi_{l\bar\sigma}^\dagger)^T$, the effective action in Eq. (2) becomes,

$$S = \int d\tau d^3 r \left[\sum_{l,j} \Delta_l \hat{\mathcal{V}}_{lj} \Delta_j e^{i(\theta_l - \theta_j)} - \sum_l \mathrm{Tr}\ln(1 + \hat{G}_{0l}\Sigma_l) \right] \tag{B1}$$

where the Green's function satisfies,

$$\hat{G}_{0l}^{-1} = -\sigma_0 \partial_\tau + \Delta_l \sigma_1 - \sigma_3(-\frac{\nabla^2}{2m_l} - \mu_l) \tag{B2}$$

and the self-energy follows as,

$$\Sigma_l = -\left(\frac{i\nabla\theta_l \cdot \nabla}{2m_l}\right)\sigma_0 + \left[-i\frac{\partial_\tau\theta_l}{2} - \frac{1}{2m_l}\left(\frac{\nabla\theta_l}{2}\right)^2\right]\sigma_3 \tag{B3}$$

where σ_μ's are the usual Pauli matrices.

Consider small amplitude deviations of the phases from the stable state $\theta_l = \theta_{0l} + \phi_l$, the action in Eq. (B1) can be expanded with respect to the ϕ_l's as[49,54]

$$S[\phi] = \sum_n \int d^3 q \hat{\phi}(-w_n, -q)^T \mathcal{M}\hat{\phi}(w_n, q) \tag{B4}$$

where $\hat{\phi}(w_n, q) = (\phi_\alpha, \phi_\beta, \phi_\gamma)^T(w_n, q)$ with $w_n = 2n\pi/T$, and the matrix,

$$\mathcal{M} = \frac{1}{V_0} \begin{pmatrix} \mathcal{K}_\alpha - \lambda\epsilon_{\alpha\beta} - \eta\epsilon_{\alpha\gamma} & \lambda\epsilon_{\alpha\beta} & \eta\epsilon_{\alpha\gamma} \\ \lambda\epsilon_{\alpha\beta} & \mathcal{K}_\beta - \lambda\epsilon_{\alpha\beta} - \eta\epsilon_{\beta\gamma} & \eta\epsilon_{\beta\gamma} \\ \eta\epsilon_{\alpha\gamma} & \eta\epsilon_{\beta\gamma} & \mathcal{K}_\gamma - \eta(\epsilon_{\alpha\gamma} + \epsilon_{\beta\gamma}) \end{pmatrix} \tag{B5}$$

with $\mathcal{K}_l = N_l(w_n^2 + \bar{v}_{Fl}^2 q^2/2)$, $\epsilon_{lj} = \cos(\theta_{0l} - \theta_{0j})\Delta_{0l}\Delta_{0j}$, where N_l and $\bar{v}_{Fl}$ are respectively the density of states and average Fermi velocity of the l-band.

It is worth noting that the relative phase $\theta_{0l} - \theta_{0j}$, and hence the most stable order parameter configuration, depends on the relative magnitude and signs of the original inter-band interactions. For example, if all inter-band interactions are attractive as in our (9) and (12), the obvious most favorable state has all three order parameters in phase, i.e. $\epsilon_{lj} = 1$. In this case, now consider a rough approximation, $N_\alpha = N_\beta = N_\gamma = N_0$ and $\bar{v}_{F\alpha} = \bar{v}_{F\beta} = \bar{v}_{F\gamma} = \bar{v}_{F0}$, and take the amplitude of the gaps to be the same on all bands. After an analytic continuation, the dispersion relations for the phase modes may be obtained

by diagonalizing (B5),

$$w_G^2 = \frac{1}{2}\bar{v}_{Fl}^2 q^2 \tag{B6}$$

$$w_{L1}^2 = -3\frac{\Delta_0^2}{N_0 V_0}\eta + \frac{1}{2}\bar{v}_{Fl}^2 q^2 \tag{B7}$$

$$w_{L2}^2 = -\frac{\Delta_0^2}{N_0 V_0}(\eta + 2\lambda) + \frac{1}{2}\bar{v}_{Fl}^2 q^2 \tag{B8}$$

Here w_G denotes the usual $U(1)$ Goldstone mode, which would be massive had we properly included the vector potential in our formalism; w_{L1} and w_{L2} are the relative phase Leggett modes. Crucially, the excitation gap of the $L1$ mode, as determined by the γ-α/β inter-band Josephson coupling, may be considerably smaller than the superconducting gap. This is the soft Leggett mode we anticipated. Interestingly, in our case described by, e.g. (9) and (10), the L_2 mode is over-damped. This mode is related primarily to a relative phase oscillation between the two 1D bands dominated by an inter-band interaction. The readers are referred to Marciani et al.[51] for a more extensive discussion of the models containing dominant inter-band interactions.

Similar analyses carry through when the Josephson couplings take different signs. An interesting scenario arises when the inter-band interactions are frustrated (Sec IV), where a much softer Leggett mode is shown to be present[49,54]. From our calculations, this mode is given by $w_{L_1}^2 = \frac{3\Delta_0^2}{2N_0 V_0}\frac{|\eta|}{|\lambda|}|\eta|$. To summarize, a relatively soft Leggett mode exists in all scenarios, provided the ground state features comparable pairing gaps on the three bands.

Appendix C: Two near-degenerate solutions

Here we discuss the scenario where two nearly degenerate attractive order parameter configurations emerge,

$$\hat{\Delta}_{1\boldsymbol{k}} = \Delta_1 \begin{pmatrix} \eta_{1\alpha}\phi_\alpha(\boldsymbol{k}) \\ \eta_{1\beta}\phi_\beta(\boldsymbol{k}) \\ \eta_{1\gamma}\phi_\gamma(\boldsymbol{k}) \end{pmatrix} , \quad \hat{\Delta}_{2\boldsymbol{k}} = \Delta_2 \begin{pmatrix} \eta_{2\alpha}\phi_\alpha(\boldsymbol{k}) \\ \eta_{2\beta}\phi_\beta(\boldsymbol{k}) \\ \eta_{2\gamma}\phi_\gamma(\boldsymbol{k}) \end{pmatrix} , \tag{C1}$$

where $\hat{\eta}_i = (\eta_{i\alpha}, \eta_{i\beta}, \eta_{i\gamma})^T$ ($i = 1, 2$) are eigen vectors to (A4) with eigenvalues λ_1 and λ_2 (assume $|\lambda_1| \gtrsim |\lambda_2|$, $T_{c1} \gtrsim T_{c2}$), and the two fields Δ_1 and Δ_2 describe the amplitude of the superconducting order parameter in the corresponding solutions. In correspondence with the interactions given in (9), for example, $\hat{\eta}_1 = (0.33, 0.31, 0.89)^T$ and $\hat{\eta}_2 = (0.70, 0.67, -0.25)^T$. Note we have included in (C1) the form factors of the gaps on the respective bands for clarity. We are interested in the possibility of TRSB in connection

with a complex superposition of the two configurations. This may be best examined within an effective Ginzburg-Landau theory.

We wish to see if it is favorable for Δ_2 to coexist with the primary Δ_1 below the superconducting transition and form a complex order parameter. The free energy density reads,

$$\begin{aligned} f &= \frac{\alpha_1}{2}|\Delta_1|^2 + \frac{\alpha_2}{2}|\Delta_2|^2 \\ &+ \frac{\beta_1}{4}|\Delta_1|^4 + \frac{\beta_2}{4}|\Delta_2|^4 + \frac{\beta_{12}}{4}|\Delta_1|^2|\Delta_2|^2 \\ &+ \frac{\beta'}{4}|\Delta_1|^2(\Delta_1^*\Delta_2 + \Delta_1\Delta_2^*) + \frac{\beta''}{4}|\Delta_2|^2(\Delta_1^*\Delta_2 + \Delta_1\Delta_2^*) \\ &+ \frac{\beta}{4}(\Delta_1^*\Delta_2 + \Delta_1\Delta_2^*)^2 + ... , \end{aligned} \tag{C2}$$

where "..." stands for higher order terms, $\alpha_i \sim (T-T_{c,i})/T_{c,i}$, and all of the β-coefficients can be derived from the microscopic band structure and (C1). Here Δ_1 and Δ_2 share the same point group symmetry and $U(1)$ symmetry (instead of separate $U(1)$), thus the terms with β' and β'' are allowed.

It can be shown that $\beta_{1,2}, \beta_{12}, \beta > 0$, while β' and β'' can take both signs and are in general non-vanishing. Note in Maiti and Chubukov[50], $\beta' = \beta'' = 0$ due to the particular structure of the eigenbasis resulting from the effective multi-band interactions of their model. In our case for the type of interactions similar to (9) and (12), $\beta', \beta'' \neq 0$ and their magnitudes are of the same order as β.

Although Δ_2 is not expected to condense right below T_{c1}, the coupling between Δ_1 and Δ_2 associated with the β' term immediately induces a non-vanishing Δ_2 growing with Δ_1 as $|\Delta_2| \propto |\Delta_1|^3 \propto [(T_c - T)/T_c]^{\frac{3}{2}}$. Similarly the third possible order parameter (which is not near-degenerate and not explicitly written down in (C1)) will mix in below T_{c1}, but, in general, with a smaller amplitude. These sub-dominant components grow slower than Δ_1, but this nevertheless suggests that determining the low temperature multi-band gap amplitudes requires going beyond the weak-coupling approximations we used.

Irrespective of how a non-vanishing Δ_2 may arise below T_{c1}, when the two fields coexist, their relative phase is determined by the last three quartic terms in the free energy, of which the β-term favors a TRSB complex superposition, while the β'- and β''-terms favor non-TRSB order parameters. Since $|\Delta_1| \gg |\Delta_2|$, the β' term dominates. Thus we conclude that our system is unlikely to sustain a TRSB complex multi-band order parameter.

[1] A. J. Leggett, Prog. Theor. Phys. **36**, 901 (1966).

[2] P.W. Anderson, Phys. Rev. **110**, 827 (1958).

[3] Y. Maeno, T.M. Rice, and M. Sigrist, Physics Today **54**, 42 (2001).

[4] A.P. Mackenzie, and Y. Maeno, Rev. Mod. Phys. **75**, 657 (2003).

[5] C. Kallin, and A.J. Berlinsky, J. Phys.: Condens. Matter **21**, 164210 (2009).

[6] M.W. Haverkort, I.S. Elfimov, L.H. Tjeng, G.A. Sawatzky, and A. Damascelli, Phys. Rev. Lett. **101**, 026406 (2008).

[7] C.N. Veenstra, *et al.*, Phys. Rev. Lett. **112**, 127002 (2014).

[8] C.G. Fatuzzo, *et al.*, Phys. Rev. B **91**, 155104 (2015).

[9] See C. Kallin, Rep. Prog. Phys. 75, 042501 (2012), and references therein.

[10] C. Kallin and A.J. Berlinsky, Rep. Prog. Phys. **79**, 054502 (2016).

[11] Y. Maeno, S. Kittaka, T. Nomura, S. Yonezawa, and K. Ishida, J. Phys. Soc. Jpn. **81**, 011009 (2012), and references therein.

[12] D.F. Agterberg, T.M. Rice, and M. Sigrist, Phys. Rev. Lett. **78**, 3374 (1997).

[13] S. NishiZaki, Y. Maeno, and Z.Q. Mao, J. Phys. Soc. Jpn. **69**, 572 (2000).

[14] I.A. Firmo, S. Lederer, C. Lupien, A.P. Mackenzie, J.C. Davis, and S.A. Kivelson, Phys Rev. B **88**, 134521 (2013).

[15] T. Scaffidi, J.C. Romers, and S.H. Simon, Phys. Rev. B **89**, 220510(R) (2014).

[16] K. Deguchi, Z.Q. Mao, H. Yaguchi, and Y. Maeno, Phys. Rev. Lett. **92**, 047002 (2004); K. Deguchi, Z.Q. Mao, and Y. Maeno, J. Phys. Soc. Jpn. **73**, 1313 (2004).

[17] S.J. Ray, A.S. Gibbs, S.J. Bending, *et al.*, Phys. Rev. B **89**, 094504 (2014).

[18] M.E. Zhitomirsky, and T.M. Rice, Phys. Rev. Lett. **87**, 057001 (2001).

[19] e.g. T. Nomura and K. Yamada, J. Phys. Soc. Jpn. **71**, 1993 (2002).

[20] S. Raghu, A. Kapitulnik, S.A. Kivelson, Phys. Rev. Lett. **105**, 136401 (2010).

[21] J. Garaud, D.F. Agterberg, and E. Babaev, Phys. Rev. B **86**, 060513(R) (2012).

[22] Q.H. Wang, C. Platt, Y. Yang, C. Honerkamp, F.C. Zhang, W. Hanke, T.M. Rice and R. Thomale, Europhys. Lett. **104**, 17013 (2013).

[23] J.W. Huo, T.M. Rice and F.-C. Zhang, Phys. Rev. Lett. **110**, 167003 (2013).

[24] M. Tsuchiizu, Y. Yamakawa, S. Onari, Y. Ohno, and H. Kontani, Phys. Rev. B **91**, 155103 (2015).

[25] Dieter Vollhardt and Peter Wölfle, *The Superfluid Phases of Helium 3*, Dover Publications (1990).

[26] G.M. Luke, Y. Fudamoto, K.M. Kojima, *et al.*, Nature **394**, 558 (1998).

[27] K. Ishida, H. Mukuda, Y. Kitaoka, K. Asayama, Z.Q. Mao, Y. Mori, and Y. Maeno, Nature (London) **394**, 558 (1998).

[28] J. A. Duffy, S.M. Hayden, Y. Maeno, Z. Mao, J. Kulda, and G.J. McIntyre, Phys. Rev. Lett. **85**, 5412 (2000).

[29] K.D. Nelson, Z.Q. Mao, Y. Maeno, and Y. Liu, Science **306**, 1151 (2004).

[30] J. Xia, Y. Maeno, P.T. Beyersdorf, M.M. Fejer, and A. Kapitulnik, Phys. Rev. Lett. **97**, 167002 (2006).

[31] M. Matsumoto and M. Sigrist, J. Phys. Soc. Jpn. **68**, 994 (1999).

[32] J.R. Kirtley, C. Kallin, C.W. Hicks, E.-A. Kim, Y. Liu, K.A. Moler, Y. Maeno, K.D. Nelson, Phys. Rev. B **76**, 014526 (2007).

[33] C.W. Hicks, J.R. Kirtley, T.M. Lippman, N.C. Koshnick, *et al.*, Phys. Rev. B **81**, 214501 (2010).

[34] P.J. Curran, S.J. Bending, W.M. Desoky, A.S. Gibbs, S.L. Lee, A.P. Mackenzie, Phys. Rev. B **89**, 144504 (2014).

[35] Ying Liu, private communication (2016).

[36] Y. Imai, K. Wakabayashi, and M. Sigrist, Phys. Rev. B **85**, 174532 (2012); Phys. Rev. B **88**, 144503 (2013).

[37] S. Lederer, W. Huang, E. Taylor, S. Raghu, and C. Kallin, Phys. Rev. B **90**, 134521 (2014).

[38] A. Bouhon and M. Sigrist, Phys. Rev. B **90**, 220511(R) (2014).

[39] T. Scaffidi and S.H. Simon, Phys. Rev. Lett. **115**, 087003 (2015).

[40] Y. Tada, W. Nie, and M. Oshikawa, Phys. Rev. Lett. **114**, 195301 (2015).

[41] W. Huang, E. Taylor, and C. Kallin, Phys. Rev. B **90**, 224519 (2014).

[42] W. Huang, S. Lederer, E. Taylor, C. Kallin, Phys. Rev. B **91**, 094507 (2015).

[43] K. Deguchi, M.A. Tanatar, Z.Q. Mao, T. Ishiguro, and Y. Maeno, J. Phys. Jpn. Soc. **71**, 2839 (2002).

[44] S. Yonezawa, T. Kajikawa, and Y. Maeno, Phys. Rev. Lett. **110**, 077003 (2013).

[45] A. Ramires and M. Sigrist, arXiv:1605.03827 (2016).

[46] D.F. Agterberg, V. Barzykin, and L.P. Gor'kov, Phys. Rev. B **60**, 14868 (1999).

[47] K. Voelker and M. Sigrist, arXiv:cond-mat/0208367.

[48] V. Stanev and Z. Tesanovic, Phys. Rev. B **81**, 134522 (2010).

[49] S.-Z. Lin and X. Hu, Phys. Rev. Lett. **108**, 177005 (2012).

[50] S. Maiti and A.V. Chubukov, Phys. Rev. B **87**, 144511 (2013).

[51] M. Marciani, L. Fanfarillo, C. Castellani, and L. Benfatto, Phys. Rev. B **88**, 214508 (2013)

[52] P.K. Biswas, *et al.*, Phys. Rev. B **87**, 180503 (2013).

[53] Y. Sidis, M. Braden, P. Bourges, B. Hennion, S. NishiZaki, Y. Maeno, and Y. Mori, Phys. Rev. Lett. **83**, 3320 (1999).

[54] Y. Ota, M. Machida, T. Koyama, and H. Aoki, Phys. Rev. B **83**, 060507(R) (2011).

[55] D.J. Scalapino, E. Loh, Jr., and J.E. Hirsch, Phys. Rev. B **34**, 8190(R) (1986).

[56] Note that due to a notational difference, $\lambda_{\text{SOC}} = 0.1t$ in Ref. 15 corresponds to $\lambda_{\text{SOC}} = 0.2t$ in DFT and ARPES literature[6].

[57] The other solutions are $(0.70, 0.67, -0.25)^T$ (also with an attractive eigenvalue) and $(-0.77, 0.63, 0.00)^T$.

[58] T.P. Devereaux and D. Einzel, Phys. Rev. B **51**, 16336 (1995).

[59] M. Khodas, A.V. Chubukov, and G. Blumberg, Phys. Rev. B **89**, 245134 (2014).

[60] S. Maiti and P.J. Hirschfeld, Phys. Rev. B **92**, 094506 (2015).

[61] G. Blumberg, A. Mialitsin, B.S. Dennis, M.V. Klein, N.D. Zhigadlo, and J. Karpinski, Phys. Rev. Lett. **99**, 227002 (2007).

[62] P.J. Hirschfeld, W.O. Putikka, and P. Wölfle, Phys. Rev. Lett **69**, 1447 (1992).

[63] S. Higashitani and K. Nagai, Phys. Rev. B **62**, 3042 (2000).

[64] H-Y. Kee, Y.B. Kim, and K. Maki, **62**, 5877 (2000).

[65] H-Y. Kee, K. Maki, and C.H. Chung, Phys. Rev. B **67**, 180504(R) (2003).

[66] J.A. Sauls, H. Wu, and S.B. Chung, Front. Phys. **3**, 36 (2015).

[67] S.B. Chung, S. Raghu, A. Kapitulnik, and S.A. Kivelson, Phys. Rev. B **86**, 064525 (2012).

[68] I.J.R. Aitchison, P. Ao, D.J. Thouless, and X.-M. Zhu, Phys. Rev. B **51**, 6531 (1995).

Chapter 7

Conclusions

Despite more than twenty years of study, the unconventional superconductivity in Sr_2RuO_4 continues to attract considerable interest. This material exhibits highly two-dimensional electronic structure with simple Fermi surface geometry, and is an ideal Fermi liquid free of any other competing orders at the temperatures immediately above the superconducting transition. Moreover, superconductivity occurs without the need of doping. These salient features are not available in many other unconventional superconductors, such as the cuprates and iron-based superconductors.

A wide range of measurements have given strong support for spin-triplet odd-parity time-reversal symmetry breaking superconductivity in this material, making chiral p-wave order the most probable candidate ground state. However, such an order cannot be straightforwardly reconciled with several key experiments, the most notable of which is the absence of spontaneous surface currents.

In this thesis and in the associated publications, we have presented a general theory of the edge currents in chiral superconductors. We showed that edge current is not protected by the topology of the chiral ground state, and that it is sensitive to microscopic details such as band and gap structures. In particular, in the presence of a highly anisotropic superconducting gap

potentially relevant to Sr_2RuO_4, the edge current may be significantly reduced compared with the prediction based on a simple isotropic chiral *p*-wave model. When combined with surface disorder, this would lead to substantial further suppression of the edge current, which may be compatible with the stringent experimental upper bounds placed on the size of the surface current in this compound.

As a side product of our studies on Sr_2RuO_4, we found that, rather surprisingly, the integrated edge current (and hence the total orbital angular momentum in the case of a finite system) at a sharp confining edge vanishes identically for any continuum chiral superconductors with higher angular momentum Cooper pairing. In this regard, chiral *p*-wave is special! In lattice models, the net edge current for non-*p*-wave superconductors may not vanish but is significantly smaller than that of a simple isotropic chiral *p*-wave superconductor. In the limit of a soft confining edge, the orbital angular momentum and the corresponding total integrated edge current is recovered. These results hold important meaningful implications for the "angular momentum paradox" in ^{3}He A-phase which has been scrutinized for decades. In particular, we show that the total orbital angular momentum of a finite size chiral superfluid in rigid confinement is not straightforwardly related to the Cooper pair angular momentum.

Finally, we also delved into the superconducting mechanism of Sr_2RuO_4 and studied a few novel aspects of the multi-band nature of the superconductivity in this material. Our calculations elucidated the possible origin for the multiple bands to superconduct with comparable gap amplitudes, and pointed out the existence of a soft Leggett mode as a test of this conclusion. On account of the edge current problem and a few other measurements that are inconsistent with chiral *p*-wave pairing, we also examined the possibility of a novel multi-band TRSB superconductivity which does not require chiral pairing. However, within our model, Sr_2RuO_4 lacks the frustrated inter-band interactions required for the formation of such order.

In this thesis, we primarily focussed on issues related to the absence of observable edge currents and did not cover the other outstanding issues regarding the putative chiral p-wave order in Sr_2RuO_4. One example concerns the size of the chiral domains. The μSR [29] and Josephson interferometry [31] measurements are consistent with domains of the order of one μm, while the interpretations of the SQUID tunneling [21] and the Kerr effect [30] measurements require much larger domains. Another example is the absence of split superconducting transitions in the presence of an in-plane magnetic field. For an in-plane field oriented along the crystalline a-axis, the proposed two-component chiral order is expected to lead to two successive transitions corresponding respectively to the onset of the two components.[42] An early specific heat measurement showed indication of multiple transitions [108], which is however not observed in more recent measurements on much smaller single crystalline samples.[109] Thus more thorough theoretical investigations are needed in order to fully understand the nature of the unconventional superconductivity in Sr_2RuO_4.

Bibliography

[1] H. Kamerlingh Onnes, Comm. Phys. Lab. Univ. Leiden, Nos. 119, 120, 122 (1911).

[2] J. Bardeen, L.N. Cooper, J.R. Schrieffer, Phys. Rev. **106**, 162 (1957); Phys. Rev. **108**, 1175 (1957).

[3] Y. Maeno, H. Hashimoto, K. Yoshida, S. Nishizaki, *et al*, Nature (London) **372**, 532 (1994).

[4] A.P. Mackenzie, and Y. Maeno, Rev. Mod. Phys. **75**, 657 (2003).

[5] J.G. Bednorz and K.A. Müller, Z. Phys. B **64**, 189 (1986).

[6] P.A. Lee, N. Nagaosa, and X.-G. Wen, Rev. Mod. Phys. **78**, 17 (2006).

[7] A. Damascelli *et al.*, Phys. Rev. Lett. **85** 5194 (2000).

[8] C. Bergemann, S.R. Julian, A.P. Mackenzie, S. NishiZaki and Y. Maeno Phys. Rev. Lett. **84**, 2662 (2000).

[9] T. Oguchi, Phys. Rev. B **51**, 1385 (1995).

[10] C.N. Veenstra, *et al.*, Phys. Rev. Lett. **112**, 127002 (2014).

[11] M.W. Haverkort, I.S. Elfimov. L.H. Tjeng, G.A. Sawatzky, and A. Damascelli, Phys. Rev. Lett. **101**, 026406 (2008).

[12] C.G. Fatuzzo, *et al.*, Phys. Rev. B **91**, 155104 (2015).

[13] Y. Maeno, T.M. Rice, and M. Sigrist, **54**, 42 Physics Today (2001).

[14] C. Kallin, and A.J. Berlinsky, J. Phys.: Condens. Matter **21**, 164210 (2009).

[15] C. Kallin, Rep. Prog. Phys. **75**, 042501 (2012).

[16] Y. Maeno, S. Kittaka, T. Nomura, S. Yonezawa, and K. Ishida, J. Phys. Soc. Jpn. **81**, 011009 (2012).

[17] C. Kallin, and A.J. Berlinsky, Rep. Prog. Phys. **79**, 054502 (2016).

[18] A.P. Mackenzie, R.K.W. Haselwimmer, A.W. Tyler, G.G. Lonzarich, Y. Mori, S. Nishizaki, and Y. Maeno, Phys. Rev. Lett. **80**, 161 (1998).

[19] K. Ishida, H. Mukuda, Y. Kitaoka, K. Asayama, Z.Q. Mao, Y. Mori, and Y. Maeno, Nature (London) **394**, 558 (1998).

[20] J. A. Duffy, S.M. Hayden, Y. Maeno, Z. Mao, J. Kulda, and G.J. McIntyre, Phys. Rev. Lett. **85**, 5412 (2000).

[21] K.D. Nelson, Z.Q. Mao, Y. Maeno, and Y. Liu, Science **306**, 1151 (2004).

[22] J. Jang, D.G. Ferguson, V. Vakaryuk, R. Budakian, S.B. Chung, P.M. Goldbart, and Y. Maeno, Science **331**, 186 (2011).

[23] X. Cai, Y.A. Ying, N.E. Staley, Y. Xin, D. Fobes, T.J. Liu, Z.Q. Mao, and Y. Liu, Phys. Rev. B **87**, 081104(R) (2013).

[24] X. Cai, Y.A. Ying, B. Zakrzewski, D. Fobes, T.J. Liu, Z.Q. Mao, and Y. Liu, arXiv:1507.00326 (2015).

[25] S.B. Chung, H. Bluhm, and E.A. Kim, Phys. Rev. Lett. **103**, 057003 (2007).

[26] V. Vakaryuk and A.J. Leggett, Phys. Rev. Lett. **99**, 197002 (2009).

[27] H.-Y. Kee and M. Sigrist, arXiv:1307.5859v1 (2013).

[28] K. Roberts, R. Budakian, and M. Stone, Phys. Rev. B **88**, 094503 (2013).

[29] G.M. Luke, Y. Fudamoto, K.M. Kojima, M.I. Larkin, *et al*, Nature (London) **394**, 558 (1998).

[30] J. Xia, Y. Maeno, P.T. Beyersdorf, M.M. Fejer, and A. Kapitulnik, Phys. Rev. Lett. **97**, 167002 (2006).

[31] F. Kidwingira, J.D. Strand, D.J. Van Harlingen, and Y. Maeno, Science **314**, 1267 (2006).

[32] H. Wang, J. Luo, W. Lou, J. Wei, J.E. Ortmann, Z.Q. Mao, Y. Liu, arXiv:1605.07712.

[33] Dieter Vollhardt and Peter Wölfle, *The Superfluid Phases of Helium-3*, Dover Pbulications (1990).

[34] T.M. Rice, and M. Sigrist, J. Phys.: Condens. Matter **7**, L643 (1995).

[35] K.K. Ng and M. Sigrist, Europhys. Lett. **49**, 473 (2000).

[36] Grigory E. Volovik, *The Universe in a Helium Droplet*, Oxford University Press, (2003).

[37] A.J. Leggett Rev. Mod. Phys. **47**, 331 (1975).

[38] D.J. Thouless, M. Kohomoto, M.P. Nightingale, and M. den Nijs, Phys. Rev. Lett. **49**, 405 (1982).

[39] G.E. Volovik, JETP Lett., **70**, 609 (1999).

[40] M.Z. Hasan and C.L. Kane, Rev. Mod. Phys. **82**, 3045 (2010).

[41] X.L. Qi and S.C. Zhang, Rev. Mod. Phys. **83**, 1057 (2011).

[42] M. Sigrist and K. Ueda, Rev. Mod. Phys. **63**, 239 (1991).

[43] N.B. Kopnin and M.M. Salomaa, Phys. Rev. B **44**, 9667 (1991).

[44] N. Read and D. Green, Phys. Rev. B **61**, 10267 (2000).

[45] E. Majorana, Nuovo Cimento **14**, 171 (1937).

[46] D.A. Ivanov, Phys. Rev. Lett. **86**, 268 (2001).

[47] C. Nayak, S.H. Simon, A. Stern, M. Freedman and S. Das Sarma, Rev. Mod. Phys. **80**, 3 (2008).

[48] M. Stone, and R. Roy, Phys. Rev. B **69**, 184511 (2004).

[49] R. Jackiw and C. Rebbi, Phys. Rev. D **13**, 3398 (1976).

[50] P.W. Anderson and P. Morel, Phys. Rev. 123, 1911 (1961).

[51] G.E. Volovik, JETP Letters 22, 108 (1975).

[52] M.C. Cross, J. Low Temp. Phys. 26, 165 (1977).

[53] M. Ishikawa, Prog. Theor. Phys. 57, 1836 (1977).

[54] A.J. Leggett and S. Takagi, Annals of Physics 110, 353 (1978).

[55] M.G. McClure and S. Takagi, Phys. Rev. Lett. 43, 596 (1979).

[56] N.D. Mermin and P. Muzikar, Phys. Rev. B **21**, 980 (1980).

[57] J.A. Sauls, Phys. Rev. B **84**, 214509 (2011).

[58] M. Matsumoto and M. Sigrist, J. Phys. Soc. Jpn. **68**, 994 (1999).

[59] A. Furusaki, M. Matsumoto, and M. Sigrist, Phys. Rev. B **64** 054514 (2001).

[60] J.R. Kirtley, C. Kallin, C.W. Hicks, E.-A. Kim, Y. Liu, K.A. Moler, Y. Maeno, K.D. Nelson, Phys. Rev. B **76**, 014526 (2007).

[61] C.W. Hicks, J.R. Kirtley, T.M. Lippman, N.C. Koshnick, *et al*, Phys. Rev. B **81**, 214501 (2010).

[62] P. Curran, S.J. Bending, W. Desoky, A.S. Gibbs, A.S. Lee, A.P. Mackenzie, Phys. Rev. B **89**, 094504 (2014).

[63] P.E.C. Ashby and C. Kallin, Phys. Rev. B **79**, 224509 (2009).

[64] S. Kashiwaya, H. Kashiwaya, H. Kambara, T. Furuta, H. Yaguchi, Y, Tanaka, and Y. Maeno, Phys. Rev. Lett. **107**, 077003 (2011).

[65] S. Lederer, W. Huang, E. Taylor, S. Raghu, and C. Kallin, Phys. Rev. B **90**, 134521 (2014).

[66] T. Scaffidi and S.H. Simon, Phys. Rev. Lett. **115**, 087003 (2015).

[67] Y. Imai, K. Wakabayashi, and M. Sigrist, Phys. Rev. B **85**, 174532 (2012); Y. Imai, K. Wakabayashi, and M. Sigrist, Phys. Rev. B **88**, 144503 (2013).

[68] G. Baskaran, Physica B: Condensed Matter, **223&224**, 490 (1996).

[69] T. Takimoto, Phys. Rev. B **62**, 14641(R) (2000).

[70] T. Kuwabara, and M. Ogata, Phys. Rev. Lett. **85**, 4586 (2000).

[71] T. Nomura and K. Yamada, J. Phys. Soc. Jpn. **69**, 3678 (2000).

[72] T. Nomura and K. Yamada, J. Phys. Soc. Jpn. **71**, 1993 (2002).

[73] S. Raghu, A. Kapitulnik, S.A. Kivelson, Phys. Rev. Lett. **105**, 136401 (2010).

[74] C.M. Puetter, Hae-Young Kee, EPL **98**, 27010 (2012).

[75] J. Huo, T.M. Rice and F.-C. Zhang, Phys. Rev. Lett. **110**, 167003 (2013).

[76] Q.H. Wang, C. Platt, Y. Yang, C. Honerkamp, F.C. Zhang, W. Hanke, T.M. Rice, T. Thomale, Europhys. Lett. **104**, 17013 (2013).

[77] T. Scaffidi, J.C. Romers, S.H. Simon, Phys. Rev. B **89**, 220510 (2014).

[78] M. Tsuchiizu, Y. Yamakawa, S. Onari, Y. Ohno, H. Kontani, Phys. Rev. B **91**, 155103 (2015).

[79] S. NashiZaki, Y. Maeno, and Z.Q. Mao, J. Phys. Soc. Jpn. **69**, 572 (2000).

[80] I.A. Firmo, S. Lederer, C. Lupien, A.P. Mackenzie, J.C. Davis, and S.A. Kivelson, Phys. Rev. B **88**, 134521 (2013).

[81] K. Deguchi, Z.Q. Mao, H. Yaguchi, and Y. Maeno, Phys. Rev. Lett. **92**, 047002 (2004); K. Deguchi, Z.Q. Mao, and Y. Maeno, J. Phys. Soc. Jpn. **73**, 1313 (2004).

[82] M.E. Zhitomirsky, and T.M. Rice, Phys. Rev. Lett. **87**, 057001 (2001).

[83] Chapter 6, A. Altland and B. Simons, *Condensed Matter Field Theory*, Cambridge University Press, (2006).

[84] Chapter 7, C. Mudry, *Lecture Notes on Field Theory in Condensed Matter Physics*, World Scientific, (2014).

[85] S.-I. Suzuki and Y. Asano, arXiv:1602.03994.

[86] B.A. Bernevig, with T.L. Hughes, *Topological Insulators and Topological Superconductors*, Princeton University Press, (2013).

[87] W. Huang, E. Taylor and C. Kallin, Phys. Rev. B **90**, 224519 (2014).

[88] A. Bouhon and M. Sigrist, Phys. Rev. B **90**, 220511(R) (2014).

[89] W. Huang, S. Lederer, E. Taylor, C. Kallin, Phys. Rev. B **91**, 094507 (2015).

[90] Y. Tada, W. Nie, and M. Oshikawa, Phys. Rev. Lett. **114**, 195301 (2015).

[91] T. Ojanen, Phys. Rev. B **93**, 174505 (2016).

[92] A. Shitade and Y. Nagai, Phys. Rev. B **93**, 174517 (2016).

[93] R. Joynt and L. Taillefer, Rev. Mod. Phys. **74**, 235 (2002).

[94] M.H. Fischer, *et al.*, Phys. Rev. B **89**, 020509 (2014).

[95] K. Takada, H. Sakurai, E. Takayama-Muromachi, F. Izumi, R.A. Dilanian and T. Sasaki, Nature **422**, 53 (2003).

[96] R. Nandkishore, L.S. Levitov, and AV. Chubukov, Nat. Phys. **8**, 158 (2012).

[97] G.E. Volovik, JETP **67**, 1804 (1988).

[98] Phys. Lett. A **246**, 549 (1998).

[99] D.F. Agterberg, T.M. Rice, and M. Sigrist, Phys. Rev. Lett. **97**, 3374 (1997).

[100] A. J. Leggett, Prog. Theor. Phys. **36**, 901 (1966).

[101] M. Braden, *et al.*, Phys. Rev. B **66**, 064522 (2002).

[102] D.F. Agterberg, V. Barzykin, and L.P. Gor'kov, Phys. Rev. B **21**, 14868 (1999).

[103] K. Voelker and M. Sigrist, arXiv:cond-mat/0208367.

[104] V. Stanev and Z. Tesanovic, Phys. Rev. B **81**, 134522 (2010).

[105] S.-Z. Lin and X. Hu, Phys. Rev. Lett. **108**, 177005 (2012).

[106] P.K. Biswas, *et al.*, Phys. Rev. B **87**, 180503 (2013).

[107] H. Murakawa, K. Ishida, K. Kitagawa, Z.Q. Mao, and Y. Maeno, Phys. Rev. Lett. **93**, 167004 (2004).

[108] K. Deguchi, M.A. Tanatar, Z.Q. Mao, T. Ishiguro, and Y. Maeno, J. Phys. Jpn. Soc. **71**, 2839 (2002).

[109] S. Yonezawa, T. Kajikawa, and Y. Maeno, Phys. Rev. Lett. **110**, 077003 (2013).

[110] L.P. Gor'kov, Soviet Phys. JETP, **9**, 1364 (1959).

[111] J. Goldstone and F. Wilczek, Phys. Rev. Lett. **47**, 986 (1981).

[112] M. Stone, Phys. Rev. B **31**, 6112 (1985).

[113] B. Horovitz and A. Golub, Phys. Rev. B **68**, 214503 (2003).

[114] B. Braunecker, P.A. Lee, and Z. Wang, Phys. Rev. Lett. **95**, 017004 (2005).

Appendix A

Derivation of Ginzburg-Landau free energy

Here we outline the derivation of the Ginzburg-Landau free energy of multi-component superconductors with arbitrary pairing symmetries, up to the quartic order in the order parameter amplitudes. The theory is expected to provide excellent phenomenological descriptions near T_c [42]. The original microscopic derivation of Ginzburg-Landau theory for an s-wave superconductor was due to Gor'kov[110]. Here we adopt a functional integral approach[83, 84] and restrict the discussions to a one-band model. Generalizations to multi-band models are straightforward.

For a general two-component superconductor, we write the position-dependent order parameter as $\Delta(\mathbf{r}, \mathbf{r}') = \Delta_1(\mathbf{r}, \mathbf{r}') + \Delta_2(\mathbf{r}, \mathbf{r}')$, where $\mathbf{r}\&\mathbf{r}'$ are the coordinates of the electrons constituting the Cooper pairs. In a uniform system, this order parameter may be Fourier transformed to obtain the gap function $\Delta_{0\mathbf{k}} = \Delta_{10}f_{1\mathbf{k}} + \Delta_{20}f_{2\mathbf{k}}$, where $\mathbf{k}$ is the relative momentum of the two electrons, and $f_{1\mathbf{k}}$ and $f_{2\mathbf{k}}$ are real form factors characteristic of the symmetry of the Cooper pair wavefunctions. We start from the functional of the form of (2.1) in which the electrons are already integrated out,

$$S[\Delta^*, \Delta] = \int_0^\beta d\tau \int d\mathbf{r} \int d\mathbf{r}' \left(\frac{|\Delta_1(\mathbf{r}, \mathbf{r}')|^2}{V_1(\mathbf{r}, \mathbf{r}')} + \frac{|\Delta_2(\mathbf{r}, \mathbf{r}')|^2}{V_2(\mathbf{r}, \mathbf{r}')} - \text{Tr} \ln \hat{G}^{-1}(\tau, \mathbf{r}, \mathbf{r}') \right), \qquad (7.1)$$

where the Gor'kov Greens function is given by,

$$
\hat{G}^{-1}(\tau, \mathbf{r}, \mathbf{r}') = \begin{pmatrix} -\partial_\tau - \hat{H}_0(\mathbf{r}, \mathbf{r}') & \Delta_1(\mathbf{r}, \mathbf{r}') + \Delta_2(\mathbf{r}, \mathbf{r}') \\ \Delta_1^*(\mathbf{r}, \mathbf{r}') + \Delta_2^*(\mathbf{r}, \mathbf{r}') & -\partial_\tau + \hat{H}_0^*(\mathbf{r}, \mathbf{r}') \end{pmatrix}, \tag{7.2}
$$

Assume translational invariant effective interactions $V_i(\mathbf{r}, \mathbf{r}')$ which depend only on the center-of-mass (COM) coordinate of the Cooper pairs, $(\mathbf{r} + \mathbf{r}')/2$, the first two terms in the integrand of (7.1) reduces to $|\Delta_i((\mathbf{r} + \mathbf{r}')/2)|^2/V_i$, i.e. without explicit dependence on the relative co-ordinate. The last part in (7.1) may be expanded perturbatively in powers of Δ_i. Using the relation,

$$
\begin{aligned}
\text{Tr} \ln \hat{G}^{-1} &= \text{Tr} \ln(\hat{G}_0^{-1} + \hat{\Delta}) = \text{Tr} \ln \hat{G}_0^{-1}(1 + \hat{G}_0 \hat{\Delta}) \\
&= \text{const.} + \text{Tr} \ln(1 + \hat{G}_0 \hat{\Delta}) \\
&= \text{const.} - \frac{1}{2n} \sum_{n=0}^{\infty} \text{Tr}[\hat{G}_0 \hat{\Delta}]^{2n},
\end{aligned} \tag{7.3}
$$

after a Fourier transformation to momentum space using the COM and relative momenta $\mathbf{q}$ and $\mathbf{k}$, and to Matsubara frequency space with no external frequency (not considering dynamics), the expansion returns the following second and fourth order terms,

$$
S_2 = \sum_{\mathbf{q}} \left\{ \frac{|\Delta_{1\mathbf{q}}|^2}{V_1} + \frac{|\Delta_{2\mathbf{q}}|^2}{V_2} + \frac{T}{2L^d} \sum_{w,\mathbf{k}} \text{Tr}\left[\hat{G}_0(w, \mathbf{k} + \frac{\mathbf{q}}{2})\hat{\Delta}_{\mathbf{k},\mathbf{q}}^* \hat{G}_0(w, \mathbf{k} - \frac{\mathbf{q}}{2})\hat{\Delta}_{\mathbf{k},-\mathbf{q}}\right] \right\}, \tag{7.4}
$$

and

$$
\begin{aligned}
S_4 = \sum_{\mathbf{q},\mathbf{q_1},\mathbf{q_2}} \frac{T}{4L^d} \sum_{w,\mathbf{k}} \quad & \text{Tr}[\hat{G}_0(w, \mathbf{k} + \frac{\mathbf{q}}{2})\hat{\Delta}_{\mathbf{k},\mathbf{q}}^* \hat{G}_0(w, \mathbf{k} - \frac{\mathbf{q_1}}{2})\hat{\Delta}_{\mathbf{k},-\mathbf{q_1}} \hat{G}_0(w, \mathbf{k} + \frac{\mathbf{q_2}}{2})\hat{\Delta}_{\mathbf{k},\mathbf{q_2}}^* \\
& \cdot \hat{G}_0(w, \mathbf{k} - \frac{\mathbf{q} - \mathbf{q_1} + \mathbf{q_2}}{2})\hat{\Delta}_{\mathbf{k},-(\mathbf{q}-\mathbf{q_1}+\mathbf{q_2})}],
\end{aligned} \tag{7.5}
$$

where

$$\hat{G}_0(w,\mathbf{k}) = \begin{pmatrix} \frac{1}{iw-\xi_{\mathbf{k}}} & 0 \\ 0 & \frac{1}{iw+\xi_{-\mathbf{k}}} \end{pmatrix} = \begin{pmatrix} g(w,\mathbf{k}) & 0 \\ 0 & \bar{g}(w,\mathbf{k}) \end{pmatrix}, \tag{7.6}$$

and,

$$\hat{\Delta}_{\mathbf{k},\mathbf{q}} = \begin{pmatrix} 0 & \Delta_{1\mathbf{q}}f_{1\mathbf{k}}+\Delta_{2\mathbf{q}}f_{2\mathbf{k}} \\ \Delta^*_{1\mathbf{q}}f_{1\mathbf{k}}+\Delta^*_{2\mathbf{q}}f_{2\mathbf{k}} & 0 \end{pmatrix}. \tag{7.7}$$

The gradient-free terms in the free energy are associated with an expansion with vanishing COM momentum, $\mathbf{q} = 0$. Employing this condition to both (7.4) and (7.5) and explicitly evaluating the traces, we obtain,

$$
\begin{aligned}
S_{20} &= \left[\frac{1}{V_1} + \frac{T}{L^d}\sum_{w,\mathbf{k}} g(w,\mathbf{k})\bar{g}(w,\mathbf{k})f^2_{1\mathbf{k}} \right] |\Delta_1|^2 + \left[\frac{1}{V_2} + \frac{T}{L^d}\sum_{w,\mathbf{k}} g(w,\mathbf{k})\bar{g}(w,\mathbf{k})f^2_{2\mathbf{k}} \right] |\Delta_2|^2 \\
&= \frac{\alpha_1(T)}{2}|\Delta_1|^2 + \frac{\alpha_2(T)}{2}|\Delta_2|^2 ,
\end{aligned} \tag{7.8}
$$

where $\frac{\alpha_i(T)}{2} = \frac{1}{V_i} + \frac{T}{L^d}\sum_{w,\mathbf{k}} g(w,\mathbf{k})\bar{g}(w,\mathbf{k})f^2_{i\mathbf{k}} \sim (T - T_{c,i})/T_{c,i}$, and

$$
\begin{aligned}
S_{40} &= \frac{T}{2L^d}\sum_{w,\mathbf{k}}[g(w,\mathbf{k})\bar{g}(w,\mathbf{k})]^2 \left[(\Delta_1 f_{1\mathbf{k}} + \Delta_2 f_{2\mathbf{k}})(\Delta^*_1 f_{1\mathbf{k}} + \Delta^*_2 f_{2\mathbf{k}}) \right]^2 \\
&= \frac{\beta_1}{4}|\Delta_1|^4 + \frac{\beta_2}{4}|\Delta_2|^4 + \frac{\beta_{12}}{4}|\Delta_1|^2|\Delta_2|^2 + \frac{\beta'}{4}(\Delta^*_1\Delta_2 + \Delta_1\Delta^*_2)^2 \\
&\quad + \frac{\beta_3}{4}|\Delta_1|^2(\Delta^*_1\Delta_2 + \Delta_1\Delta^*_2) + \frac{\beta_4}{4}|\Delta_2|^2(\Delta^*_1\Delta_2 + \Delta_1\Delta^*_2) ,
\end{aligned} \tag{7.9}
$$

with the following relations,

$$\beta_1 = 2\frac{T}{L^d}\sum_{w,\mathbf{k}}[g(w,\mathbf{k})\bar{g}(w,\mathbf{k})]^2 f^4_{1\mathbf{k}} , \tag{7.10}$$

$$\beta_2 = 2\frac{T}{L^d}\sum_{w,\mathbf{k}}[g(w,\mathbf{k})\bar{g}(w,\mathbf{k})]^2 f_{2\mathbf{k}}^4, \tag{7.11}$$

$$\beta_{12} = 4\frac{T}{L^d}\sum_{w,\mathbf{k}}[g(w,\mathbf{k})\bar{g}(w,\mathbf{k})]^2 f_{1\mathbf{k}}^2 f_{2\mathbf{k}}^2, \tag{7.12}$$

$$\beta' = 2\frac{T}{L^d}\sum_{w,\mathbf{k}}[g(w,\mathbf{k})\bar{g}(w,\mathbf{k})]^2 f_{1\mathbf{k}}^2 f_{2\mathbf{k}}^2 = \frac{\beta_{12}}{2}, \tag{7.13}$$

$$\beta_3 = 2\frac{T}{L^d}\sum_{w,\mathbf{k}}[g(w,\mathbf{k})\bar{g}(w,\mathbf{k})]^2 f_{1\mathbf{k}}^3 f_{2\mathbf{k}}, \tag{7.14}$$

$$\beta_4 = 2\frac{T}{L^d}\sum_{w,\mathbf{k}}[g(w,\mathbf{k})\bar{g}(w,\mathbf{k})]^2 f_{1\mathbf{k}} f_{2\mathbf{k}}^3. \tag{7.15}$$

Note that although the first four β-coefficients do not vanishing, the last two may by symmetry, such as for a p-wave superconductor with $f_{1\mathbf{k}} \sim k_x$ and $f_{2\mathbf{k}} \sim k_y$.

The lowest order gradient terms in the free energy are obtained from a small-$\mathbf{q}$ expansion of the second term in (7.4). Keeping the expansion up to the quadratic order of $\mathbf{q}$ (terms associated with linear order of $\mathbf{q}$ vanish),

$$
\begin{aligned}
S_{2\partial} &= \sum_{i,j=1,2}\sum_{l,m=x,y}\left\{\frac{T}{L^d}\sum_{w,\mathbf{k}}f_{i\mathbf{k}}f_{j\mathbf{k}}\frac{\partial^2}{\partial q_l \partial q_m}\left[g(w,\mathbf{k}+\frac{\mathbf{q}}{2})\bar{g}(w,\mathbf{k}-\frac{\mathbf{q}}{2})\right]_{\mathbf{q}\to 0}\right\}\cdot q_l q_m \Delta_{i\mathbf{q}}^* \Delta_{j\mathbf{q}} \\
&= \sum_{i,j=1,2}\sum_{l,m=x,y}k_{lm}^{ij}q_l q_m \Delta_{i\mathbf{q}}^* \Delta_{j\mathbf{q}} \tag{7.16} \\
&\to \sum_{i,j=1,2}\sum_{l,m=x,y}k_{lm}^{ij}\partial_l \Delta_i^* \partial_m \Delta_j, \tag{7.17}
\end{aligned}
$$

where q_l is the l-th component of $\mathbf{q}$, and in the final step we have performed a Fourier transformation back to real space. Finally, the k-coefficients are given by,

$$
\begin{aligned}
k_{lm}^{ij} &= \frac{T}{L^d} \sum_{w,\mathbf{k}} f_{i\mathbf{k}} f_{j\mathbf{k}} \frac{\partial^2}{\partial_{\mathbf{q_l}} \partial_{\mathbf{q_m}}} \left[g(w, \mathbf{k} + \frac{\mathbf{q}}{2}) \bar{g}(w, \mathbf{k} - \frac{\mathbf{q}}{2}) \right]_{\mathbf{q} \to \mathbf{0}} \\
&\propto \oint_{FS} \frac{d\mathbf{k}}{\sqrt{v_{\mathbf{k},l}^2 + v_{\mathbf{k},m}^2}} v_{\mathbf{k},l} v_{\mathbf{k},m} f_{i\mathbf{k}} f_{j\mathbf{k}} \\
&\equiv \langle v_{\mathbf{k},l} v_{\mathbf{k},m} f_{i\mathbf{k}} f_{j\mathbf{k}} \rangle_{FS} ,
\end{aligned}
\tag{7.18}
$$

where the final expression is a Fermi surface integral, with $v_{\mathbf{k},l}$ the l-th component of the Fermi velocity. This can be directly used to obtain, e.g. the k_3-coefficient in (2.6).

Appendix B

Semiclassical derivation of integrated edge current in chiral superconductors

Here we derive the integrated edge current of chiral superconductors with arbitrary Cooper pair angular momentum $L_z = m\hbar$. Our analysis is based on the semiclassical approach developed by Stone and Roy[48] for chiral p-wave superfluids. They mapped the specular and Andreev reflection of an incident quasi-particle wave at the edge (Fig.7.1) to the reflection and transmission of Dirac waves at the domain wall of a one-dimensional twisted mass Dirac Hamiltonian, i.e. a Dirac Hamiltonian with opposite masses on the two sides of the normal ("domain wall").[111, 112] For such a 1D Dirac problem, excess charge Q accumulates at the domain wall, due to the formation of edge states as well as the phase shift of the extended continuum states. The spontaneous current arising from the occupied quasi-particle states with momenta parallel to an incident trajectory is given by Qv_{F_y}, i.e. a product of the component of Fermi velocity parallel to the edge and the amount of accumulated charge of the corresponding 1D twisted-mass Dirac Hamiltonian.
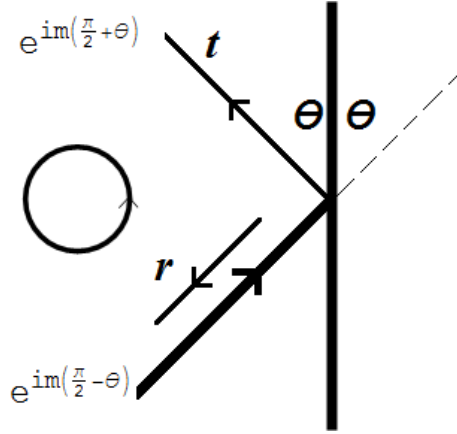
Figure 7.1: Specular and Andreev reflection of a quasiparticle wave at an ideal boundary. The angle θ is measured with respect to the positive y-direction parallel to the edge and increases in clockwise sense. The chirality imposes a diretional-dependent phase to each propagating wave, i.e. for the incident wave, $\phi_{\text{in}} = m(\pi/2 - \theta)$, while for the specularly-reflected wave $\phi_{\text{out}} = m(\pi/2 + \theta)$, both originating from the superconducting gap function $\Delta_k = \Delta_0 e^{im\theta_k}$ where θ_k denote the direction of the wavevector with respect to the x-direction. Translating to the effective 1D Dirac Hamiltonian, the specular and Andreev reflections correspond respectively to transmission and reflection of an incident Dirac wave. The arrow in on circle indicates the chirality of the Cooper pairing.

Generalizing the derivation in Stone and Roy[48] to arbitrary m, one can show that the total amount of accumulated charge arising from the extended continuum states with incident trajectory shown in Fig.7.1 is,

$$Q_{\text{con}}(\theta) = \text{Const.} - \Delta \sin(m\theta) e^{-2\Delta|\sin(m\theta)||x|} + \int_{\Delta}^{\infty} \frac{dk}{2\pi} \frac{\Delta \sin(2m\theta)}{k^2 - \Delta^2 \sin^2(m\theta)} \frac{k}{\sqrt{k^2 - \Delta^2}} e^{-2k|x|},$$

(7.19)

where the constant is θ-independent and will be dropped in the following discussions, while the second term is a pole contribution that is present only if $2i\pi < 2m\theta < (2i+1)\pi$ (negative energy edge modes exist for these incident angles), with i being an integer. Integrating over

85

x from $-\infty$ to ∞, this second term gives total charge -1. After the same x-integration, and rescaling the variable by taking $x = k/\Delta$, the last term becomes,

$$\int_1^\infty \frac{dx}{2\pi} \frac{\sin(2m\theta)}{x^2 - \sin^2(m\theta)} \frac{1}{\sqrt{x^2 - 1}} = \frac{2m\theta}{2\pi}, \quad -\pi < 2m\theta < \pi \qquad (7.20)$$

This expression is a 2π periodic function of $2m\theta$. Notice that in Fig.7.1, θ runs from 0 to π. For $2m\theta$ not in the range $(-\pi, \pi)$, it is given by $\mathrm{mod}(2m\theta + \pi, 2\pi) - \pi$, except when $2m\theta$ is odd multiples of π where there exists a discontinuity due to the loss of edge modes to the upper continuum. Note also that this would lead to vanishing accumulated charges for incident angles corresponding to the upper ends of the chiral edge branches. Physically this is because for these angles the phases of the incident wave and the specularly-reflected wave (or the transmitted wave in the mapping to the 1D problem in Fig.7.1), are equivalent, i.e. $\phi_{\mathrm{out}} - \phi_{\mathrm{in}} = \mathrm{mod}\, 2\pi$ in Fig.7.1. To be more concrete, we consider in the following the first three representative cases with $m = 1, 2, 3$, i.e. chiral p-, d-, f-wave superfluids.

7.0.1 Chiral p-wave   For chiral p-wave, $n = 1$. For the geometry shown in Fig.7.1, a chiral edge dispersion peels off the lower continuum at an incident angle $\theta = 0$ and makes it way to the upper continuum as θ increases from 0 to π (Fig.2.3). The dispersion is expressed as,

$$E_{k_y} = -\Delta \cos\theta = -\Delta k_y/k_F \ . \qquad (7.21)$$

Notice the group velocity of the edge dispersion is in opposite sense to the actual flow of the current. Due to charge-neutrality, the current carried by each of the individual edge mode is independent of their group velocity and is simply proportional to its wavevector parallel to the edge, k_y/m^*. The expression in Eq.7.20 now simplifies to,

$$\begin{cases} \dfrac{\theta}{\pi} & 0 < \theta < \dfrac{\pi}{2} \\[3em] \dfrac{\theta}{\pi} - 1 & \dfrac{\pi}{2} < \theta < \pi \end{cases} \tag{7.22}$$

Taking into account the pole contribution, Eq.7.19 follows as,

$$Q_{\mathrm{con}}(\theta) = \frac{\theta}{\pi} - 1. \quad 0 < \theta < \pi \tag{7.23}$$

This is the charge drawn to the "domain wall" of the 1D twisted-mass Dirac problem as induced by the reflection of the continuum states. Note that as explained before, the accumulated charge is zero for $\theta = \pi$.

Translating back to our 2D problem, (7.23) corresponds to a total amount of current $j_{\mathrm{con}}(\theta) = Q_{\mathrm{con}}(\theta) k_F \cos\theta / m^*$ resulting from all of the phase-shifted occupied continuum states with incident trajectory angle θ. In the ground state, the occupied bound states correspond to incident angles $\theta \in (0, \pi/2)$, and each carries one unit charge, $Q_{\mathrm{edge}} = 1$. Taken together, the total accumulated charge at $\theta = \pi$ is zero, a manifestation of sudden loss of bound state at the upper end of the chiral edge dispersion.

One can now compute the spontaneous current for any particular incident angle, where the continuum contribution is,

$$J_{\mathrm{con}}^p = \frac{1}{2} \int_\pi^0 \frac{-k_F \sin\theta \, d\theta}{2\pi} \frac{k_F \cos\theta}{m^*} \left(\frac{\theta}{\pi} - 1 \right) = -\frac{k_F^2}{16\pi m^*} \tag{7.24}$$

where the factor $1/2$ accounts for double counting[48] in arriving at Eq.(7.19), m^* is the effective mass of carrier which is not to be confused with the angular momentum of the Cooper

pairs. The occupied edge states exist for incident angles $\theta \in (0, \pi/2)$. Hence the bound state contribution follows as,

$$J_{\text{edge}}^p = \frac{1}{2} \int_{\pi/2}^0 \frac{-k_F \sin\theta d\theta}{2\pi} \frac{k_F \cos\theta}{m^*} = \frac{k_F^2}{8\pi m^*} \tag{7.25}$$

Thus the continuum state contribution is half of the edge state contribution, and in opposite direction! These results are obtained by both Stone and Roy[48], and Sauls[57]. The total edge current of a chiral p-wave superfluid is then,

$$J^p = \frac{k_F^2}{16\pi m^*} = \frac{\rho}{4m^*} \tag{7.26}$$

for a spinless model. This current flows in positive y direction, and induces a macroscopic angular momentum (had the superfluid been confined in a finite disk) coinciding with the sum of the angular momentum of the Cooper pairs!

7.0.2 Chiral d-wave   For chiral d-wave, $m = 2$. As shown in Fig.2.3, there exists two branches of topologically protected edge modes with the same chirality. The edge dispersion is given by

$$E_{k_y} = \begin{cases} -\Delta\cos(2\theta) = \Delta(k_F^2 - 2k_y^2)/k_F^2 & 0 \le \theta \le \frac{\pi}{2} \\ \\ \Delta\cos(2\theta) = -\Delta(k_F^2 - 2k_y^2)/k_F^2 & \frac{\pi}{2} < \theta \le \pi \end{cases} \tag{7.27}$$

In the following, the bulk of the analysis in the previous section carries through, with the only complication that one now needs to compute the accumulated charge for $\theta \in (0, \pi/2)$ and $\theta \in (\pi/2, \pi)$ separately. In addition, the occupied edge mode in this case correspond respectively to incident angles $\theta \in (0, \pi/4)$ and $\theta \in (\pi/2, 3\pi/4)$ for the two branches of edge

dispersion. A detailed analysis leads to the following piecewise function for the accumulated charge from the continuum states,

$$Q_{\text{con}}(\theta) = \begin{cases} \frac{2\theta}{\pi} - 1 & 0 \leq \theta \leq \frac{\pi}{2} \\ \\ \frac{2\theta}{\pi} - 1 - 1 & \frac{\pi}{2} < \theta \leq \pi \end{cases} \tag{7.28}$$

which again satisfies the requirement that the accumulated charge be zero for the incident trajectory associated with the wavevectors at the upper ends of the chiral branches, i.e. for incident angles $\theta = \pi/2$ and $\theta = \pi$. The current arising from the phase-shifted continuum states then follows as,

$$\begin{aligned} J_{\text{con}}^d &= \frac{1}{2} \int_{\pi/2}^{0} \frac{-k_F \sin\theta \, d\theta}{2\pi} \frac{k_F \cos\theta}{m^*} \left(\frac{2\theta}{\pi} - 1 \right) + \frac{1}{2} \int_{\pi}^{\pi/2} \frac{-k_F \sin\theta \, d\theta}{2\pi} \frac{k_F \cos\theta}{m^*} \left(\frac{2\theta}{\pi} - 2 \right) \\ &= 0 \end{aligned} \tag{7.29}$$

Similarly, the edge state contribution reads,

$$\begin{aligned} J_{\text{edge}}^d &= \frac{1}{2} \left(\int_{\pi/4}^{0} + \int_{3\pi/4}^{\pi/2} \right) \frac{-k_F \sin\theta \, d\theta}{2\pi} \frac{k_F \cos\theta}{m^*} \\ &= 0 \end{aligned} \tag{7.30}$$

It has been shown before[113, 114] that the edge state contribution should vanish in a chiral d-wave. Here we have moved one step further by showing that the continuum contribution is zero as well! Taken together, the total edge current of a chiral d-wave superfluid vanishes,

$$J^d = 0 \tag{7.31}$$

It is also interesting to see from (7.29) and (7.30) that the one-half relation between the contin-uum and edge state contribution does not hold in chiral d-wave models. In fact, this relation is a peculiar property of chiral p-wave superfluids, and is absent for all higher angular momen-tum Cooper pairings, as will be illustrated further in the next section.

7.0.3 Chiral f-wave   For chiral f, $m = 3$. Figure 2.3 shows the three branches of chiral edge modes of an isotropic chiral f-wave model, where,

$$E_{k_y} = \begin{cases} -\Delta\cos(3\theta) = \Delta(3k_F^2 k_y - 4k_y^3)/k_F^3 & 0 \leq \theta \leq \frac{\pi}{3} \\ \\ \Delta\cos(3\theta) = -\Delta(3k_F^2 k_y - 4k_y^3)/k_F^3 & \frac{\pi}{3} < \theta < 2\pi/3 \\ \\ -\Delta\cos(3\theta) = \Delta(3k_F^2 k_y - 4k_y^3)/k_F^3 & \frac{2\pi}{3} < \theta \leq \pi \end{cases} \tag{7.32}$$

Notice that in the ground state the occupied edge modes correspond to incident angles $\theta \in (0, \pi/6), (\pi/3, \pi/2)$ and $(2\pi/3, 5\pi/6)$. With some analyses analogous to the previous sections, one can show that the accumulated charge from the continuum is,

$$Q_{\mathrm{con}}(\theta) = \begin{cases} \frac{3\theta}{\pi} - 1 & 0 \leq \theta \leq \frac{\pi}{3} \\ \\ \frac{3\theta}{\pi} - 2 & \frac{\pi}{3} < \theta \leq 2\pi/3 \\ \\ \frac{3\theta}{\pi} - 3 & \frac{2\pi}{3} < \theta \leq \pi \end{cases} \tag{7.33}$$

Evaluating the current explicitly,

$$J^f = J^f_{\text{edge}} = J^f_{\text{con}} = 0 \tag{7.34}$$

i.e. the edge current of a chiral f-wave superfluid is also zero! Similar calculations can be generalized to $m > 3$, all of which have $J^m = J^m_{\text{edge}} = J^m_{\text{con}} = 0$.

Appendix C

Spectral asymmetry and integrated edge currents

In Eq. (17) of the publication in Chapter 4, we expressed the total integrated current of the ground state of a chiral p-wave superconductor across the two edges of a cylindrical geometry in terms of the so-called spectral asymmetry of the energy spectrum. Here we give a derivation of the integrated current, assuming two open boundaries in x-direction and periodic boundary condition in y.

The translational invariance in y allows one to Fourier transform the Hamiltonian along that direction. For each wavevector k_y, the BdG equation reads,

$$\hat{H}_{k_y}(x) \begin{pmatrix} u_{j,k_y}(x) \\ v_{j,k_y}(x) \end{pmatrix} = E_{j,k_y} \begin{pmatrix} u_{j,k_y}(x) \\ v_{j,k_y}(x) \end{pmatrix}, \tag{7.35}$$

where E_{j,k_y} is the energy of the j-th quasi-particle state, and the wavefunction satisfies the following normalization relation,

$$\int dx \left(|u_{j,k_y}(x)|^2 + |v_{j,k_y}(x)|^2 \right) = 1. \tag{7.36}$$

The corresponding BdG Hamiltonian may be expressed in terms of the quasi-particle operators $H_{\text{BdG}} = \sum_{j,k_y} \left(E_{j,k_y} \gamma^\dagger_{j,k_y} \gamma_{j,k_y} - E_{j,k_y} \bar{\gamma}_{j,-k_y} \bar{\gamma}^\dagger_{j,-k_y} \right)$. Using these operators, the fermion field can be decomposed as the following,

$$\psi(x) = \sum_{k_y,j} \left(u_{j,k_y}(x) \gamma_{j,k_y} + v_{j,k_y}(x) \bar{\gamma}^\dagger_{j,-k_y} \right). \tag{7.37}$$

Specific to the problem under consideration, the usual particle-hole redundancy of the BdG Hamiltonian is manifest in the following: for each state (labeled j) with wavevector k_y and wavefunction $(u,v)^T$, there exists another state (labeled $\bar{j}$) at wavevector $-k_y$ with the exact opposite energy and with a wavefunction $(v^*, -u^*)^T$, i.e.

$$E_{j,k_y} = -E_{\bar{j},-k_y}. \tag{7.38}$$

Next, use the current operator $\hat{I}(x) = \psi^\dagger(x) \hat{V}_y(x) \psi(x)$ to evaluate the current density distribution, where $\hat{V}_y = -i\partial_y$ is the y-component of the velocity operator. The derivation below is only valid when $\hat{V}_y$ is independent of the x-coordinate, thus we drop the the explicit x-dependence of the operator hereafter. In the ground state, the current density is computed as the following,

$$I(x) = \langle \hat{I}(x) \rangle = \sum_{k_y} \sum_{E_{j,k_y} > 0} V_{k_y} |v_{j,k_y}(x)|^2, \tag{7.39}$$

where $\langle \rangle$ stands for a ground state expectation where the ground state is taken as the vacuum of positive-energy states, and we made a simplification by using V_{k_y} to denote the y-component velocity operator. Usually, when the normal state single-particle Hamilton in momentum space is expressed in separable forms of k_x and k_y, V_{k_y} is only explicitly dependent on k_y, such as $V_{k_y} = k_y/m$ for a continuum model and $V_{k_y} = t \sin k_y$ for a tight-binding model on a square lattice with only nearest neighbor (NN) hoppings. For more general lattice models, V_{k_y}

may also depend on $|k_x|$, e.g. $V_{k_y} = t' \cos k_x \sin k_y$ for a square lattice with only next nearest neighbor (NNN) hoppings. In this case, for our derivation to be valid, it is required that $|k_x|$ be a good quantum number, i.e. there should not be external potential variation along x-direction within the geometry.

Similar to (7.39), the time-reversed current density is given by,

$$
\begin{aligned}
-I(x) &= \langle \hat{I}(x)^* \rangle = \sum_{k_y} \sum_{E_{j,k_y}>0} V_{-k_y} |u_{j,k_y}(x)|^2 = -\sum_{k_y} \sum_{E_{j,k_y}>0} V_{k_y} |u_{j,k_y}(x)|^2, \quad \text{or,} \\
I(x) &= \sum_{k_y} \sum_{E_{j,k_y}>0} V_{k_y} |u_{j,k_y}(x)|^2.
\end{aligned}
\tag{7.40}
$$

Consequently, the final expressions on the right-hand-side of (7.39) and (7.40) equal one another,

$$
I(x) = \sum_{k_y} \sum_{E_{j,k_y}>0} V_{k_y} |v_{j,k_y}(x)|^2 = \sum_{k_y} \sum_{E_{j,k_y}>0} V_{k_y} |u_{j,k_y}(x)|^2.
\tag{7.41}
$$

Note that in both (7.39) and (7.40), only the positive-energy states are summed over. In fact, by utilizing the particle-hole redundancy (7.38), the current may also be evaluated using the negative-energy states. This yields a current opposite to (7.39),

$$
I(x)' = -I(x) = \langle \hat{I}(x) \rangle' = \sum_{k_y} \sum_{E_{j,k_y}<0} V_{k_y} |u_{j,k_y}|^2 = \sum_{k_y} \sum_{E_{j,k_y}<0} V_{k_y} |v_{j,k_y}|^2,
\tag{7.42}
$$

where $\langle \rangle'$ denotes a ground state expectation where the ground state is taken as the vacuum of negative-energy states, and the last equation follows the same lines as those leading to (7.41).

Combining (7.41) and (7.42) leads to the following expression for the current density,

$$
\begin{aligned}
I(x) &= \frac{1}{4} \Big[\sum_{k_y} \sum_{E_{j,k_y}>0} V_{k_y} |v_{j,k_y}(x)|^2 + \sum_{k_y} \sum_{E_{j,k_y}>0} V_{k_y} |u_{j,k_y}(x)|^2 \\
&\quad - \sum_{k_y} \sum_{E_{j,k_y}<0} V_{k_y} |v_{j,k_y}(x)|^2 - \sum_{k_y} \sum_{E_{j,k_y}<0} V_{k_y} |u_{j,k_y}(x)|^2 \Big] \\
&= \frac{1}{4} \sum_{k_y} \Bigg[\sum_{E_{j,k_y}>0} V_{k_y} (|v_{j,k_y}(x)|^2 + |u_{j,k_y}(x)|^2) - \sum_{E_{j,k_y}<0} V_{k_y} (|v_{j,k_y}(x)|^2 + |u_{j,k_y}(x)|^2) \Bigg] .
\end{aligned}
$$
(7.43)

The integrated current across the geometry may then be written as,

$$
I = \int dx \, I(x) = \frac{1}{4} \sum_{k_y} V_{k_y} \left[\sum_{E_{j,k_y}>0} - \sum_{E_{j,k_y}<0} \right] = \frac{1}{4} \sum_{k_y} V_{k_y} \eta_{k_y} , \tag{7.44}
$$

where in the second equation we have used the normalization condition (7.36), and η_{k_y} is the spectral asymmetry defined as,

$$
\eta_{k_y} = \sum_j \mathrm{sgn}[E_{j,k_y}] . \tag{7.45}
$$

Thus the spectral asymmetry at each k_y gives the difference between the number of positive- and negative-energy quasi-particle states. An additional factor of 2 must be included in (7.44) for spinful systems. This concludes our derivation!